ACOUSTICAL AND VIBRATIONAL PROCEDURES FOR INVESTIGATING THE MODAL RESPONSE OF STRUCTURES

P.G. WILLIAMS

ACOUSTICAL AND VIBRATIONAL PROCEDURES FOR INVESTIGATING THE MODAL RESPONSE OF STRUCTURES

BY

© P. G. WILLIAMS, B.A. (OXON)

A thesis submitted to the School of Graduate

Studies in partial fulfilment of the

requirements for the degree of

Master of Engineering

Faculty of Engineering and Applied Science

Memorial University of Newfoundland

St. John's Newfoundland Canada

ACOUSTICAL AND VIBRATIONAL PROCEDURES FOR INVESTIGATING THE MODAL RESPONSE OF STRUCTURES

"It is a tale told by an idiot, full of sound and fury"

William Shakespeare (Macbeth)

ABSTRACT

The modal characteristics of structures are normally established experimentally through the use of accelerometers and force transducers to measure the frequency response under different excitation frequencies. Variations in the modal frequencies and the mode shapes can be determined for different structural modifications. Modal properties can also be determined through measurement of the acoustical properties of the structure, particularly in the quantity and direction of acoustic energy flow. Such measurements, because they are non-contacting, offer the advantage of eliminating modification of the modal response due to the mass of the accelerometers as well as ease of use where accelerometer attachment is difficult, for example, on fibre composite structures. Experiments were designed to investigate the ease and accuracy of such acoustic measurements by comparing results from the acoustic energy flow methods with more classical vibrational techniques.

The structure was then modified through the introduction of a machined notch and the acoustic modal properties measured again for comparison.

A method is presented for the use of acoustic energy flow mapping in the detection of structural defects which result in the modification of the modal frequencies and amplitudes.

ACKNOWLEDGEMENTS

This thesis was completed at the Faculty of Engineering and Applied Science and at the Centre for Cold Ocean Resource Engineering, Memorial University of Newfoundland. Funding for the research was provided by CANMET. Special thanks go to Dr. Jack Clark, Director of C-CORE for supporting this research through C-CORE, and to my thesis supervisor Dr. Jacques Guigne, Seabed Geotechnics Group Leader, C-CORE for his enthusiasm and for lending his expertise in acoustics to this project.

The author is indebted to Dr. A.S.J. Swamidas for, among other things, bringing me to St. John's in the first place, as well as for assisting in the supervision throughout this study.

Many thanks to Technical Services for the fabrication of specimens and related apparatus, and to Austin Bursey, Structures Laboratory Technician for his expertise in keeping equipment running.

Finally, I would like to thank my wife Rachel for her continuous support throughout the writing up of this thesis and for ensuring its completion.

TABLE OF CONTENTS

LIST OF FIGURES

LIST OF TABLES

NOTATIONS

a_i magnitude of accceleration (m/s^2) in i direction (i=x,y,z)

I_i magnitude of intensity (W/m^2) in i direction (i = x,y,z)

I_0 reference intensity level (W/m^2)

L_I intensity level (dB)

L_{IR} intensity level measured by a system due to instrumentation errors(dB)

L_K reactivity index of sound field (dB)

L_{K0} residual intensity index of a measuring system (dB)

L_P pressure level (dB)

L_{PR} pressure level measured during calibration of a measurement system(dB)

p pressure level (Pa)

p_0 reference pressure level (Pa)

ρc characteristic impedance

ρ density (kg/m^3)

c speed of sound (m/s)

PREFACE

It should be noted that the practical research presented in this thesis was completed at the beginning of 1990 and was specifically based on the use of a digital filtering, pressure-pressure transducer technique. There are several other techniques suitable for measuring intensity and since this work, research has moved on in some of the directions suggested by it. Guigne et al 1992 investigated the use of an FFT analyzer to obtain more detailed information regarding modal parameters, including intensity mapping. Klein et al (1994) look at the changes in modal parameters arising from fatigue cracking in cantilever beams. However, the work presented in this thesis provides an important underpinning of the subsequent research and is considered to stand as an original piece of research.

1.0 INTRODUCTION

It has long been recognised that the acoustic radiation properties of a structure are tied to its mechanical properties - for example, the Mersenne Laws relate the natural frequency of a plucked string to its tension and linear density (Stephens and Bate, 1966). The use of a simple acoustic measuring device which detects the variations in pressure allows measurement of this acoustic radiation. A single microphone can only be used to measure scalar quantities - the frequency and power of an acoustic transmission. Associated with an acoustic transmission, there may be energy propagation, represented by the acoustic intensity vector. Measurement of the acoustic intensity vector enables the energy flow in an acoustic field to be mapped and allows the identification of energy sources and sinks.

The hypothesis presented at the start of this thesis is that any mechanical changes which occur in a structure, for example, fatigue cracking, will lead to a change in the vibration modes and hence also to the radiated acoustic energy. Any technique that is developed in air can be transferred to an underwater environment with facility due to the fact that acoustic properties can be measured as easily in water as in air through the use of hydrophones.

1.1 STATEMENT OF OBJECTIVES

The measurement of acoustic energy and surface energy in order to map energy flow patterns in and around structures is well established (Pavic, 1976, Rasmussen at al 1983 and Hashimoto and Tagawa, 1987). The aim of this research was to investigate the applicability of these measurements to the determination of the underlying structural vibration. Following that, the ability to detect variations in the structural vibrations arising from structural changes was investigated. The vibrational characteristics of simple structures (cantilever beams) were theoretically determined using vibration theory (Stephens and Bate, 1966) as well as by finite element techniques (Bathe and Wilson, 1976). The experimental vibration characteristics were then measured and compared with the energy flow measurements. Band-saw cuts were introduced to modify the structure and the resultant changes to the energy flow measured. The changes to the energy flow were analyzed to determine the correlation with the actual structural modifications.

The evaluation of acoustic intensity scanning data is often complicated by the determination of significant frequency bands (Guigné et al 1988) and new measurement techniques were required to be developed. In order for the acoustic scanning technique to be applied underwater, the transducer set-up for such measurements had to be developed. The transducers were evaluated for intensity scanning by carrying out measurements on a vibrating beam in an underwater environment.

1.2 ORGANIZATION OF THESIS

This thesis is divided into six chapters. Chapters one and two introduce the research and place it in the context of current knowledge.

Chapter three introduces the concept of acoustic intensity and then presents the theoretical equations which describe this property. From the theoretical equations are developed approximations relating acoustic intensity to simple measurements of pressure. These approximations show how practical measurement of acoustic intensity is possible using a variety of microphone arrays. Surface intensity is then introduced and it is shown that measurement methods, analogous to that used for acoustic intensity, can be used through the substitution of accelerometers for microphones.

In order to expand the applicability of the method, a hydrophone array which allows the acoustic intensity to be measured underwater is described.

The practical methods used in the research are described in detail in Chapter Four and the results obtained from the experimental procedures are then presented and discussed in Chapter Five.

These results are summarised in Chapter Six, which also outlines proposals for further investigation in this field.

2.0 STATE-OF-THE-ART IN RELATING ACOUSTICAL INTENSITY MAPPING TO VIBRATIONAL RESPONSE

Vibration and acoustics are two closely related subjects which have given rise to a large volume of research into the measurement and control of both. The topic can be broken down as a function of frequency. At lower frequencies the concern is with the vibration of structures which can give rise to mechanical damage. Examples of these might be an offshore platform of a welded tubular construction where the wave loading induced vibration could lead to fatigue (Whittome & Dodds, 1983), or the infamous Tacoma narrows bridge where a wind loading induced resonance lead to its collapse (Stephens and Bate, 1966). In the audible range of the frequency spectrum the problem concentrates on the effect of sound levels on the environment because of the concerns of health and safety, and this has led on, for example, to the development of acoustic baffles to reduce radiated noise levels (Tinti, 1992). Additionally, investigations into the sources of noise can then be linked to methods of reducing the levels of radiated acoustic energy at the source, or can lead to identification of a mechanical problem giving rise to the unwanted noise.

There has been a long tradition of using the acoustic response of a structure to determine its vibration characteristics as they relate to its mechanical properties. Since the advent of the railway, iron and steel carriage wheels, have been regularly tapped and the note produced analyzed by the experienced engineer to determine whether the wheel

was cracked or otherwise damaged. Similarly, the existence of wear or misalignment problems in rotating machinery could be detected by an experienced operator from the sound of the equipment. The introduction of transducers such as accelerometers and microphones and their associated amplification and recording equipment has led to the development of more rigorous procedures for the measurement of vibration and noise. Coupled with microprocessor based analyzers and computers for post-processing the analysis of such data can reveal extensive information for the structural engineer. Additionally, predictive models have become more powerful and accurate through the use of computers to perform numerical integrations (Fillipa, 1983) or finite element analysis (Cragg, 1972, Petyt, 1983).

2.1 LITERATURE REVIEW

2.1.1 Vibration and Acoustic Transmission

The most important source of radiated noise is the vibration of elastic surfaces. This vibration can arise from either mechanical excitation or from external acoustic excitation. An additional problem in predicting noise levels arises when the area of acoustic interest formed an enclosed space. Again taking a musical analogy, notes on a pipe organ are the result of a resonance of an air column (Sen, 1990). Similarly, any enclosed air space will have acoustic resonances (Petyt, 1983). Particular problems can arise if the structural resonances are close to an acoustic resonance.

The levels of noise radiating from a vibrating structure are related by the Helmholtz equation (Filippa, 1983) which can be solved by various methods. One of these is numerical integration (Fyfe and Ismail, 1987, Seebert and Khurana, 1988) and this approach is called the boundary element method (BEM) (Wendland, 1983). The BEM is based on an assumption that the source is radiating into free space but Fyfe et al (1989) have used it, along with curve fitting modal identification techniques to analyze closed regions. They compared this method with the finite element method and showed that the two methods were in close agreement, with some reductions in modelling times being possible in the boundary element method. Brughmans et al (1992) also made use of the BEM to analyze closed volumes and concluded from their results that high pressure levels were caused by structural resonances while acoustic resonances led to peaks in the structure acceleration levels.

Grosveld et al (1988) used finite element techniques to solve the Helmholtz equations as a method for predicting structural-acoustic interactions, where noise levels in an enclosed space were of interest. In this case, the structure and acoustic models were coupled by a finite element solution to the structure-fluid interaction. Both external acoustic sources and direct mechanical excitations were modelled. They concluded that the acoustic response dominated the structural contribution.

Rather than solve the structural-acoustical coupling, Sung et al (1991) determined the acoustical modes for a vehicle interior using finite element analysis. The structural

modes for the vehicle body were determined experimentally using modal testing. The coupling coefficients between the two are then calculated from the solution to the wave equation and the appropriate elastic or rigid boundary conditions. Since these coefficients are a measure of the similarity between mode shapes and frequencies, they can be used to identify the structural component contributing the most to the noise levels. Structural modification to reduce noise levels can then be carried out.

A different approach to predicting structure born noise was given by Okubo et al (1988). This is based on the point source model in which each point in a structure is assumed to be an independent noise source. The acoustic intensity radiated by discrete areas of the structure can be estimated and the noise at any point near the structure can then be calculated by integrating the independent noise source intensity vectors.

The relationship between structural vibration and the resulting acoustic radiation was developed by Leuridan et al (1989). They used a model based on the mechano-acoustical impedances between structural response and sound pressure measurements. They used transfer functions and coherence analysis principles and found good agreement with experimental results.

When a structure is immersed in a fluid, effects such as reverse fluid loading become important. Park and Lee (1990) carried out an analytical investigation into these effects using Timoshenko-Mindlin plate theory to construct the equations for circular

plate vibration and solve the Helmholtz equation for this particular case. A reduction in natural frequencies arising from the fluid loading was shown and the effect of viscoelastic coatings on radiated power was examined.

For the case of external acoustic excitation the noise transmission properties of a structure are of interest, in particular with reference to noise control. Desai and Koval (1988) showed that the Rayleigh-Ritz method worked well at predicting transmission losses through plates at frequencies away from the lower plate resonance frequencies.

2.1.2 Prediction and Measurement of Structural Vibration and Acoustic Radiation

The motion of a vibrating structure can either be determined experimentally or predicted by using methods such as finite element analysis. Begg et al (1976) and Kenley and Dodds (1980) used accelerometers to determine the modal frequencies of a welded tubular off-shore structure with the intention of identifying structural change from a shift in modal frequency. Vibration monitoring of rotating machinery using accelerometers and a constant percentage bandwidth analyzer (Angelo, 1987) has proven extremely effective in the early detection of machinery faults.

The acoustic radiation resulting from structural vibration can also be determined by experimental and analytical methods.

As described in the previous section, the Boundary Element method can be used

in an analysis package to predict acoustic radiation levels. Fyfe and Ismail (1987) used the BEM to analyze noise radiating from vibrating cylinders. They used experimental data as the input surface vibration data and validated their predictions by using far field pressure measurements. Seybert and Khurana (1988) introduced a computer code called BEMAP and then went on to describe its application in predicting the radiating characteristics of a prototype engine using modal analysis to generate the surface vibration of the structure. Such a package can work equally well with both modal vibration data and experimentally measured response data.

Bissinger and Chowdhury (1992) compared the use of accelerometers and microphones in modal measurements. They made the important point that a microphone will give a better ranking of the effectiveness of vibrational modes as acoustic radiators. Although they concluded that an accelerometer makes a preferable transducer to measure the surface motion, they do show that modal shapes can be identified using a single microphone in both the near and far field.

With regard to the use of intensity measurements to investigate the vibrational response of simple structures, much work has been done to look at the energy flow both in and close to panels excited using loudspeakers and with a variety of damping locations (Rasmussen et al, 1988). This work reveals information about the location of sources and sinks in the structure and has been extended, for example, to the measurement of sound intensity maps over a van engine cover. As an example of how the acoustic

intensity could replace accelerometer based measurements, Rasmussen (1983) demonstrated an application in engine testing whereby the analysis of the variation in radiated acoustic intensity through one rotation cycle allowed identification of faulty engines.

Of particular interest in the work done by Tichy and Mann (1985) is the measured radiation from a plate vibrating at its modal frequency, where a second mode was close in frequency and also excited. They made use of the active and reactive intensity measurements in order to differentiate the two mode shapes.

Okubo and Tajima (1988) used the point source model to predict the acoustic intensity pattern over different structures. At the first two modal frequencies they found excellent correlation both with the mode shapes and with the measured acoustic intensity patterns.

Hashimoto and Tagawa (1987) also showed the correspondence between vibration modes and radiation noise distributions on a printer assembly. They were able to identify the structural components that gave rise to excessive noise and these were then modified to obtain the required reduction in acoustic radiation. Of interest is their use of acoustic intensity as a specific tool to measure the radiated noise. They obtain clear correspondence between vibration modes and acoustic intensity distribution.

2.1.3 Noise Control

The correlation between structural vibration and radiated noise provides a basis for noise control of structures. Moore and Reif (1987) carried out an investigation on a milling cutter by carrying out both modal analysis and radiated noise measurements. On a complex structure, this allows the area generating the most noise to be identified from local mode shapes and modal frequencies. From this, localized damping can be used effectively.

In many applications, the amount of damping that can be applied is limited, either by space or weight. The effect of localised damping on mode shapes and mode frequencies is investigated in order to assess optimisation of acoustic damping. In their approach Garibaldi et al (1990) used loss factor calculations in an analytical modal analysis.

The investigation carried out on plates (Lamancusa and Koopmann, 1991) led to possible noise control methods which avoided the use of added damping materials. Using finite element analysis and a discretized form of the Rayleigh integral they identified a mode shape which acted as a "weak radiator" of sound. Rather than use damping material to reduce radiated sound, they varied the thickness of the plate in order to force the plate into the "weak radiator" mode.

The problem associated with quantifying acceptable noise levels was detailed by

Castagna (1992). He also described a limitation that can arise in using modal analysis to identify structural noise sources. He found that the normal modes did not relate to the observed noise problem and identified the source as a complex mode, which he defines as 'a mode of vibration...when all of the response locations are displayed without phase restrictions'.

Acoustic measurements are usually associated with noise levels that fall in the frequency band of the human ear response. These measurements related to sound monitoring and control are generally carried out using microphones to record sound pressure levels. Analyses have traditionally been based on one-third octave or other fractional octave measurements because of the nature of human hearing, (Bruel & Kjaer, 1987).

There are problems associated with using pressure to measuring sound levels, particularly in relation to identifying sound sources when there is a high level of background noise, and it has long been realised that the measurement of acoustic intensity, which is a vector parameter, has a number of advantages of the use of the scalar pressure (Pascal and Lu, 1985). Schultz (1975) discussed the failure of effective practical measuring equipment but with the overcoming of these obstacles a number of applications were developed. Tichy and Mann (1985) developed theoretical expressions for acoustic near fields of radiators and standing waves and then measured the intensity vortex for two cases. Rasmussen (1984,1985) and Kelly (1988) have both detailed the

principle advantages of acoustic intensity over pressure as being the ability to measure a vector quantity and the improvement in the signal-to-noise ratio that could be achieved. In particular, by integrating the measured intensity over a surface containing a sound source, the sound power for that source can be determined irrespective of the background noise.

The principal area of application of acoustic intensity has been in transportation systems where it is important that the vibrational response of the various vehicle components are such that they fall outside those areas where the ear is most sensitive. The use of acoustic intensity measurements in such applications is well established because of the improvement in the noise to signal ratio and the directionality of the measured signal. For example, Rasmussen (1988) made use of acoustic intensity, sound pressure level and accelerometer measurements in order to identify the source of noise arising from a rail vehicle and then linked the source to an engineering problem of excess wheel/rail wear. Bennett (1987) used an acoustic intensity technique to identify sound sources on an articulated loading shovel and a rotary pump which were generating excessive noise emissions; Atarashi (1988) made use of intensity measurements to investigate turbo machinery.

An extensive analysis of engine noise using acoustic intensity (Tinti, 1992) allowed determination of sound power levels as well as of noise source ranking while the engine is in a test frame in a semi-reverberant room. The ranking of sound sources also

allowed acoustical shield locations to be selected, as well as a subsequent measurement of the efficiency of each shield.

2.1.4 Other Applications of Acoustic Monitoring

There are a number of other areas where acoustic methods are being used to investigate vibration for engineering reasons other than the control of noise levels. Nilles and Dauby (1976) described an application of sound intensity in the monitoring and control of the reduction process in the steel making process whereby the sound intensity is used to control the volume of oxygen used in the blow. The problem of bubble cavitation on a marine propeller has been investigated using a hydrophone pair for measurement of acoustic intensity (Technisch Physiche Dienst, 1983). In both of these applications, the particular merit of the intensity measurement technique arises from the problems arising from high signal-to-noise ratios.

2.3 SUMMARY

The papers reviewed above clearly outline the relationship between radiated acoustic noise and the underlying structural vibrations. A number of theoretical and analytical relationships are introduced and then developed or verified through various practical measurements. Although there are a number of different approaches, they all generally adhere to the following steps:

a) Source characterization, i.e., underlying structural vibrations.

b) Coupling parameters between structural and acoustic effects.

c) Determination of sound field.

The principle aim of most structural-acoustic vibration problems is noise control. Again a few important guidelines emerge from the reviewed research:

a) Identification of the intended final noise requirements - for example, it will not be practical to reduce noise levels for a diesel engine to those of an electric motor.

b) Noise control can be effected by modification of the underlying structural response to alter mode shapes or shift modal frequencies.

c) Noise control can also be achieved through the use of acoustic shields which attenuate noise form particular sources.

A number of significant points relating to the practical measurements of acoustic radiation and structural vibration can be summarised from the reviewed authors:

a) The conclusion of Bissinger and Chowdhury (1992) that acoustic methods can be effective in experimental modal analysis. They use pressure measurements to

determine mode shapes.

b) Seybert and Kurana (1988) recognize the benefits of using acoustic intensity in the analysis of structural-acoustic interactions but do not carry out any practical measurements.

c) The findings of Tichy and Mann (1985), Hashimoto and Tagawa (1987), and Okubo et al (1988) all of whom obtain correlations between practical intensity measurements and mode shapes.

Given the possibilities of acoustic intensity as described by those authors who have used it, it is surprising that more researchers do not make use of it as a tool. A number of authors make use of pressure measurements but describe the problem associated with background noise. This problem can be avoided by the use of anechoic and reverberation chambers but these are not always easily accessible.

This research sets out to explore in depth the capabilities of acoustic intensity as a tool for modal analysis and to define some appropriate practical measurement procedures as well as determine the limitations of the method. The advantages mentioned by Bissinger and Chowdhury (1992) of using a non-contacting transducer are investigated further, in particular with respect to applications in underwater environments.

3.0 PHYSICS OF ACOUSTICS

In physical terms, acoustics is concerned with the propagation of energy from a source through an elastic medium by the progression of a mechanical vibration. In air, pressure variations caused by a moving surface such as a fan blade are propagated away from the source. These can be detected by a thin diaphragm such as the human ear or a microphone which converts the air pressure variation back into a mechanical vibration and then converts the mechanical vibration into an electrical impulse. However, the measurement of pressure yields a scalar value and hence no information regarding the direction of energy flow or the source of the energy can be obtained from such measurements. In order to obtain this information, we need to be able to measure Acoustic Intensity which is a vector quantity giving a measure of the power transmitted through a medium. The first requirement is, therefore, a reliable intensity measuring device. The following presentation of the physics and measurement of intensity was based on Fahy (1989) and various publications by Bruel and Kjaer (1986, 1987, 1988) who are acknowledged as one of the leaders in acoustic instrumentation.

3.1 DEFINITION OF INTENSITY

The instantaneous acoustic power density Ψ (W/m^2) is defined from Figure 3.1 as the energy transported in a specified direction per unit surface and unit time (Rossi, 1988). An equation for this value is derived as follows.

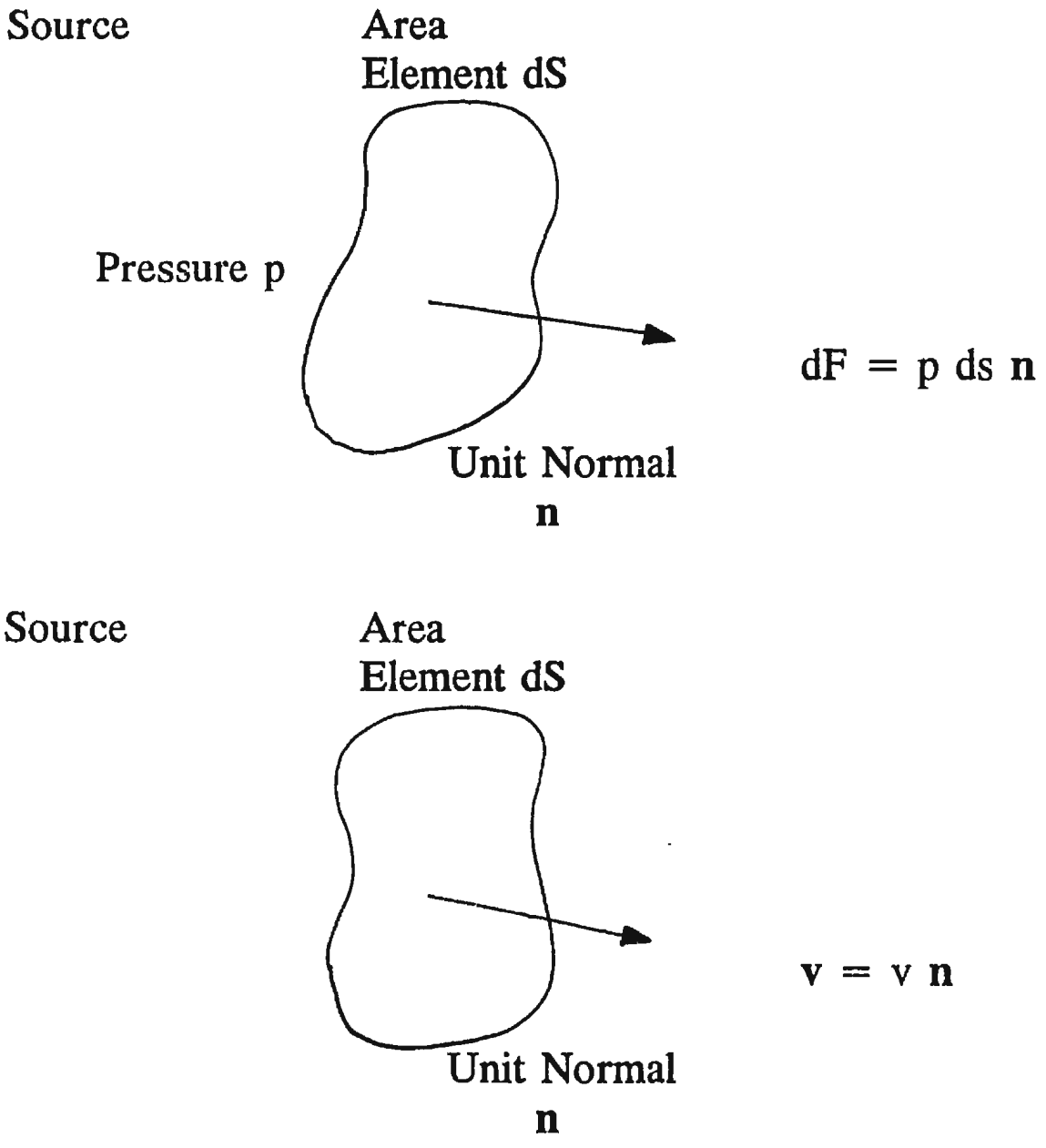

Figure 3.1 Definition of Sound Power and Acoustic Intensity

For an area element dS with unit normal **n**, the force exerted on this element by a pressure p is given by

$$dF = p \times dS \times \mathbf{n} \qquad N \qquad (3.1)$$

Assuming longitudinal waves, the particle velocity **v** is

$$\mathbf{v} = v \times \mathbf{n} \qquad m/s \qquad (3.2)$$

The work done by dF gives the energy transferred through dS during time dt, and this is given from

$$dW = (p\, dS\, \mathbf{n} \cdot v\, \mathbf{n}) \times dt$$

$$= p \times v \times dS \times dt \qquad J \qquad (3.3)$$

From the definition of the instantaneous acoustic power density, it can be seen that Ψ is given by the product of the particle velocity and the instantaneous pressure.

$$\Psi = p\, v \qquad W/m^2 \qquad (3.4)$$

The acoustic intensity I (W/m^2) is defined as the mean value of the instantaneous

acoustic power density. The acoustic intensity is a vector given by the time averaged product of the instantaneous pressure, p(t) and the particle velocity, v(t), in the equation

$$\mathbf{I} = \overline{p(t) \cdot v(t)} \qquad (3.5)$$

where the bar denotes a time averaging. Dimensionally we can see that this is correct:

$$\text{Intensity} = \frac{\text{Power}}{\text{Area}} = \frac{\text{Energy}}{\text{Area x Time}}$$

$$= \frac{\text{Force x Distance}}{\text{Area x Time}}$$

$$= \text{Pressure x Velocity} \qquad (3.6)$$

For a free field in which the sound wave arrives only from the direction of the source (spherical wave), the intensity is derived as follows (Fahy, 1989). For a plane harmonic wave the pressure and the particle velocity are related by:

$$v = p/(\rho c) \qquad \text{Pa} \qquad (3.7)$$

and substituting Eqn. (3.7) into Eqn. (3.5) we get

$$I = \frac{p^2_{rms}}{\rho c} \qquad W/m^2 \qquad (3.8)$$

where ρc is the characteristic impedance of the material, ρ is the density and c the speed of sound in the material.

3.2 DECIBEL SCALES

Most acoustic properties are represented using a logarithmic quantity because they are measurable over a number of orders of magnitudes (Sen 1989). The logarithmic quantity corresponds to the base 10 logarithm of the ratios of two measurements of the same property. The logarithmic ratio of two values is presented in the dimensionless quantity called the bel, or, more usually, in decibels (dB) where 1 dB is one-tenth of a Bel. For certain properties the logarithmic quantity, or level, is given as the logarithmic ratio of the measured value to a standard reference value. The sound pressure level and intensity levels, in decibels are given by:

$$L_p = 10 \log_{10} (p^2/p^2_o) \qquad dB \qquad (3.9)$$

$$L_I = 10 \log_{10} (I/I_o) \qquad dB \qquad (3.10)$$

where p_o equals 20 μPa. This value is chosen because it corresponds approximately to the threshold of hearing. The reference value I_o for intensity measurement is 1 pW/m^2, and this is chosen so that under free field conditions the pressure levels and intensity levels are nearly equal. In fact, under free field conditions we can substitute for I in Eqn. (3.10) using Eqn. (3.8)

$$L_I = 10 \log_{10} (p^2/(\rho.c.I_o)$$

$$= L_p - 10 \log_{10} (\rho \, . \, c. \, I_o/p^2_o)$$

$$= L_p - 10 \log_{10} (\rho \, . \, c/400) \qquad (3.11)$$

and under standard conditions, $\rho c = 415$ and the correction factor represented by the second term in Eqn. (3.11) is 0.16 dB.

When a directional characteristic is represented using a decibel scale, the usual notation is, for example, 65 dB(-) where the sign indicates the direction of flow relative to the measurement point. Standard notation takes positive as flow away from the surface or structure being investigated. Confusion should be avoided with -65 dB which represents a very small value.

3.3 SOUND FIELDS

Acoustic propagation involves energy flow but there can still be a time-variant pressure field in which the net intensity is zero. From the definition of intensity as the time averaged product of the particle velocity and the pressure we can see from Figure 3.2 that when the velocity and pressure are in phase, then the instantaneous acoustic power density variations are also in phase, and the acoustic intensity will be non-zero. If there is a phase shift of 90° then there will still be a variation in the instantaneous acoustic power density, but the time averaged acoustic intensity will be zero (Figure 3.3). An active field is one in which there is energy flow; a reactive field is one in which there is no net energy flow. An example of a purely reactive field is a standing wave in a pipe. Sound fields are also described as Free field or Diffused field. In a free field there are no reflections (e.g. an anechoic chamber) and the sound field is active. In a diffused field the sound is reflected from all surfaces so that it travels in all directions with equal magnitude and probability (e.g. a reverberation chamber). The net intensity is zero and we have a reactive sound field.

In the near field of a source (defined as less than 1/4 of a wavelength from the surface) the air acts as a mass-spring system storing energy and hence the sound field is reactive. By measuring intensity in the near field, this reactive component is ignored and only the active component is measured. Because the measurements can be made close to the source, the signal-to-noise ratio of the measurement is improved.

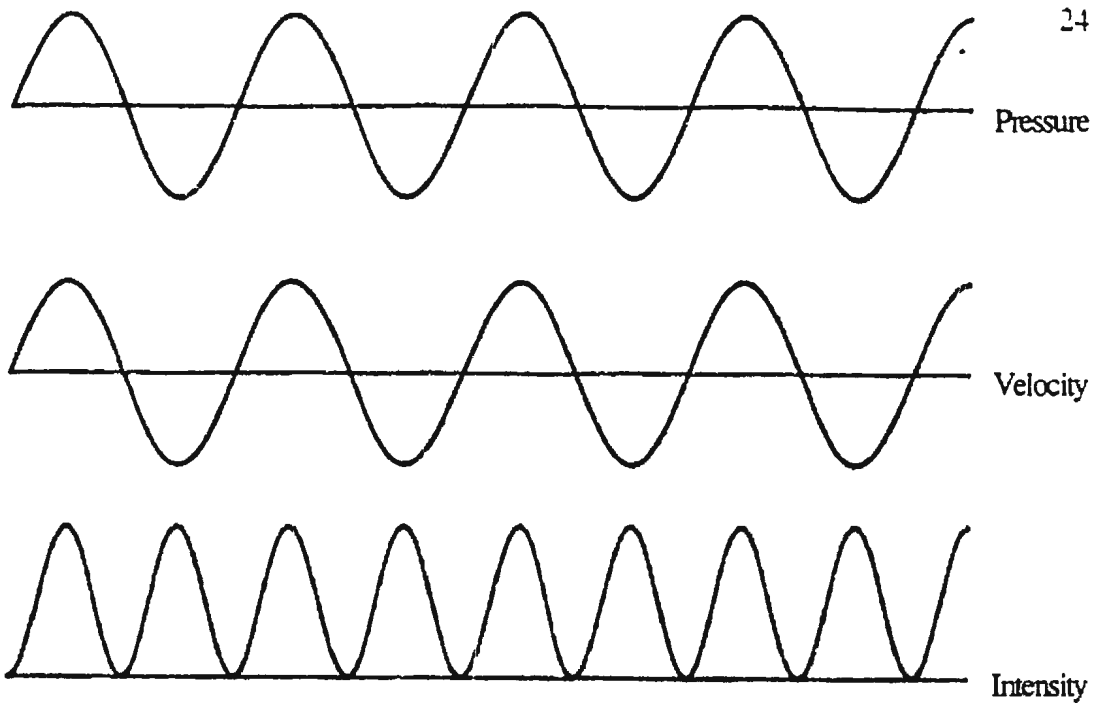

Time Averaged Intensity $\neq 0$

Figure 3.2 Instantaneous Acoustic Power Density for Particle Velocity and Pressure In Phase.

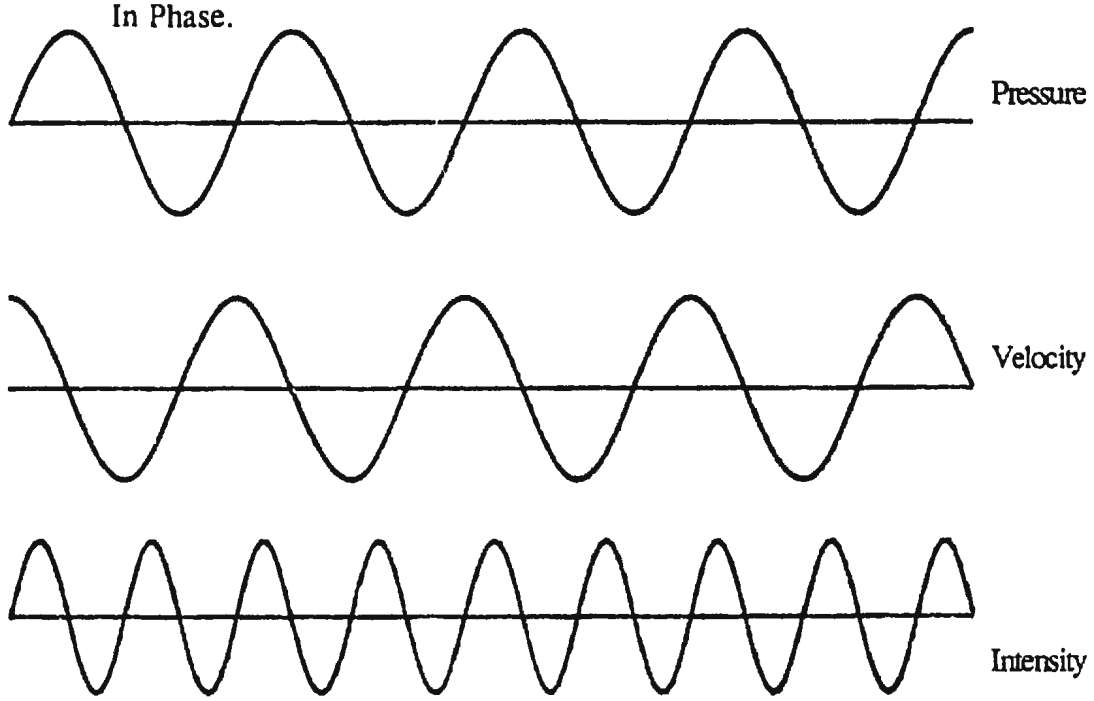

Time Averaged Intensity = 0

Figure 3.3 Instantaneous Acoustic Power Density for Particle Velocity and Pressure 90° Out of Phase.

3.4 MEASUREMENT OF ACOUSTIC INTENSITY

Acoustic intensity can be measured (Fahy, 1989) in either the time domain through the use of digital filters or the frequency domain using an FFT analyzer. Time domain measurements were made throughout this research and this is the method which is discussed in detail here.

3.4.1 Finite Difference Approximation

From Euler's equation we know that, for a sound field propagating in a fluid, the particle acceleration, a, is given by the ratio of the pressure gradient to the fluid density ρ:

$$a = \frac{dv}{dt} = \frac{1}{\rho}\frac{dp}{dr} \tag{3.12}$$

The particle velocity can thus be obtained by integrating the particle acceleration as follows

$$v = \frac{1}{\rho}\int \frac{dp}{dr}\,dt \tag{3.13}$$

The pressure gradient is a continuous function which, for two closely spaced microphones, can be approximated using a finite difference method (Forssen & Crocker 1983, Rasmussen 1985):

$$\frac{dp}{dr} = \frac{p_b - p_a}{\Delta r} \qquad (3.14)$$

where p_b and p_a are the pressures measured at the two microphones separated by Δr (Figure 3.4). This gives an approximation for the pressure gradient at the centre of microphone pair; the pressure at this point is derived from the average pressure measured at the two microphones:

$$p = \frac{p_b + p_a}{2} \qquad (3.15)$$

Substituting Eqns. (3.13), (3.14) and (3.15) into Eqn. (3.5) we see that in practice intensity can be computed from:

$$I = \frac{p_a + p_b}{2\rho\Delta r} \overline{\int (p_b - p_a)\, dt} \qquad (3.16)$$

where the bar denotes time averaging.

There are inherent limitations in the measurement of intensity using two closely spaced microphones and the finite difference approximation for the derivation of the particle velocity (Watkinson 1984). The use of this technique in measuring sound intensity introduces a number of errors which limit the useful frequency range of the

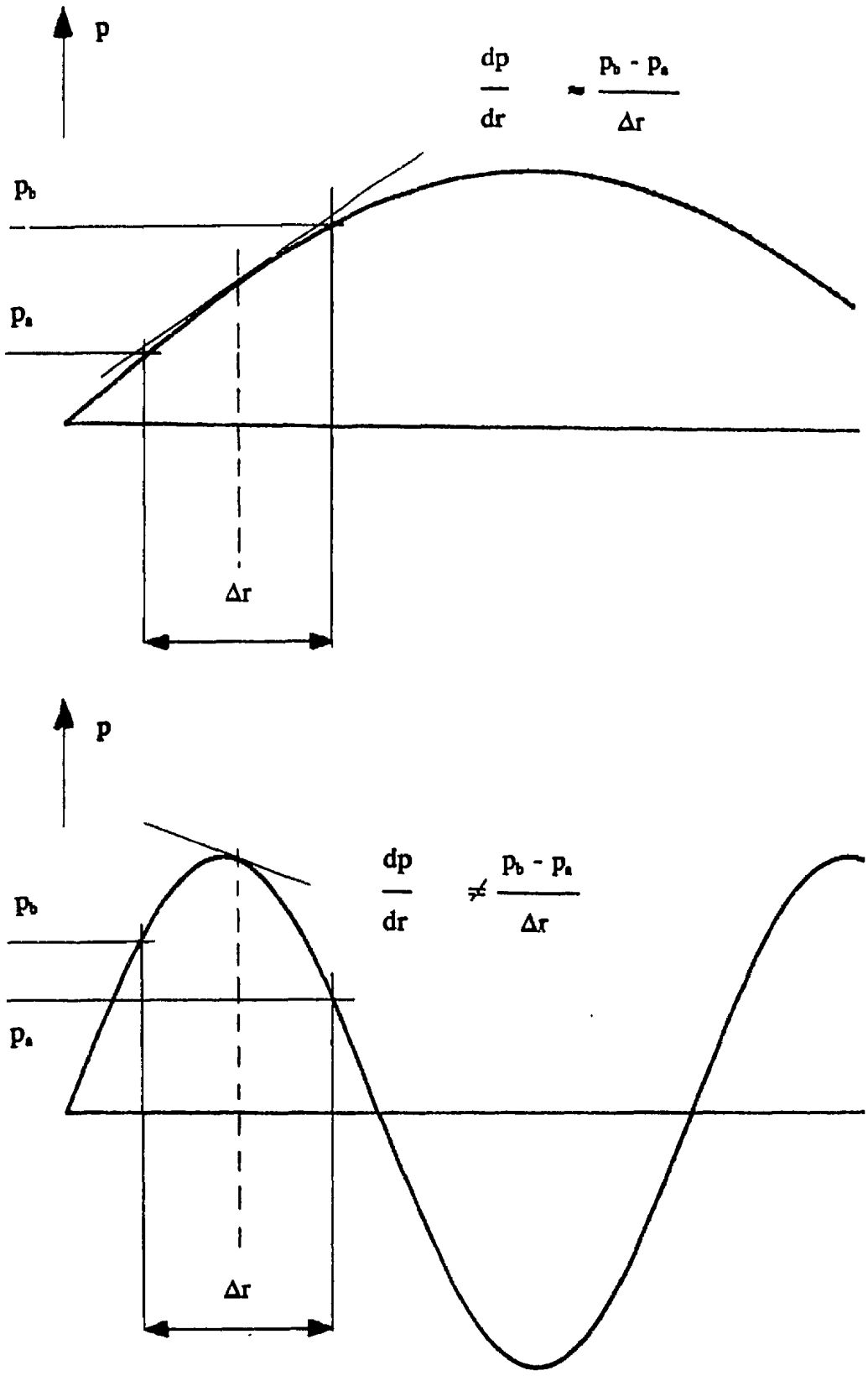

Figure 3.4 Finite Difference Approximation for pressure Gradient Measurement Using Two Transducers

system. These errors have been well studied (Thompson and Tree 1981, Gade 1985, Rasmussen 1984) and can be grouped into the following categories:

a) Finite difference approximation errors at high frequencies

b) Errors arising from phase mismatch when the phase difference between the two element positions is small

c) Random Errors

3.4.2 Finite Difference Approximation Errors

When the wavelength of the pressure variation is small compared to the effective microphone spacing, the finite difference approximation becomes inaccurate. This gives rise to an upper frequency limit to the accurate measurement of intensity. In order to measure intensity accurately the wavelength measured must be greater than six times the spacer distance. At 10 kHz, and using the value of 343 m/s for the speed of sound, the wavelength is 34.3 mm and we can see that we require a space 5.7 mm or smaller. Increasing the spacing reduces the upper frequency limit; reducing the spacing increases the upper frequency limit.

3.4.3 Phase Errors

The phase difference ϕ between the pressure measured at two points, p_a and p_b separated by a distance Δr can be calculated as

$$\phi = \frac{\Delta r \times 360^\circ}{\lambda} \qquad (3.17)$$

where λ is the wavelength. In order for the calculations in Eqn. (3.16) to be correct, the phase ϕ must be detected with a much smaller error, ϕ_{err}.

Rearranging Eqn. (3.8) in terms of c, and substituting into Eqn. (3.17) for the wavelength λ (=c/f), we get (Rasmussen, 1984):

$$\phi = \frac{\Delta r \,.\, f \,.\, \rho \,.\, I}{p^2_{rms}} \,.\, 360° \qquad (3.18)$$

Using $p_{rms} = 0.36$ pa,

$I = 10^{-4}$ W/m^2

$\Delta r = 12$ mm

$\rho = 1.21$ kg/m^3

$f = 1$ kHz

the phase calculated from Eqn. (3.18) is 4°. In order to measure the correct intensity, the phase mismatch between p_a and p_b must be of the order of 0.4°. If this phase mismatch is not achieved then the spacing Δr must be increased with reference to the finite difference approximation errors described in the previous section. Additionally, as the frequency of measurement gets lower, the microphone spacing Δr must be increased in order to maintain the same phase difference and hence minimise the phase errors.

From Eqn. (3.18), we can see that the phase difference between the signals is

dependent on the frequency being measured and on the spacing of the microphones, as well as on the ratio between the measured intensity levels and the measured pressure levels. In summary, phase errors can be reduced by correct choice of microphone spacings.

3.4.4 Random Errors

When measuring sound intensity the random errors in the measured values are a function of the BT-product, where B is the bandwidth of the filter and T is the averaging time, and also on the ratio of the sound intensity to sound pressure in the sound field. In a reactive field this ratio increases and so the BT-product must increase in order to maintain the same random error limits as in an active sound field (see Figure 3.5).

3.4.5 Directionality and Reactivity

A two microphone probe will measure the component of the intensity vector in the line of the two transducers. If the vector lies along the line of the probe, then the phase change can be calculated from the frequency and the probe spacing using Eqn. (3.17). When the intensity vector lies off the measurement axis, the phase change is reduced by a factor cos θ (Figure 3.6):

$$\phi = \frac{\cos\theta \times \Delta r \times 360^\circ}{\lambda} \qquad (3.19)$$

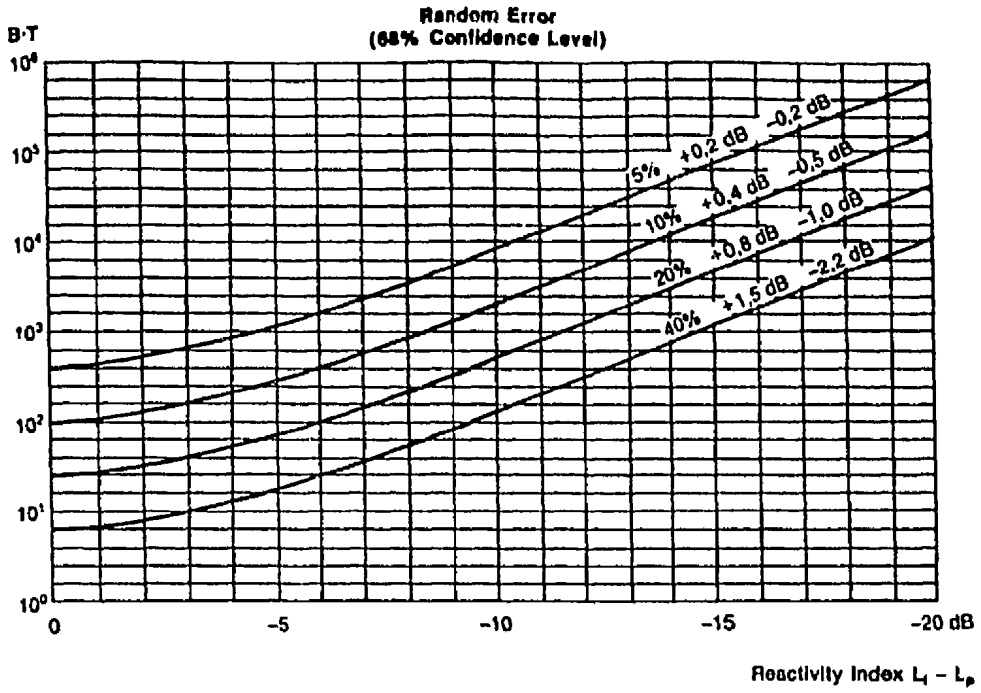

Figure 3.5 Random Errors as a Function of BT product (Bruel and Kjaer 1988)

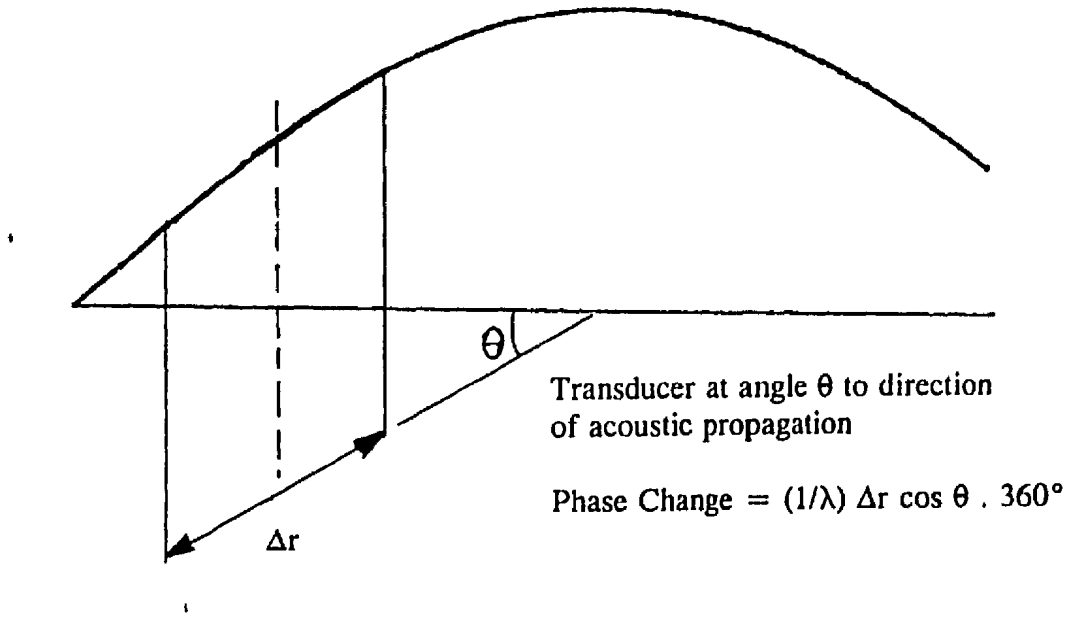

Figure 3.6 Effect of Directionality on Intensity Measurements

As the intensity vector approaches a 90° angle of incidence to the probe, the phase tends to zero and the intensity component will also tend to zero. The measurement will therefore be much more sensitive to phase errors, and the error in the measurement will be high.

Although the intensity component along a two microphone probe will vary with the angle of incidence, the pressure, being a scalar value, will remain constant. The actual phase change across the spacer can be related to the difference between the pressure and intensity levels. From Eqn. (3.18) we get:

$$\frac{I}{p^2_{rms}} = \frac{\phi}{\Delta r \,.\, 360° \,.\, f. \,\rho} \tag{3.20}$$

Multiplying by p^2_o/I_o [$= (\rho c).400/(\rho c)$] yields

$$\frac{I}{I_o} \,.\, \frac{p^2_o}{p^2_{rms}} \,.\, \frac{\rho.c}{400} = \frac{\phi \,.\, c}{\Delta r \,.\, 360° \,.\, f} \tag{3.21}$$

In terms of decibel levels, we can write this as

$$L_I - L_p + 10\ \mathrm{Log}_{10} \left[\frac{\rho.c}{400} \right] = 10\ \log_{10} \left[\frac{\phi \,.\, c}{\Delta r \,.\, 360° \,.f} \right] \tag{3.22}$$

where 10 $Log_{10}(\rho c/400)$ is a correction term arising from the choice of reference levels. The term L_I - L_p is called the reactivity index L_K. The relationship between L_K, Δr and f is shown by the nomogram in Figure 3.7.

In practical terms, measurement of the reactivity index L_K allows the phase change across the microphone pair to be calculated. This value can then be related to any system errors to determine the validity of a measured intensity level i.e., if the phase change across the probe is 1° at 1 kHz and the sensitivity of the system is only 0.5° then there will be a large error in the measured intensity level. Measurement system phase errors and measurement errors are discussed in Section 4.1.2.

3.5 PROBE CONFIGURATION FOR ACOUSTIC INTENSITY MEASUREMENTS

3.5.1 One-Dimensional Intensity Probe

An intensity probe for measurement using two pressure transducers has, as a first requirement, to be made up of two omnidirectional microphones. In order to measure intensity the two transducers (microphones) must be mounted with a fixed spacing. A number of different configurations are possible; the ideal configuration is to suspend the two microphones in space so that there are no reflection or interference effects from any supporting brackets. As this is not possible, the support brackets used must be designed to minimize any errors due to reflections. The microphones used in this research are

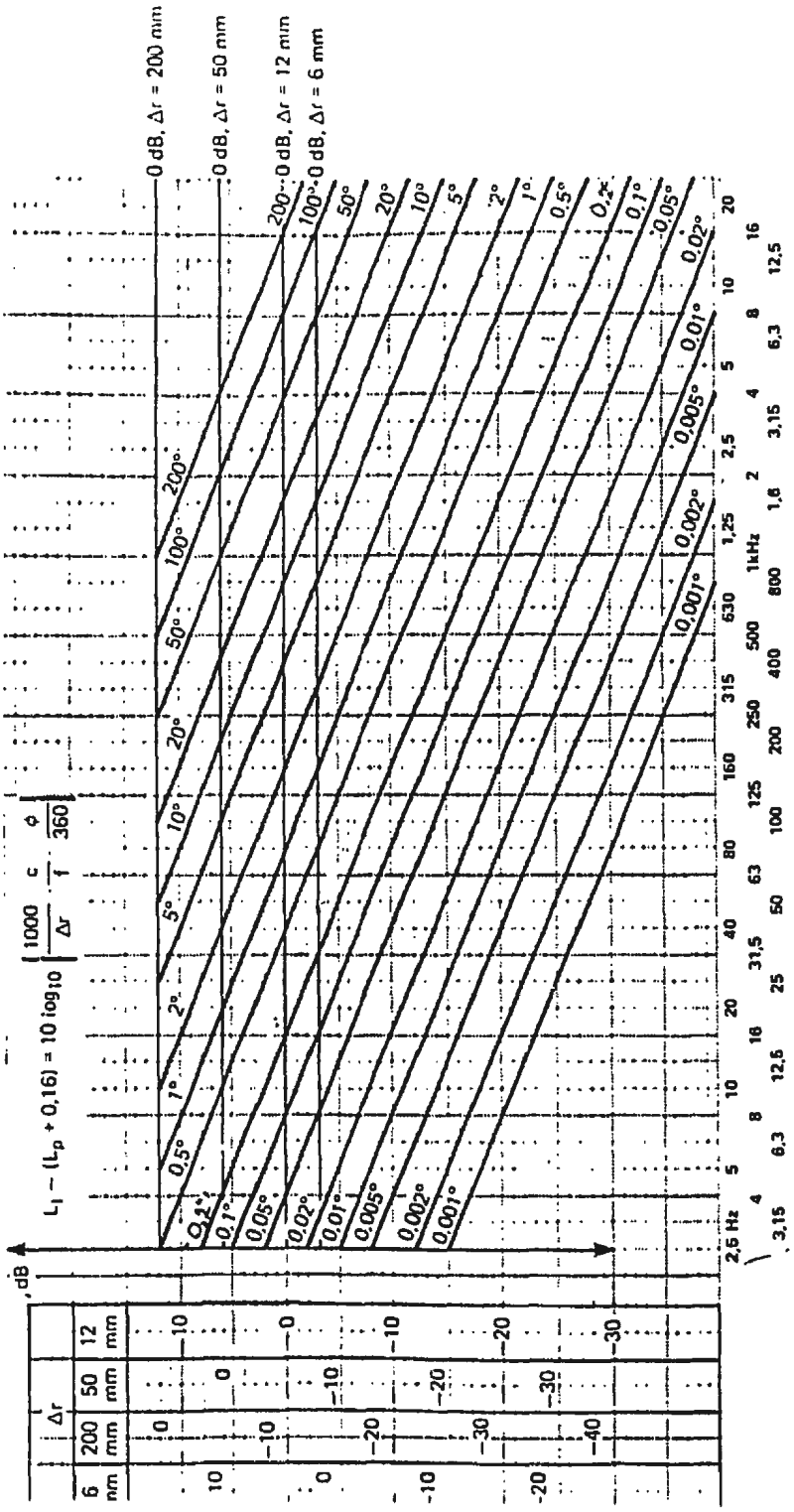

Figure 3.7 Relationship Between phase, Frequency and Reactivity Index for Different Microphone Configurations (Bruel and Kjaer 1988)

designed to be used with preamplifier units which are then used as part of the support frame. Two configurations are possible; face-to-face and side-by-side.

In the side-by-side configuration, the probes are supported and separated by a bracket mounted between the preamplifier bodies (Figure 3.8). For the face-to-face configuration a bracket and an angle piece are used to hold the microphones so that the diaphragms are facing each other (Figure 3.9). It can be seen from Figure 3.10 that while the nominal spacing for both configurations is 12 mm, the actual separation of the acoustical centres is frequency dependent and that above 1 kHz the face to face configuration gives a much smaller error.

3.5.2 Three-Dimensional Intensity Probe

Using the one-dimensional intensity probe described in Section 3.5.1 it is only possible to measure the component of the intensity vector along the line of the probe. In order to characterize the vector completely, the three orthogonal components must be measured. This is done by extending the face-to-face bracket to support three microphone pairs in a face-to-face configuration about a common acoustical centre as shown in Figure 3.11. This set up introduces two sources of error arising from the geometry of the probe and from phase errors.

Probe geometry effects are due to reflection and diffraction, and these

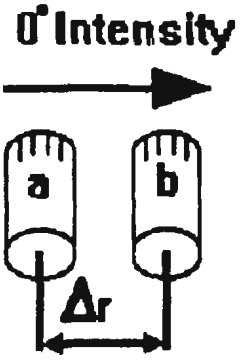

Figure 3.8 Side-by-Side Intensity Probe Configuration

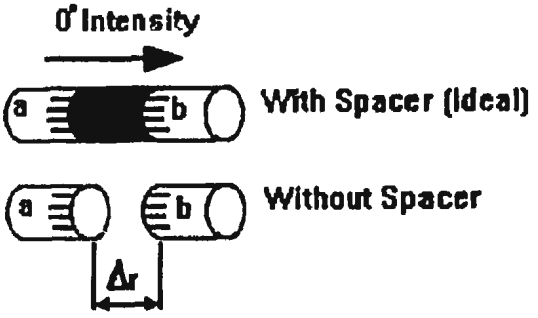

Figure 3.9 Face-to-Face Intensity Probe Configuration

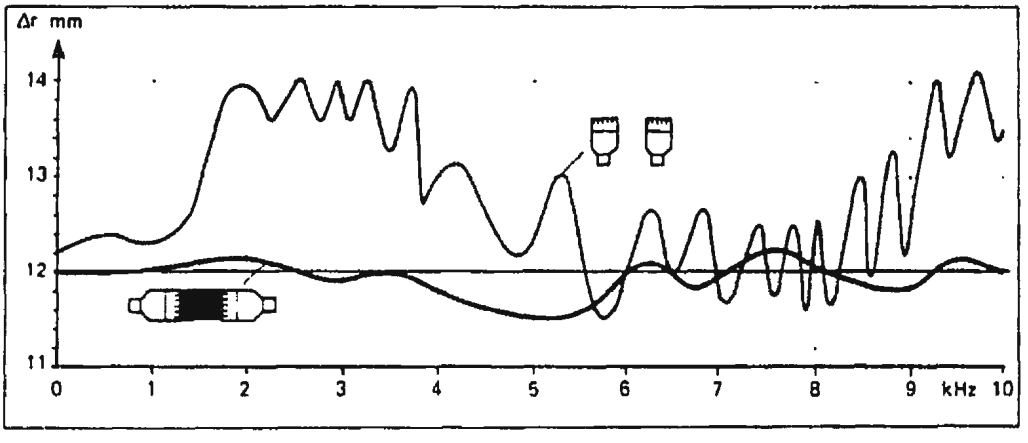

Figure 3.10 Nominal Spacing Variation as a Function of Frequency for Different Microphone Configurations (Bruel and Kjaer 3360 Manual)

Figure 3.11 Three-Dimensional Intensity Probe Configuration (Bruel and Kjaer 1988)

phenomena become more apparent at higher frequencies. By reducing the number of reflecting surfaces to a minimum, the effect of the probe geometry can be reduced.

If the intensity vector lies along or close to the direction of one of the probes, then the phase change across the microphones in the other two directions will be very small. This increases measurement errors arising from any phase errors in the system.

3.6 SURFACE INTENSITY

Acoustic measurements are usually associated with energy propagation in air or in fluid media, arising from the mechanical vibrations of some source. The simplest case is the spherical wave generated by a single point source. A non-point source can be approximated to a point source at a sufficiently large distance, but close to a structure the acoustic intensity will depend on the local vibration. Depending on the coupling between the structure and the surrounding medium, the structural vibrations can be estimated close to the surface using an acoustic probe. Alternatively, they can be measured directly through the measurement of the surface intensity vector using an accelerometer array on the structure.

When a structure vibrates there is an energy flow through it, the magnitude and direction of which can be characterized by the structure born wave intensity W. In order to measure the intensity flow in a plate, Pavic (1976) derived an expression for the

surface intensity of a two-dimensional wave and then showed how a finite difference approximation using eight accelerometers can be used experimentally. Noiseux (1970) proposed a simplified approach to measuring surface intensity in a plate. He assumed that the waves are locally one-dimensional in the far field.

For the special case of a one-dimensional sinusoidal wave travelling in a plate the time averaged structure born intensity $\bar{W}$ has been derived (Pavic, 1976) as

$$\bar{W} = \overline{\frac{B.2}{c_f^2} \frac{\partial \eta}{\partial t} \frac{\partial^3 \eta}{\partial x \partial t^2}} \qquad (3.23)$$

where c_f is the flexural phase velocity, η is the normal displacement at the point of interest and m is the mass per unit area. B is the flexural stiffness of the plate, given by

$$B = \frac{E\ h^3}{12\ (1-\mu^2)} \qquad (3.24)$$

where E is Young's modulus, h is the plate thickness, and μ is Poisson's ratio.

Two transducers placed symmetrically about the point of measurement and separated by a distance Δr (Figure 3.12) can be used to measure $\partial\eta/\partial t$ and $\partial^2\eta/\partial x \partial t$ using a finite difference approximation.

$$(\partial\eta/\partial t)\,\overline{\frac{\partial(\partial^2\eta/\partial t^2)}{\partial x}} = \frac{\overline{(\partial\eta/\partial t)_1+(\partial\eta/\partial t)_2}}{2}\,\frac{\overline{(\partial^2\eta/\partial t^2)_1-(\partial^2\eta/\partial t^2)_2}}{\Delta r} \qquad (3.25)$$

On expansion, Eqn. 3.25 can be reduced since the time averaged products $(\partial\eta/\partial t)_1$ $(\partial^2\eta/\partial t^2)_1$ and $(\partial\eta/\partial t)_2$ $(\partial^2\eta/\partial t^2)_2$ are zero, and additionally the time averaged products $(\partial\eta/\partial t)_1$ $(\partial^2\eta/\partial t^2)_2$ and $(\partial\eta/\partial t)_2$ $(\partial^2\eta/\partial t^2)_1$ are equal. Consequently:

$$(\partial\eta/\partial t)\,\overline{\frac{\partial(\partial^2\eta/\partial t^2)}{\partial x}} \approx \frac{\overline{(\partial^2\eta/\partial t^2)_1\ (\partial\eta/\partial t)_2}}{\Delta r} \qquad (3.26)$$

and substituting Eqn. 3.26 into Eqn. 3.23 we obtain

$$\bar{W} = \frac{\overline{B.2\quad (\partial^2\eta/\partial t^2)_1\ (\partial\eta/\partial t)_2}}{c_f^2\qquad \Delta r} \qquad (3.27)$$

Substituting $c_f = 2\pi f/k$ where k is the wavenumber and $k = (m/B)^{1/4}(2\pi f)^{1/2}$ we get

$$\bar{W} = \frac{\overline{(B.m)^{1/2}\qquad (\partial^2\eta/\partial t^2)_1\ (\partial\eta/\partial t)_2}}{\pi f\qquad\qquad \Delta r} \qquad (3.28)$$

The x and y components of the surface intensity can therefore be measured using a four accelerometer array with a pair of transducers along each of the x and y

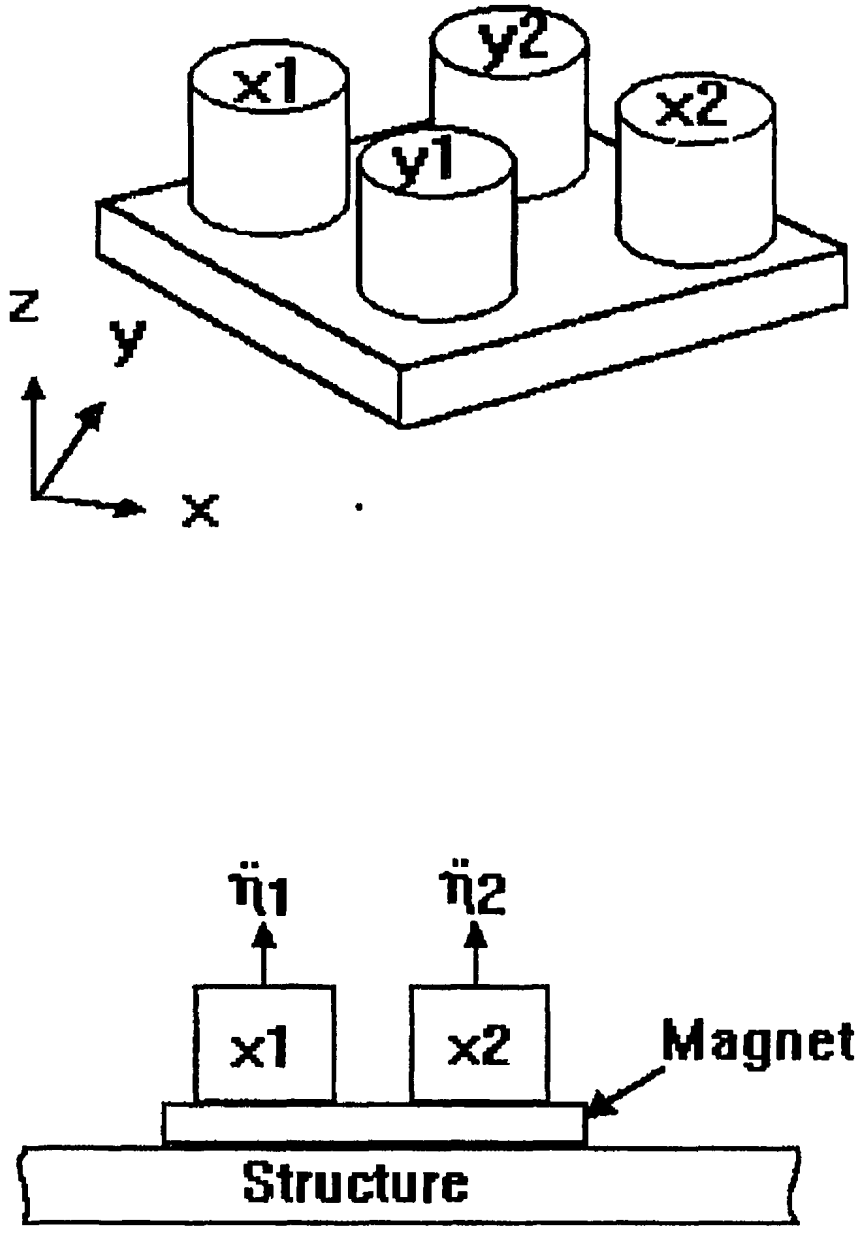

Figure 3.12 Measurement of Surface Intensity

axes. Material, frequency and boundary conditions all affect the accuracy of these measurements but Rasmussen (1986) states that 'practical measurements, however, indicate that it is reasonably accurate in many practical situations'.

3.7 INTENSITY MAPPING

The measurement of intensity in the very near field of a surface shows great promise as a new tool for investigating the reactive modal behaviour of surfaces (Rasmussen, 1988).

By measuring the near field acoustic intensity over a structure we can determine the direction and magnitude of acoustic energy flow from the surface. If the energy flow in one direction only is measured then the data can be presented in the form of contour plots by drawing lines connecting points of equal acoustic intensity. These contour plots can also be presented as three-dimensional surface plots, which are particularly revealing if the measured component is normal to the measurement surface.

If two components of the intensity vector are measured then the energy flow in the measurement plane can be represented vectorially. Measurement of all three components allow for the determination of energy flow towards sinks and radiating from sources, and this can be represented by either combined vector and contour plots, or vectorially through an interactive computer graphics display.

In order to determine error levels and data significance, two measurements are made. The first is the reactivity index (see Section 3.4.5) to determine the phase change across the microphone pair and hence the phase errors in the measurement. In a general sound field, there will be a spatial variation in the phase change and so the reactivity index should be measured at each scanning point, although a space averaged value is often sufficient (Bruel & Kjaer, 1986). The second measurement is the temporal variation in the intensity level to determine the stationarity of the energy flow in any one frequency band (Guigne et al, 1989).

3.7.1 Periodic Sound Fields

In many instances where the acoustic energy is to be measured, the source will be periodic in nature - for example, the sound field in the vicinity of an internal combustion engine will vary with the progression through the combustion cycle. By using sufficiently long averaging times, the overall sound field could be characterized over the surface of interest. However, if an energy source is to be tied to a particular event in the cycle then we must synchronize the intensity measurements with the source. By using this synchronization, the cycle can be divided into as many segments as required. In order to improve the statistical significance of any reading, each measurement is carried out by averaging data over the same window for a number of cycles. An intensity map can be generated for each segment of the cycle and the variation in the energy flow through the cycle is revealed by examining the changes in these maps through the cycle. Again, the sequence can be animated on a computer.

3.7.2 Stationarity Determination

For non-periodic sound fields we must determine whether the acoustic energy flow is constant over the period of the scanning. In general, it is found that only certain frequency bands contain stationary energy flow. The most sensitive and practical method for the evaluation of these frequency bands is deemed to be the statistical analysis of intensity versus time data collected over a time period (Guigne et al, 1990). In this technique, the microphone probe is held at one location over the surface of interest and the intensity spectrum measured and stored every second for 30 seconds, for example. The mean and standard deviation in the intensity level is then calculated for each frequency band and a standard deviation greater than one is used to indicate that the energy in that frequency band is fluctuating randomly and cannot be used to give a meaningful pattern.

3.8 SUMMARY

To summarize, the physics of acoustic measurements is detailed with particular reference to acoustic intensity. The relationship between acoustic intensity, particle velocity and pressure in a sound field is derived (Eqn. 3.4). From these relationships, different aspects of the energy flow in a sound field are analyzed and reactive and active intensity defined. A relationship between pressure and velocity using a finite difference approximation applied to Eulers equation (Eqns. 3.13 and 3.14) provides a practical method for measuring acoustic intensity. This method is developed along with an

analysis of error. Sources of error, methods of measuring error and ways of minimizing errors are all dealt with. Calibration and reference values are touched on briefly along with a description of decibel scales. Transducer types for measuring different components of an acoustic field are looked at with reference to the error measurements and other practical measurement aspects.

Because we are interested specifically in looking at the relationship between structural vibration and acoustic radiation, a direct method of measuring surface vibrations using accelerometers is described. Using a finite difference approximation an equation for surface intensity is derived, based on the relationship between two accelerometer measurements, which is analogous to that derived for acoustic intensity using microphones. This allows surface and acoustic intensity to be measured using the same measurement device.

The application of intensity measurements to modal behaviour is developed practically through the use of Intensity Mapping and a number of data presentation and measurement procedures are outlined. In order to minimize error measurements a number of steps must be followed which can be summarised as follows:

a) Determine the frequency range over the area to be investigated.

b) Measure the reactivity index over the area of interest.

c) The microphone size and spacing should then be optimised in order to minimise the finite difference approximation errors and the phase errors based on the frequency range of interest and the reactivity indices.

The temporal variation of the sound field should be analyzed and methods of dealing with periodic and non-periodic sound fields are looked at.

4.0 EXPERIMENTAL PROCEDURES

The investigations into the application of acoustic intensity mapping were carried out using a proprietary intensity analyzing system. Measurements were carried out in air to investigate the acoustic energy flow over the surface of a simple cantilever beam. The modal parameters of the beam were investigated separately. A notch was introduced into the beam using a band-saw and the acoustic energy flow was measured again. The two sets of acoustic measurements were then analyzed to identify the variations in the energy flow and relate them to the vibrational frequency and amplitude variation.

In order to investigate the extension of the technique into an underwater environment, an underwater intensity probe was calibrated and tested.

4.1 INTENSITY MAPPING

4.1.1 Acoustic Intensity Analyzer

The acoustic intensity measurements were made using the Brüel & Kjær (B & K) Sound Intensity Analyzing System Type 3360, shown in Figure 4.1. This uses a two microphone measurement system to measure acoustic intensity using Eqn. (3.16) in B & K Section 3.4.1. The B & K 3360 system consists of 42 digital filters having

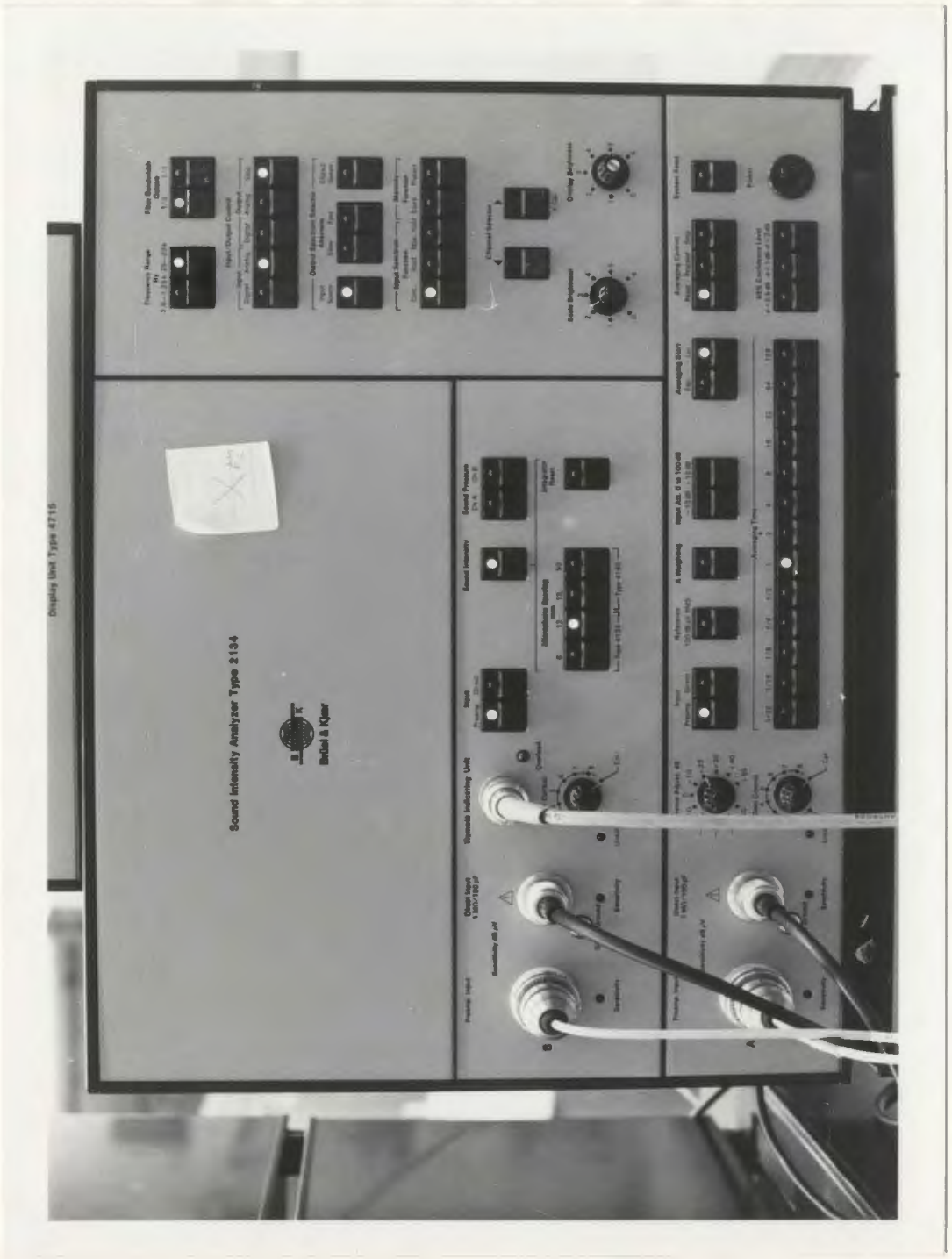

Figure 4.1 B & K Type 3360 Sound Intensity Analyzer

a bandwidth of one-third octave and centre frequencies from 1.6 to 20000 Hz. The input data is digitized and filtered, and then the manipulation to calculate intensity is performed. The output is a real time one-third octave intensity spectrum of the intensity vector component along the line of the probes. Because of digitizing constraints, the maximum upper frequency for intensity measurement is limited to 10 KHz. The actual frequency limits are set by the selection of measurement probe and spacing used for any particular measurement.

The centre frequencies for a true one-third octave spectrum are given by

$$f_{n+1} = f_n \cdot 2^{1/3} \qquad (4.1)$$

Since $2^{1/3} \approx 10^{1/10}$, the relationship

$$f_{n+1} = f_n \cdot 10^{1/10} \qquad (4.2)$$

is used for the centre frequencies of the 3360 Analyzer. In fact, the values used are the preferred centre frequencies calculated using Eqn. (4.2) (Kinsler et al. 1982). The centre frequencies calculated using Eqn. (4.2) as well as the actual centre frequencies obtained from Eqn 4.1 are given in Table 4.1 up to 4000 Hz, along with the bandwidth for each frequency slot.

TABLE 4.1 1/3 OCTAVE FILTER CENTRE FREQUENCIES

Exact Value $f_{n+1}=f_n \cdot 2^{1/3}$ (Hz)	1/3 Octave Approximation $f_{n+1}=f_n.10^{1/10}$ (Hz)	3360 Value (Hz)	Bandwidth (Hz)	Frequency Slot
1.55	1.59	1.60	0.4	2
1.95	1.99	2.00	0.5	3
2.46	2.51	2.50	0.6	4
3.10	3.16	3.15	0.7	5
3.91	3.98	4.00	1.0	6
4.92	5.01	5.00	1.2	7
6.20	6.31	6.30	1.4	8
7.81	7.94	8.00	1.8	9
9.84	10.00	10.00	2.3	10
12.40	12.59	12.50	2.9	11
15.63	15.85	16.00	3.7	12
19.69	19.95	20.00	4.6	13
24.80	25.12	25.00	5.8	14
31.25	31.62	31.50	7.2	15
39.37	39.81	40.00	9.2	16
49.61	50.11	50.00	11.5	17
62.50	63.10	63.00	14.5	18
78.75	79.43	80.00	18.4	19
99.21	100.00	100.00	23.1	20
125.00	125.89	125.00	28.9	21
157.49	158.49	160.00	37.1	22
198.52	199.53	200.00	46.3	23
250.00	251.19	250.00	57.9	24
314.98	316.23	315.00	72.9	25
396.85	398.11	400.00	92.6	26
500.00	501.19	500.00	115.8	27
629.96	630.96	630.00	145.9	28
793.70	794.33	800.00	185.3	29
1000.00	1000.00	1000.00	231.6	30
1259.92	1258.93	1250.00	289.5	31
1587.40	1584.89	1600.00	370.5	32
2000.00	1995.26	2000.00	463.1	33
2519.84	2511.89	2500.00	578.9	34
3174.80	3162.28	3150.00	729.4	35
4000.00	3981.07	4000.00	926.3	36

The bandwidth is given by $f_u - f_l$ where f_u is the upper frequency and f_l is the lower frequency of the filter. For a 1/3-octave filter, $f_u = 2^{1/3} f_l$ and the centre frequency $f_n = (f_u \cdot f_l)^{1/2}$. We can see then that the bandwidth is given by

$$\begin{aligned} w &= f_u - f_l \\ &= f_l (2^{1/3}-1) \end{aligned}$$

$$\begin{aligned} f_n &= (f_u \cdot f_l)^{1/2} \\ &= 2^{1/6} \cdot f_l \end{aligned}$$

$$\begin{aligned} w &= f_n (2^{1/3}-1)/ 2^{1/6} \\ &= f_n \times 0.232 \end{aligned} \qquad (4.3)$$

The filtering is carried out by three 2-pole filter units in series with coefficients that give a 6-pole Chebyshev filter of 1/3-octave bandwidth. Because the filters of the 3360 are digital, the filter coefficients can be changed to give different filter characteristics. A second set of filter coefficients are available to perform a 1/12-octave analysis. In order to give the same frequency range, the full 1/12-octave analysis is performed in four passes and the data is then interleaved. Because the 1/12-octave analysis is not done in real time, either the input signal must be stationary or exactly the same data must be recirculated four times (Randall, 1977).

For a 1/12-octave analysis, the bandwidth is again f_u-f_l where $f_u = 2^{1/12} \cdot f_l$. The centre frequency is given by $f_n = (f_u \cdot f_l)^{1/2}$ and the bandwidth is therefore given by 0.058 x f_n.

Two intensity probes are available, each consisting of a pair of calibrated and phase matched microphones. The Type 4181 set of two 1/2 inch microphones is provided with 12 and 50 mm spacers for a face-to-face probe configuration. Figure 4.2 shows the Type 4181 1/2" microphones with a 12 mm spacer. The centre of the spacer is 50 mm from the surface of the structure. The Type 4178 set has two 1/4 inch microphones and is provided with 12 and 6 mm spacers for a face-to-face configuration, and a 12 mm spacer for the side-by-side configuration. Figure 4.3 shows the 1/4" microphone pair in the face-to-face configuration as part of the three-dimensional intensity probe. The centre of the spacer is 25 mm from the surface of the structure.

4.1.2 Calibration Procedures

The intensity analyzer is calibrated for intensity measurement using a known sound source. This is provided by a B & K Type 3541 Sound Intensity Calibrator which provides a sound pressure level of 117.9 dB at 250 Hz. The pressure inputs of the two microphones are calibrated to these levels, and the sensitivity of the intensity level measured.

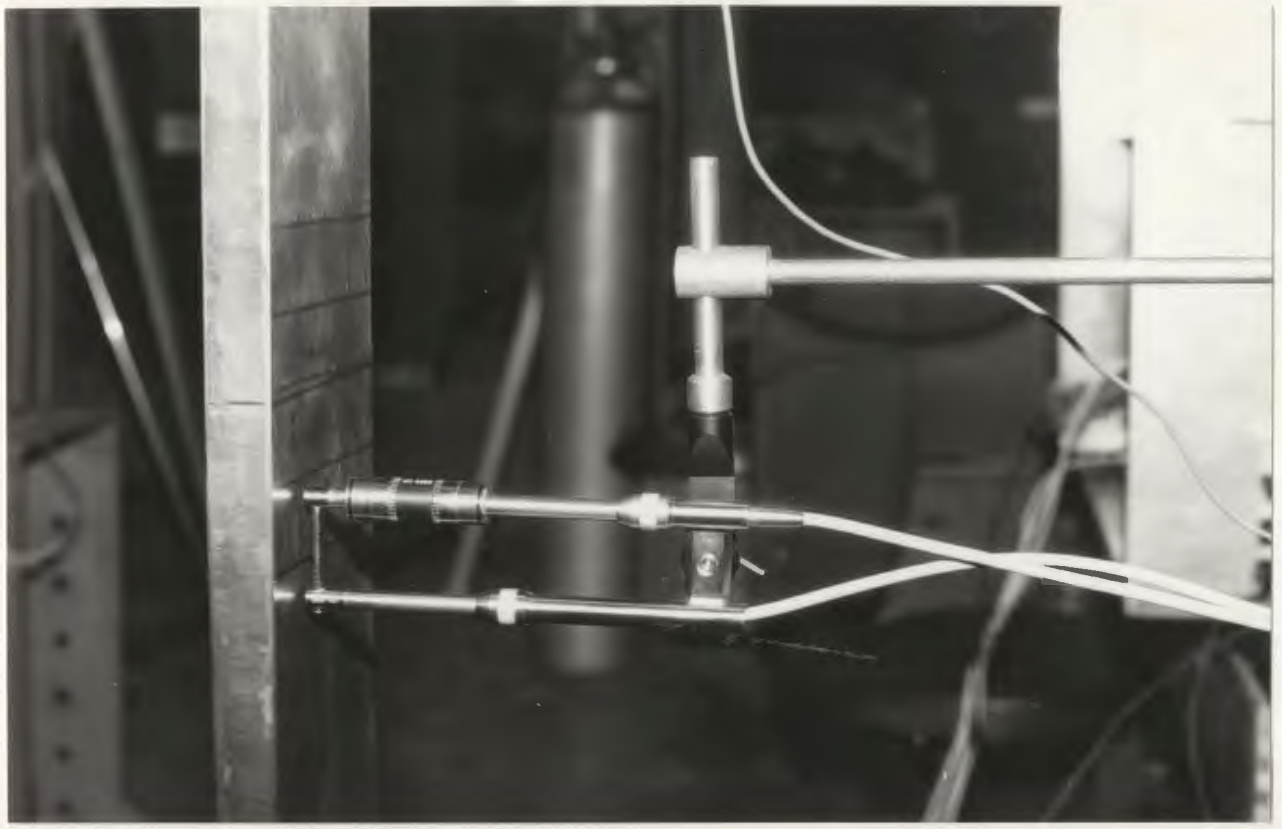

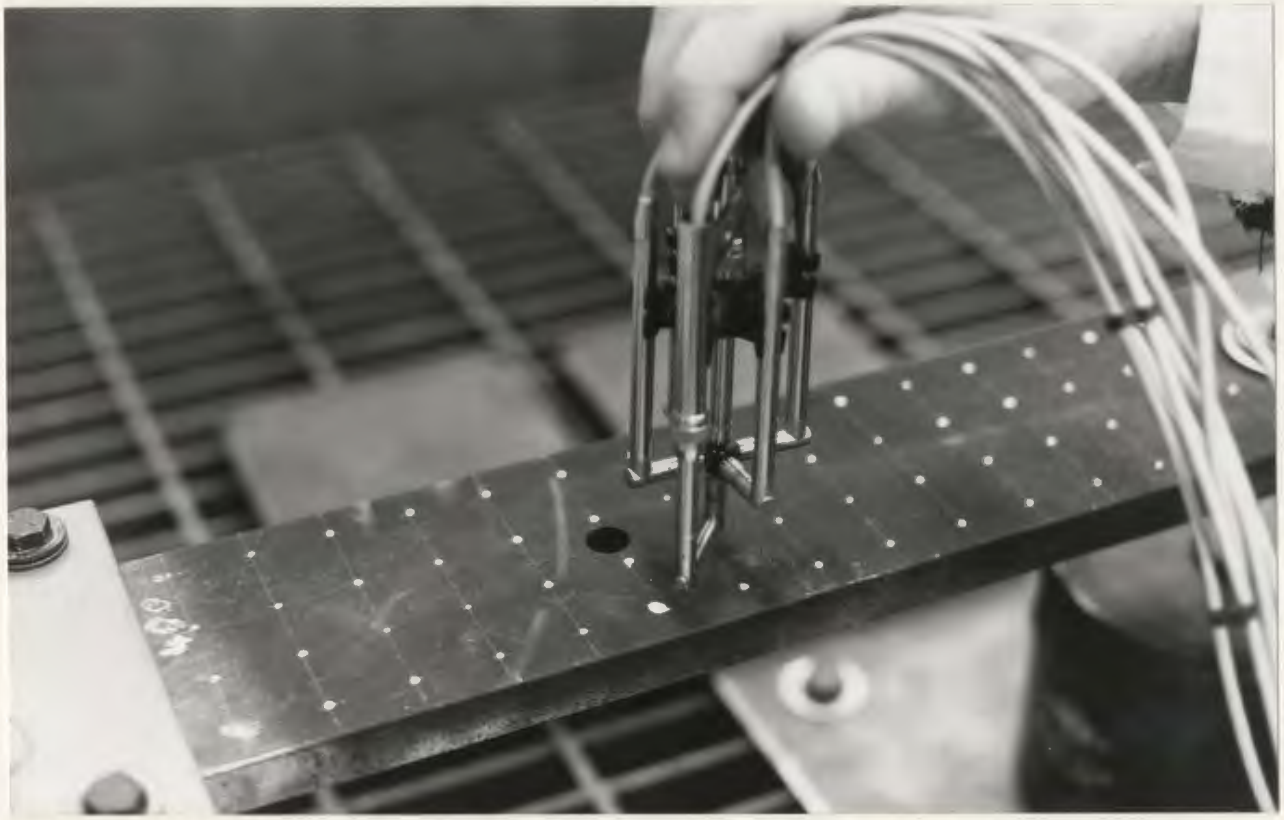

Figure 4.2 (Top) Type 4181 1/2" Microphones in Face-to-Face Configuration

Figure 4.3 (Bottom) Type 4178 1/4" Microphones in Face-to-Face Configuration

The residual intensity index L_{to} is a measure of the phase errors in the system and is important for determining the errors in subsequent intensity measurements (see Section 3.4.3). The residual intensity index of the measurement system using the 1/2 inch microphone pair can be determined as follows. The two microphones are placed into a chamber where they are subjected to a plane progressive wave with a pink noise spectrum and having 0° incidence on the probe. The actual intensity is zero, and any measured intensity, L_{IR}, is due to system error. The pressure levels are given by L_{PR} and the difference between these two levels is called the residual intensity index L_{KO} (= L_{IR} - L_{PR}). From Eqn. (3.22) we can see that the system error can be quantified as a phase error for each frequency.

$$\phi_{err} = 360° \cdot \Delta r \cdot f/c \cdot 10^{(L_{KO} + 0.16)/10} \qquad (4.4)$$

Three intensity analyzers were used during the experiments and the calibration, sensitivity levels and residual intensity in terms of phase error with respect to frequency are given in Appendix A. It can be seen that the measured phase errors are generally within the expected value of 0.3° except for unit two where they are higher than this value for both the 12 mm and 50 mm nominal spacings. These errors are discussed further in relation to the measured reactivity of the actual sound field where the difference can be related to an actual measurement error (Rasmussen, 1986).

4.1.3 Surface Intensity Array

The surface intensity in the vibrating plate is monitored by using a pair of accelerometers. In order to utilize the B & K 3360 analyzer, the following computation is required to convert the measured value into a surface intensity measurement. A finite difference approximation (Rasmussen, 1985) for the product $(\partial^2\eta/\partial t^2)_1(\partial\eta/\partial t)_2$ in Eqn. (3.28) can be derived as

$$\overline{(\partial^2\eta/\partial t^2)_1(\partial\eta/\partial t)_2} = \frac{\overline{(\partial^2\eta/\partial t^2)_1+(\partial^2\eta/\partial t^2)_2}}{2} \overline{\int (\partial^2\eta/\partial t^2)_1-(\partial^2\eta/\partial t^2)_2\, dt} \qquad (4.5)$$

and substituting Eqn. (4.5) into Eqn. (3.28) gives

$$\bar{W} = \frac{(B.m)^{1/2}}{2\pi f\Delta r} \overline{(\partial^2\eta/\partial t^2)_1+(\partial^2\eta/\partial t^2)_2 \int (\partial^2\eta/\partial t^2)_1-(\partial^2\eta/\partial t^2)_2\, dt} \qquad (4.6)$$

It can be seen from comparison between Eqns. 4.6 and 3.16 that if two accelerometer inputs are fed into the Type 3360 Analyzer, then the output can be converted to surface intensity using the following factor

$$\bar{W} = \frac{(B.m)^{1/2}}{\pi\,\Delta r_1\, f}\,\rho_o\,\Delta r\, I \qquad (4.7)$$

where ρ_o is the density of air, Δr is the nominal microphone spacing set on the unit, and

I is the intensity measured by the unit. Δr_1 is the accelerometer separation.

A surface intensity probe was fabricated from four B & K Type 4375 Accelerometers and four B & K Type 2635 Charge Amplifiers (Figure 4.4). The accelerometers used consist of three piezoelectric elements and three masses arranged in a triangular configuration around a triangular post and held in place by a high tensile clamping ring. This design gives a high sensitivity-to-mass ratio with a relatively high resonant frequency. The charge output per unit acceleration is given by calibration sheets for each unit. The measurement of acceleration levels using the Type 3360 analyzer required that the system be calibrated. This was done using a reference vibration source which provided a 10 m/s^2 acceleration at a frequency of 80 Hz. When representing acceleration levels on a decibel scale, the reference level used is 10^{-6} m/s^2 (ISO 1683).

4.1.4 Intensity Data Collection and Analysis

Data collection from the intensity analyzers was carried out using a Hewlett-Packard (HP) 310 microcomputer running HP BASIC, with a 40 MByte hard disc drive for data storage (Figure 4.5). Communication and data transfer from the B & K Type 3360 Intensity Analyzer was carried out over an IEEE-488 parallel interface. Data collection and manipulation was carried out using programmes written by the author which also incorporated into it data manipulation routines provided by Brüel & Kjær.

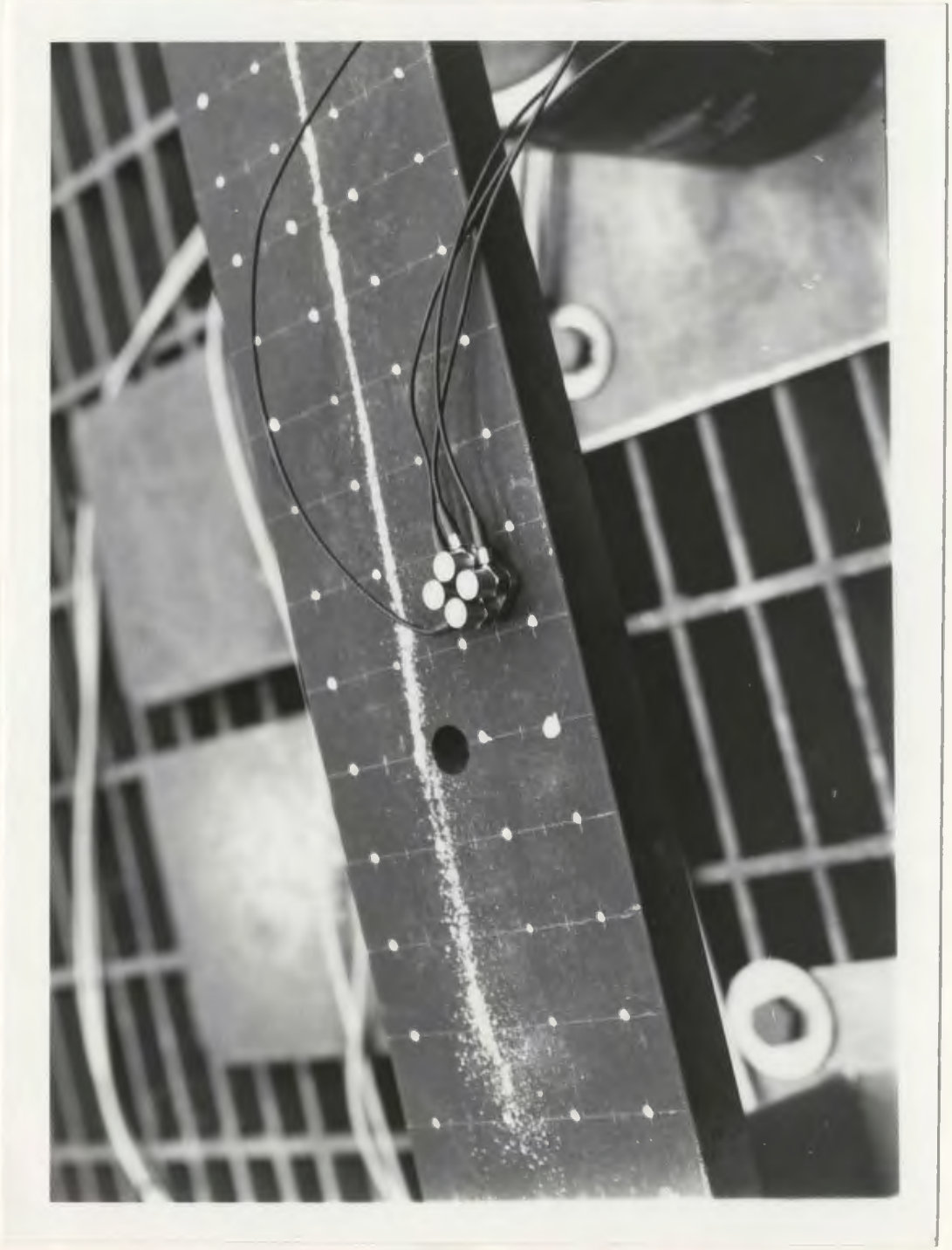

Figure 4.4 Surface Intensity Probe

Figure 4.5 HP310 Microcomputer Data Collection and Analysis System.

Before the Intensity mapping is carried out the acoustic field must be characterised. A collection grid is marked over the surface of the specimen or delineated in space using a light-weight grid fabricated from fine brass wire (Fig. 4.6).

In order to characterize the acoustic field the following readings must be made:

a) Intensity and pressure spectra at different points and at different frequency resolutions.

b) Reactivity index of the sound field.

c) Stationarity of the sound field.

The first measurements made are of the intensity and pressure spectra at different points over the surface. These are carried out using different microphone sizes and spacings in order to determine the frequency content of the acoustic field. Once the frequency range of interest is determined the appropriate microphone size and spacing can be selected. Spectra at different frequency resolutions are also made as these give an indication of the nodes and antinodes in the frequency spectrum. One-twelfth octave spectra give the highest resolution and by comparing one-twelfth and one third octave spectra it can be determined which bandwidth is necessary such that spectral nodes can be distinguished.

The determination of the Reactivity Index L_k of the sound field (Section 3.4.5) allows the phase change across the microphone pair to be determined as a function of

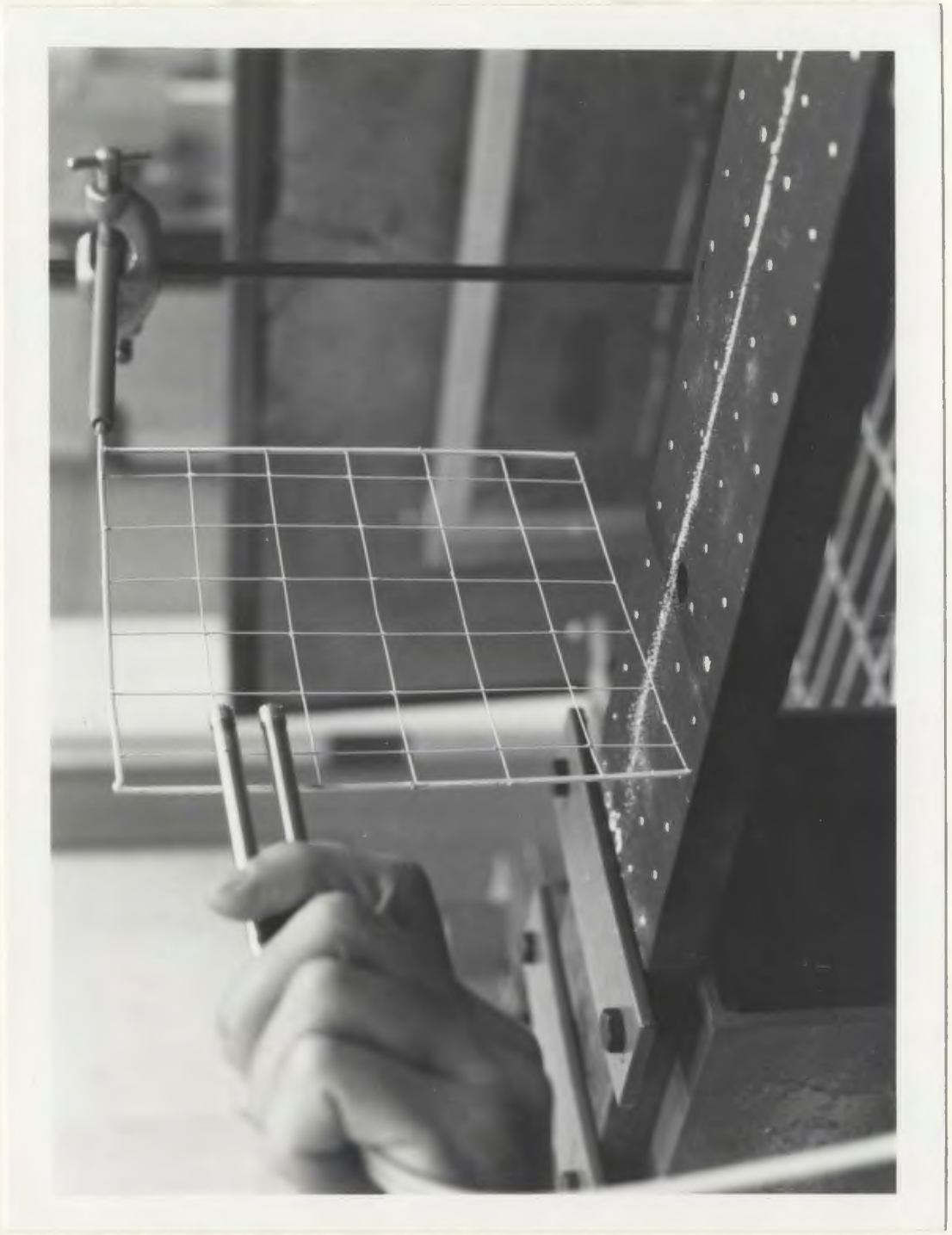

Figure 4.6 Intensity Mapping Measurements made in a Plane Normal to the Surface of the Specimer..

frequency and these can then be related back to the phase measurement errors of the system. The reactivity index was measured separately at all of the grid locations as well as being measured as a space averaged value by sweeping the probe over the area of the grid whilst taking a time average measurement. Two parameters are required to be measured; the pressure spectrum and the intensity spectrum. The reactivity index is then determined from these two spectra and the phase difference calculated for each frequency.

The stationarity of the acoustic field must be determined as discussed in Section 3.7.2. This is done by measuring the acoustic intensity spectrum at a single point over a period of time. A number of spectra are collected using a short averaging time and as short a delay as possible between measurements. The variation in the intensity level in a single frequency band is reduced to the mean and standard deviation of the intensity level (in dB). In this investigation, stationarity measurements were made at all of the grid locations used for the intensity mapping. This was carried out in order to determine whether a single stationarity reading was a sufficiently valid criterion for the selection of significant frequency bands.

In order to carry out the intensity mapping, the selected probe configuration is held at each grid point and the intensity spectrum measured and stored in the computer. Once the grid has been mapped, the data is stored and then manipulated to produce three-dimensional surface maps, contour maps, vector maps and combined vector-contour maps

to describe the flow of acoustic energy. Figure 4.7 shows the results of an intensity mapping made using a single (unidirectional) probe to measure the normal intensity component over a plate. A contour plot is illustrated. Appendix B gives details on the presentation and information contained in the contour and vector plots.

The flow diagram in Figure 4.8 shows the different steps of data collection and the analysis made on each set of data.

For measurement of two or more components of the sound field it is possible to multiplex each measurement probe into a single Intensity Analyzer. The computer uses a digital signal to control the switches in the multiplexer unit. Each microphone pair is connected in turn to the intensity analyzer where the spectrum is recorded and then transferred as a digital signal back to the computer.

However, a more accurate measure of the instantaneous intensity vector is achieved through the use of a dedicated analyzer on each channel as shown in Figure 4.9. This innovative technique was developed during this research programme. The computer initiates each intensity analyzer to carry out spectrum measurements over the same averaging period and same attenuation level. The measurements are then triggered simultaneously and once the selected averaging time has elapsed, each analyzer will freeze the spectrum data which can then be transferred sequentially to the computer.

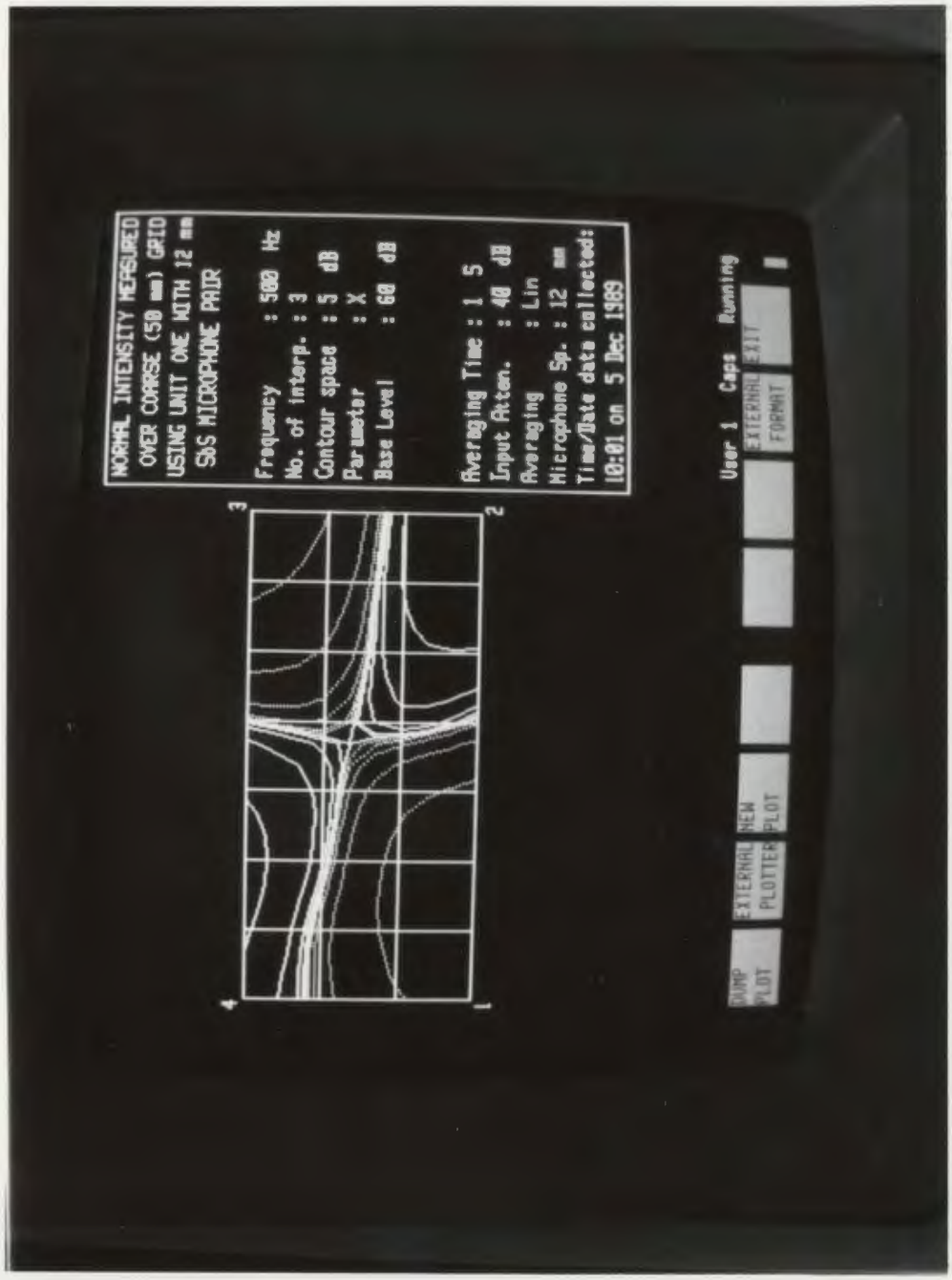

Figure 4.7 Intensity Mapping System Displaying Measurements of Intensity normal to the surface of the Specimen.

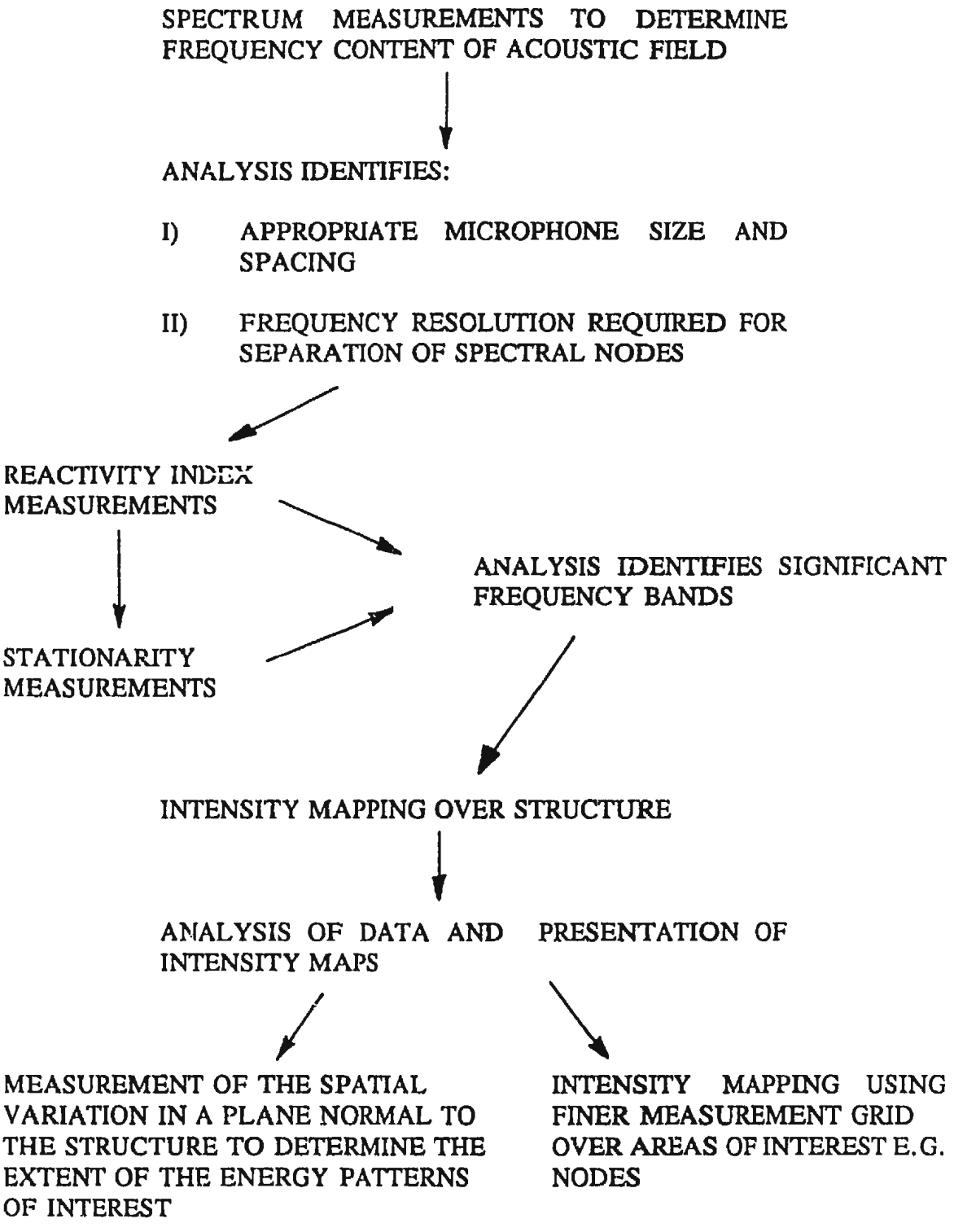

Figure 4.8 Flow Diagram of Data Collection and Analysis

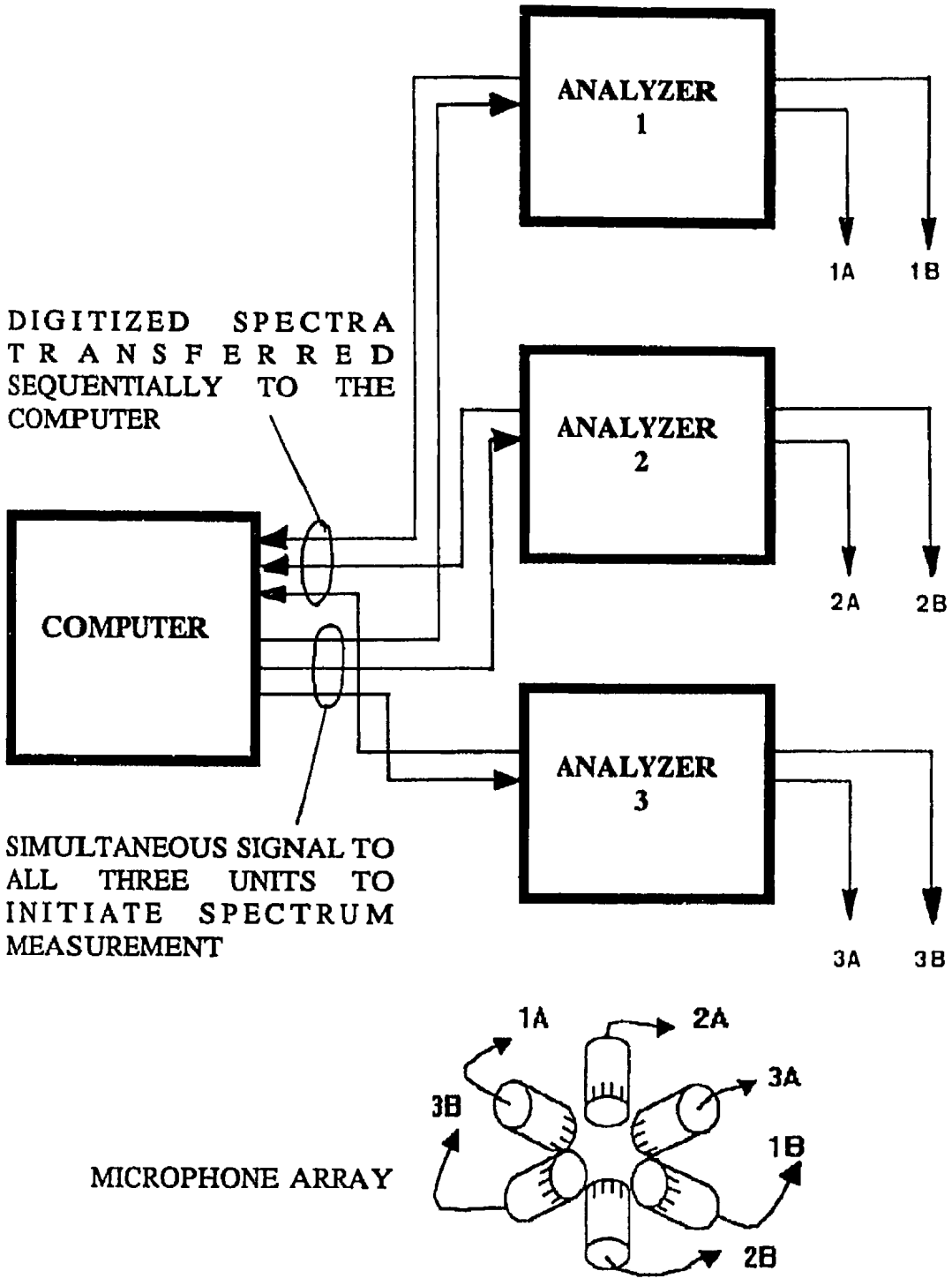

Figure 4.9 Simultaneous Measurement of probe Signals for Measurement of two or more Components of a Sound Field

4.2 UNDERWATER INTENSITY PROBE

In order to evaluate acoustic intensity scanning in an underwater environment, an underwater intensity probe was required to be calibrated and tested.

4.2.1 Phase Matching of Hydrophones

As described in Section 3.4.3, the accurate measurement of intensity is dependant on the phase errors in the measurement system. In order to minimise these, the transducers used in the intensity probe must be matched as closely in phase as possible. Because the phase errors in the transducer cannot be adjusted, pairs of transducers must be tested in order to select those with the lowest phase errors.

Six hydrophones were tested for phase matching, and three pairs were selected from the results following the method described here.

The unit designed for the phase matching of the hydrophones consists of a brass pressure unit divided into two chambers. These are separated by a diaphragm which is connected to an electromagnetic shaker unit contained in the upper chamber. The lower chamber is filled with water and the two hydrophones to be matched are introduced into it. The upper chamber is then pressurised to 10 atmospheres and the diaphragm vibrated using a noise source. The response of the two hydrophones is measured using a Bruel & Kjaer 2032 Dual Channel Signal Analyzer.

Figure 4.10 shows the equipment set-up. The resultant sound field is completely reactive, and so the sound intensity is zero in all directions. The phase difference between the two hydrophone positions will be zero and any residual intensity measured is therefore due to the phase mismatch between the hydrophones. This phase difference is calculated by downloading the spectral measurements to a Hewlett Packard computer, which also controls all of the measurements. The output is a plot of phase difference as a function of frequency.

4.2.2 Directionality Calibration of an Underwater Intensity Probe

The hydrophone pairs were checked to see how closely they conformed to the ideal cosine bell directionality pattern. This was done at the Marine Institute acoustic tank in St. John's. A fixed location source was used and the hydrophone intensity array suspended in the tank from a turntable. The acoustic intensity was measured at one degree intervals throughout a complete revolution and the directionality displayed on a stereogram (See Figure 4.11). Figure 4.12 shows the directionality of the intensity displayed using a linear, rather than Decibel scale, and shows for comparison the ideal cosine-directionality curve.

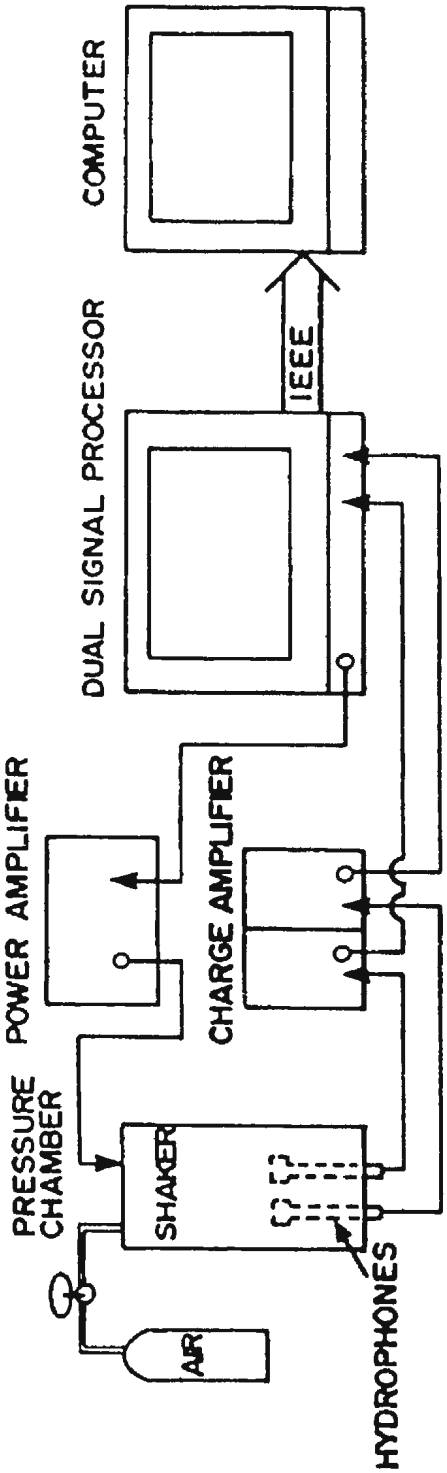

Figure 4.10 Equipment Set-up for Hydrophone Phase Matching

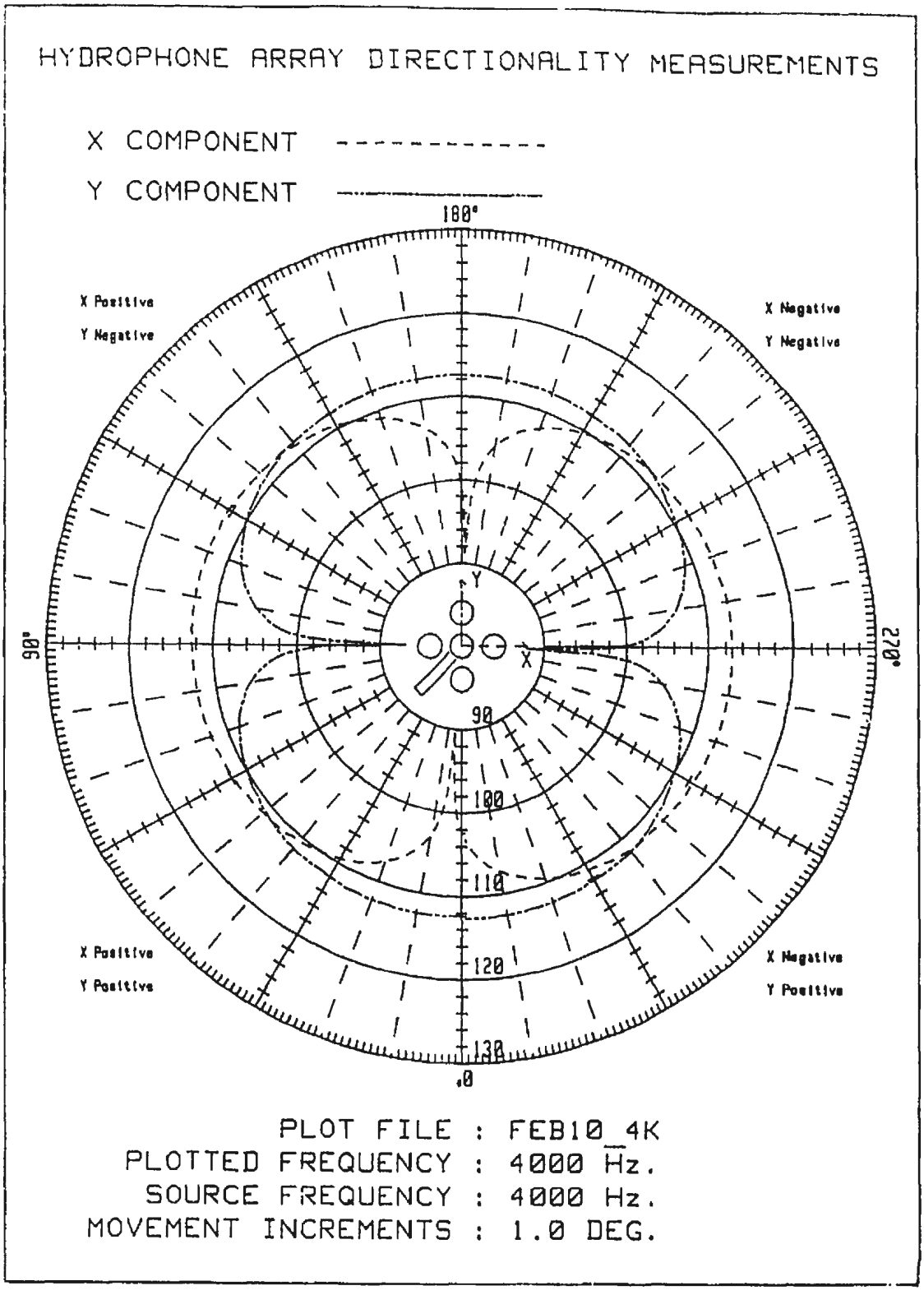

Figure 4.11 Hydrophone Directionality at 4 kHz (dB Scale)

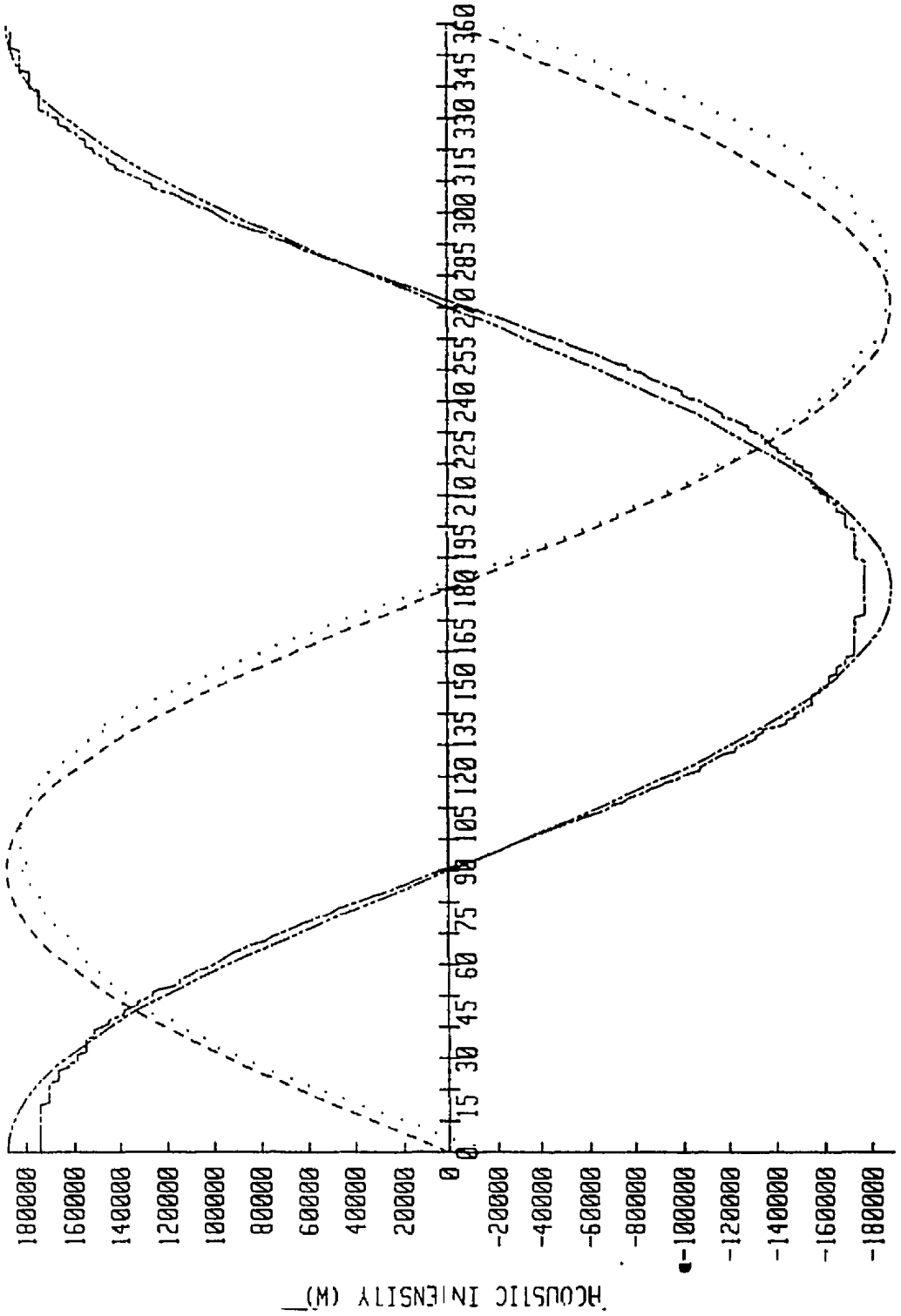

Figure 4.12 Hydrophone Directionality at 4 kHz (Linear Scale), also showing Ideal Cosine Directionality Curve

4.3 BEAM SPECIMENS AND VIBRATION SOURCE

Two different beams are used in the experimentation. Beam type I was fabricated from 6 mm thick by 75 mm wide steel strip stock and had a length of 600 mm. A hole was drilled on the centre-line, 35 mm in from one end, to provide an attachment for the excitation source (Figure 4.13). A grid for the data collection was marked onto the specimen with its origin 7.5 mm in from the edge of the plate and 10 mm from the clamp. The grid cell used had a width of 20 mm and a length of 50 mm (Figure 4.13).

Beam type II was cut from 19 mm thick steel plate stock to a width of 100 mm and a length of 600 mm. Two holes with diameters 28 mm were machined on the centre-line with centres 38 from the end (Figure 4.14). Two beams of identical dimensions and cut from the same stock were used during the measurements. The data collection grid was marked onto the specimen with its origin 12.5 mm in from the edge of the plate and 10 mm from the clamp. The grid cell had a width of 25 mm and a length of 50 mm (Figure 4.14).

The beams were clamped at one end on a short pedestal attached to a steel frame table. A small electromagnetic shaker, also attached to the table, was used to excite the beam a distance of 435 mm from the clamp (Figure 4.15).

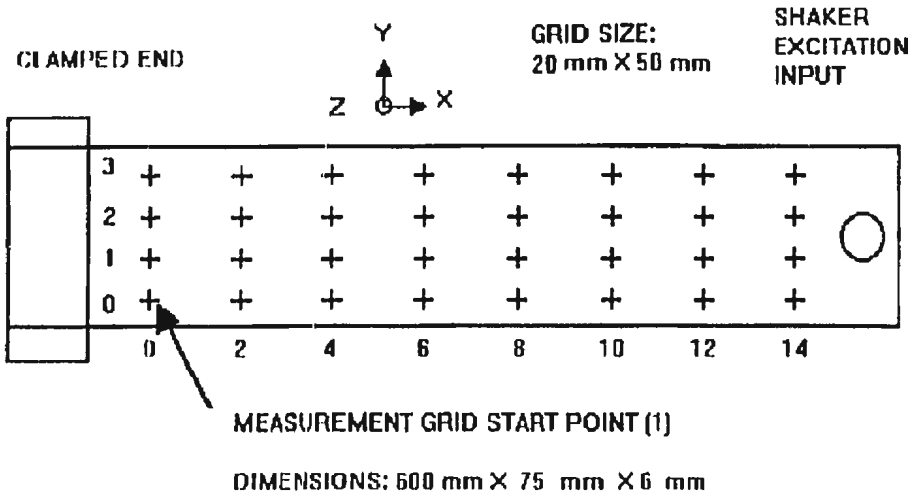

Figure 4.13 Dimensions of Beam I

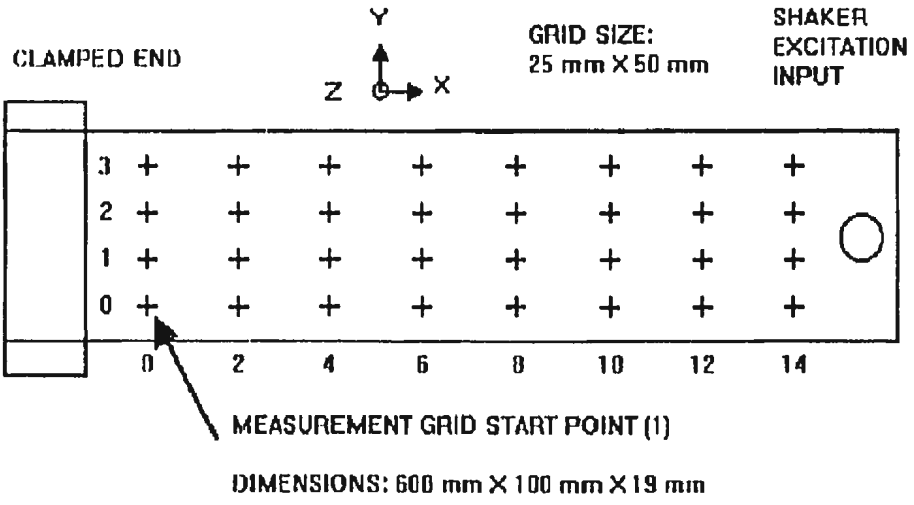

Figure 4.14 Dimensions of Beam II

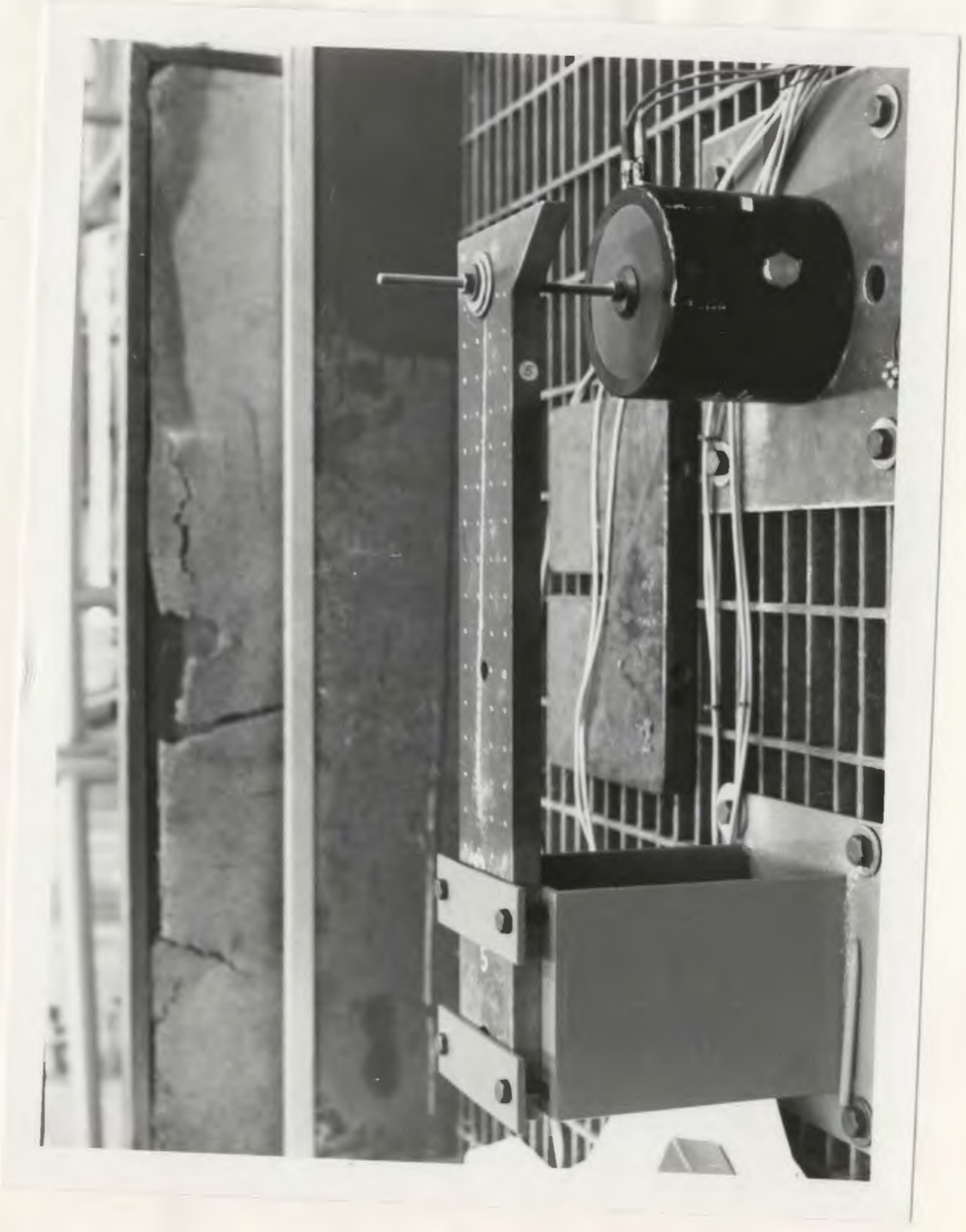

Figure 4.15 Cantilever Beam Set-up for Forced Vibration

The electromagnetic shaker is a B & K Type 4809 driven by a B & K Type 2706 Power Amplifier. Two different function generators are used to provide the excitation signal. A Wavetek Model 132 VCG/Noise Generator is used to provide a white noise excitation of variable bandwidth. An HP 3314 Digital Function Generator is used to provide single frequency excitation.

4.4 THEORETICAL AND EXPERIMENTAL VIBRATION ANALYSES

In order to provide a reference for the Acoustic Intensity Measurements, a number of 'classical' vibration analyses are carried out.

The simplest of these is the theoretical equation for the natural frequencies of a beam, given in Table 5.1.

A finite element analysis is also carried out using the computer programme SAP86 with plate elements to allow for the identification of the torsional as well as bending modes.

The simplest experimental technique used to identify mode shapes is the use of fine sand on the surface of the specimen. The frequency of excitation is then manually swept and when the beam is excited at one of its modal frequencies the sand particles migrate to the nodes and antinodes, revealing the modal shapes explicitly as in Figure

4.16.

A more detailed experimental analysis was carried out by mounting a force transducer between the shaker and the beam and measuring the cross-spectrum between the force transducer and an accelerometer placed at different grid locations over the beam. The spectral measurements were carried out using a Bruel and Kjaer Dual Channel Frequency Analyzer controlled from an HP310 computer running a state-of-the-art modal analysis software package.

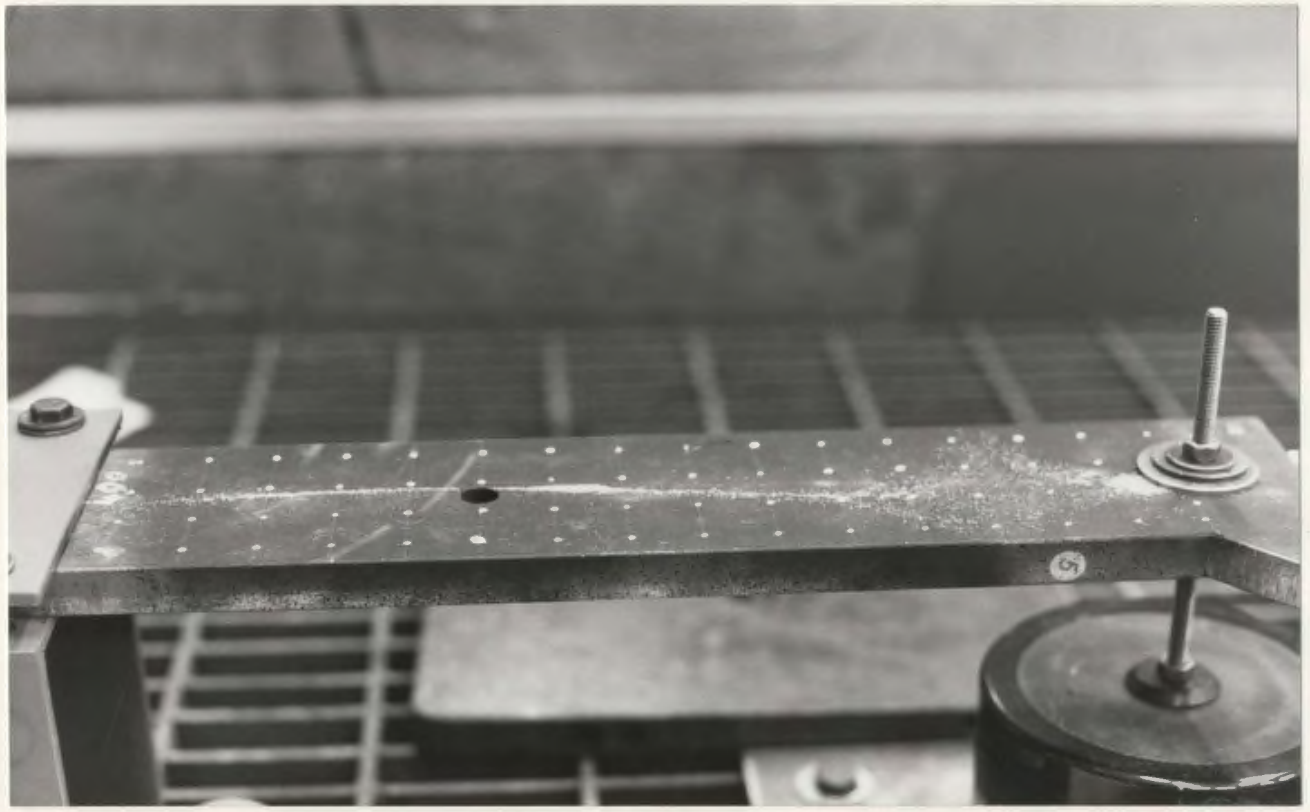

Figure 4.16 Modal Shape Revealed using Sand Patterns.

5.0 RESULTS

5.1 THEORETICAL FREQUENCY ANALYSIS

5.1.1 Beam Theory

Using the equation for the natural frequencies of vibration of a beam and the dimensions of the two plates given in Figures 4.13 and 4.14, the natural bending frequencies of the beams were calculated and are given in Table 5.1.

5.1.2 Finite Element Analysis

The two beam structures investigated were analyzed using the finite element analysis package SAP86. A grid of 20 by 3 plate elements was used to model the beam; this allowed the torsional modes to be identified in addition to the bending modes. The natural frequencies identified along with the mode type (torsional or bending) are shown in Tables 5.2 and 5.3 for Beam types I and II, respectively. Figure 5.1 shows the first two bending modes for Beam I and Figure 5.2 shows the first torsional mode for Beam I. Similar mode shapes were also obtained for Beam II.

The frequencies obtained from beam theory show slightly higher values than the results obtained from the finite element analysis package. This results from the discrete nature of the analysis, the element sizes selected and the inherent nature of finite element results which always tend to give larger values than the actual ones.

Table 5.1 **NATURAL BENDING FREQUENCIES OF BEAMS**

Material Parameters:

$E = 207 \times 10^9$ Pa

$\flat = 7.7 \times 10^3$ Kg.m^{-3}

$\rho = \flat\ w\ h$ where $\flat$ is the mass density of the beam

w is the width of the beam

h is the thickness of the beam

Structural Dimensions:

Beam I	Beam II
l = 0.435 m	l = 0.435 m
w = 0.075 m	w = 0.100 m
h = 0.006 m	h = 0.0190 m

$$\omega_n = (\beta_n l)^2 \left[\frac{E I}{\rho l^4} \right]^{1/2}$$

	Beam I		Beam II	
$\beta_n l$	ω_n (rad/S)	f_n (Hz)	ω_n (rad/S)	f_n (Hz)
3.52	167.1	26.6	529.0	84.2
22.0	1044.1	166.2	3306.3	526.2
61.7	2928.2	466.0	9272.8	1475.8

Table 5.2 **BEAM I NATURAL FREQUENCIES DETERMINED USING SAP86**

Mode Number	Frequency (Hz)	Mode Type
1	27.5	Bending
2	171.4	Bending
3	283.0	Torsional
4	479.6	Bending
5	864.2	Torsional
6	940.2	Bending
7	1489.0	Torsional
8	1555.0	Bending

Table 5.3 **BEAM II NATURAL FREQUENCIES DETERMINED USING SAP86**

Mode Number	Frequency (Hz)	Mode Type
1	83.8	Bending
2	522.2	Bending
3	663.9	Torsional
4	1460.0	Bending
5	2048.0	Torsional
6	2861.0	Bending

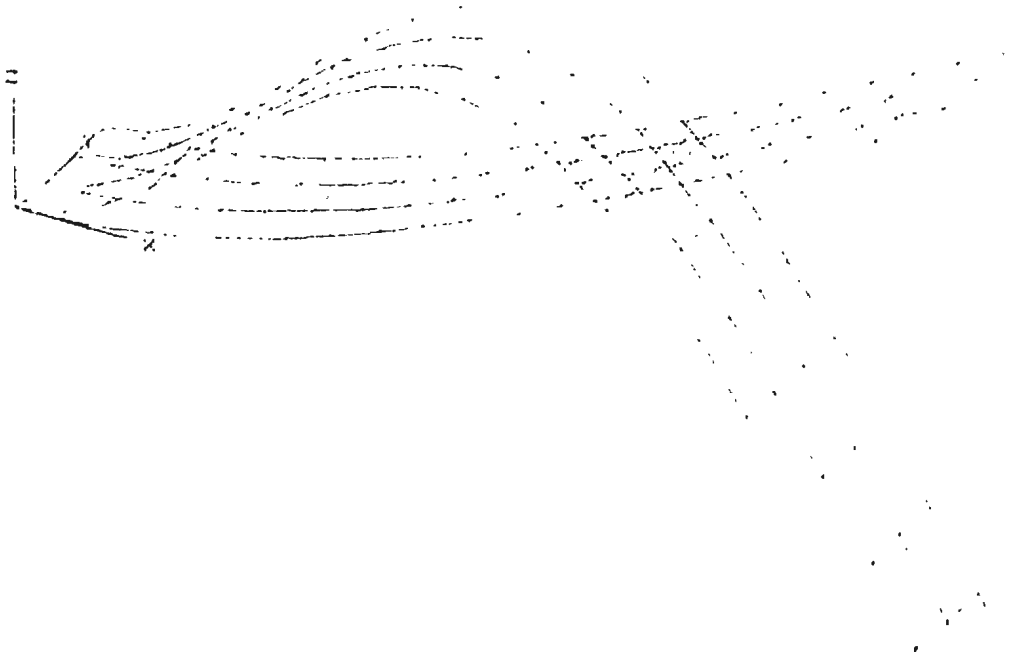

Figure 5.1 Finite Element Analysis First Two Bending Modes for Beam I.

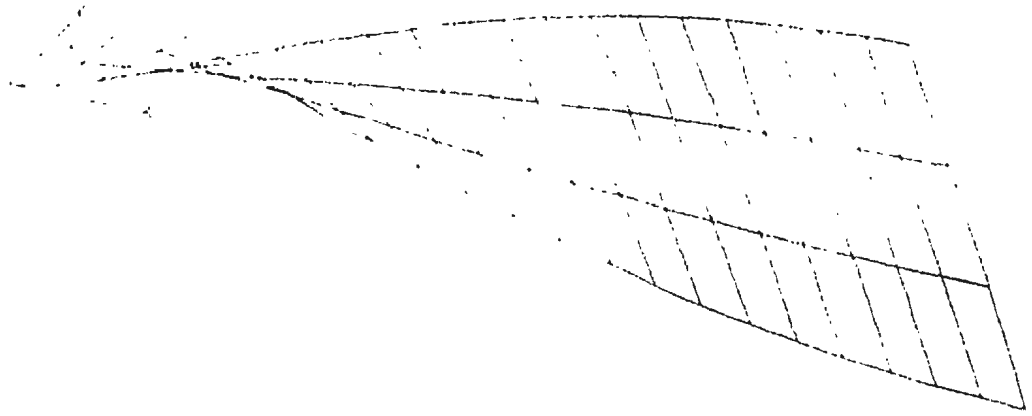

Figure 5.2 Finite Element Analysis First Torsional Mode for Beam I.

Also it is noted from Tables 5.2 and 5.3 that the ratio of the natural frequencies of the two beams is close to the ratio of the thicknesses of the beams; this is to be expected from beam theory.

An important thing to note is that the natural frequencies are closely spaced. The frequency separation of the 5th and 6th modes and also of the 7th and 8th modes are less than the bandwidth of the 1/3-octave filters at these frequencies (see Table 4.1). This immediately suggests that there may be difficulties in identifying the mode related patterns for higher frequencies from 1/3-octave acoustic spectrum.

5.2 MODAL TESTING USING AN FFT ANALYZER

Beam II was analyzed using a modal analysis software package produced by Bruel & Kjaer to perform detailed vibrational analysis using the B & K 2032 Dual Channel Frequency Analyzer controlled from an HP310 computer.

A force transducer was mounted between the shaker and the beam end, and an accelerometer placed at different grid points over the surface of the beam. At each grid location the cross spectrum between the accelerometer and the force transducer was measured. The modal frequencies were identified from the cross spectrum and the mode shapes were determined. The modal frequencies and associated mode shapes are listed in Table 5.4. Comparing these values with those given in Table 5.3 it is

Table 5.4 BEAM II NATURAL FREQUENCIES MEASURED EXPERIMENTALLY USING A MODAL ANALYSIS PACKAGE

Mode Number	Frequency (Hz)	Bending Type
1	28.6	Not Determined
2	379.5	Bending
3	504.6	Torsional
4	1023.4	Bending
5	1461.0	Torsional

Table 5.5 NATURAL FREQUENCIES MEASURED EXPERIMENTALLY

BEAM I

Mode Number	Frequency (Hz)	Bending Type
1	30	Bending
2	150	Bending
3	310	Torsional
4	395	Bending
5	600	Torsional

BEAM II

Mode Number	Frequency (Hz)	Bending Type
1	30	Not Determined
2	385	Bending
3	500	Torsional
4	1020	Bending
5	1460	Torsional

observed that the frequencies of the finite element analysis and the B & K experimental analysis package differ considerably. More will be said on these differences later in Section 5.3. The identified second, third, fourth and fifth mode shapes are displayed in Figures 5.3 (a) and (b). The first mode shape was not identified by this procedure; instead a spurious first frequency was identified, probably due to the combined motion of the clamping support and the plate.

5.3 EXPERIMENTAL MODE SHAPE DETERMINATION

The mode shapes were determined experimentally using the technique described in Section 4.4. The modal frequencies were found by adjusting the excitation frequency manually until a distinct pattern emerged in the sand. The modal frequencies are listed in Table 5.5. The patterns obtained for Beam I are shown in Figure 5.4 (a) as a bending mode and Figure 5.4 (b) as the first torsional mode.

Comparing Tables 5.2, 5.3 and 5,5, it is observed that the analytical frequencies are much higher than those obtained from the experimental analysis, indicating that the support conditions were not rigid as assumed in the theoretical analysis but rather flexible. This assumption is strengthened by the fact that in Table 5.5, the first identified modal frequency is almost the same for both of the beams indicating the combined modal frequency of the support and the beam. Consequently no proper comparisons could be made between the theoretical and experimental results. Hence no other theoretical

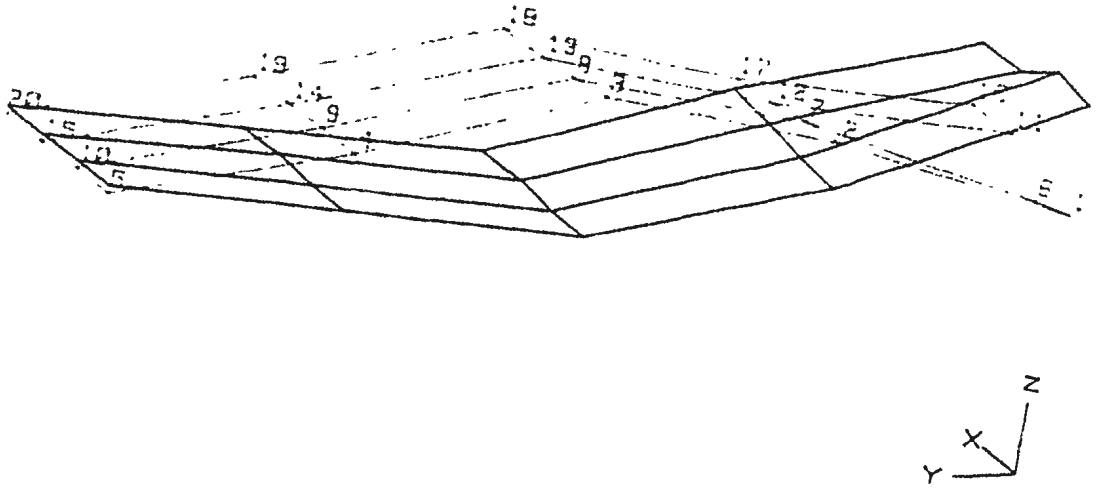

(a) Second Bending Mode

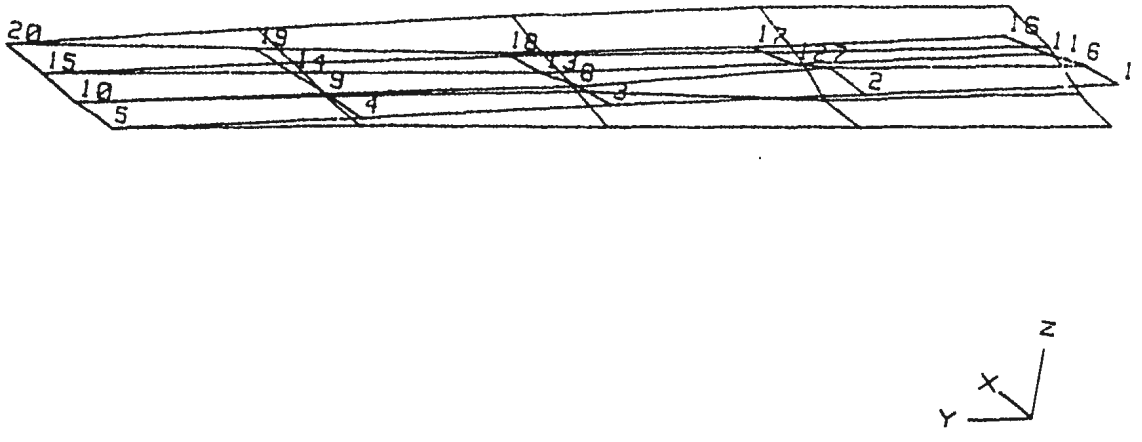

(b) First Torsional Mode

Figure 5.3 Experimental Analysis for Beam I

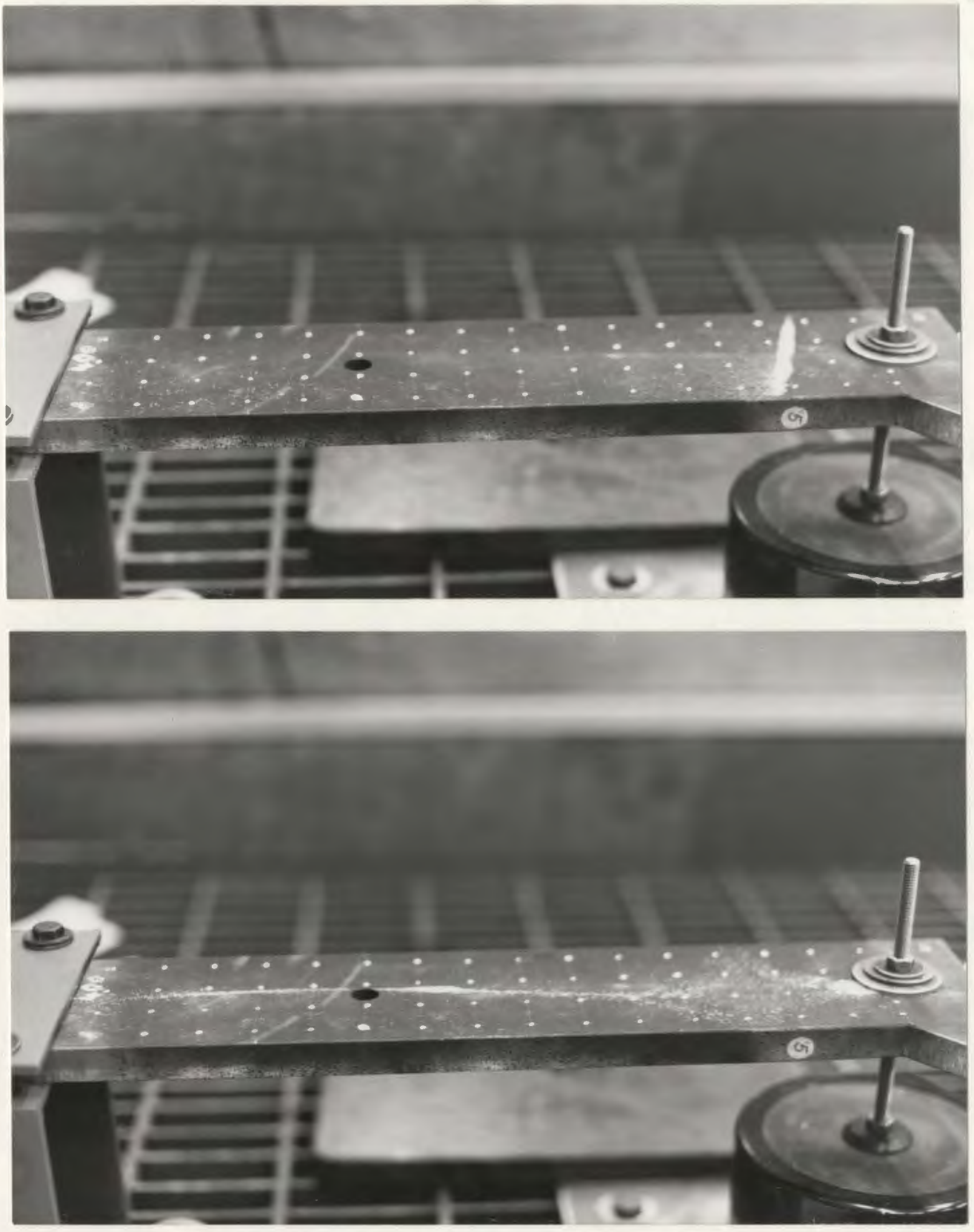

Figure 5.4 Mode shapes revealed by sand patterns.

analysis would be compared with that of the experimental. Hereafter the interpretations of the modal behaviour from the acoustical field measurements will be made only from the experimental results.

5.4 ACOUSTIC MEASUREMENTS FOR BEAM I

5.4.1 Stationarity Measurements

Stationarity measurements were made at each grid location using two 1/4" microphones in the side-by-side configuration to measure the component of the intensity vector normal to the surface of the plate. The beam was excited using 1 kHz bandwidth random noise. The data from each grid location (identified using the notation given in Figure 4.13) were analyzed to give the standard deviation (in decibels) of the measured intensity levels and these data are given in Table 5.6. It is observed that a maximum standard deviation of 4.40 dB was obtained at point (6,3) at a frequency of 500 Hz where a large acoustic intensity was observed from experimental measurements. Excepting this point, the standard deviation at most of the other points were low and this was deemed to be acceptable.

5.4.2 Reactivity Measurements

Reactivity measurements were made at a number of grid locations using two 1/4" microphones in the side-by-side configuration to measure the component of the intensity vector normal to the surface of the plate (L_I) and the corresponding pressure

Table 5.6 STATIONARITY RESULTS FOR BEAM I USING 1/4" MICROPHONE PAIR

Freq. (Hz)	Standard Deviation (dB) at different grid locations 0,0	2,0	4,0	6,0	8,0	10,0	12,0	14,0
100	a	a	a	ab	ab	b	ab	ab
125	b	b	b	b	3.02	1.62	ab	b
160	2.93	1.71	b	1.65	3.31	1.75	1.34	2.93
200	ab	2.49	1.60	1.01	0.95	1.28	0.84	ab
250	b	1.19	ab	1.74	b	1.10	0.78	b
315	ab	1.37	1.69	1.74	1.70	a	2.25	ab
400	0.93	1.07	1.92	1.37	0.97	2.60	0.96	0.93
500	b	ab	0.72	0.76	2.59	2.48	b	b
630	b	b	b	2.15	1.15	0.98	0.99	b
800	0.51	0.62	0.60	1.32	b	0.99	0.65	0.51
1000	0.76	0.58	ab	b	0.69	0.50	1.20	0.76
1250	0.33	0.97	0.52	0.36	b	0.35	0.24	0.33
1600	0.81	0.64	a	ab	0.83	0.31	0.22	0.81
2000	0.78	0.44	0.53	0.94	1.11	0.58	0 20	0.78

Freq. (Hz)	Standard Deviation (dB) at different grid locations 0,1	2,1	4,1	6,1	8,1	10,1	12,1	14,1
100	ab	ab	ab	b	b	ab	ab	b
125	b	5.23	3.19	1.68	1.29	2.10	1.00	b
160	2.93	1.22	1.74	1.84	1.19	1.29	1.42	b
200	ab	4.63	1.34	1.45	1.05	1.08	1.35	2.14
250	b	2.42	3.45	2.70	b	1.05	0.94	1.71
315	ab	1.19	1.30	1.69	3.55	1.22	3.61	2.33
400	0.93	1.21	1.06	1.12	1.05	1.76	b	2.16
500	b	ab	1.05	0.81	1.47	1.13	b	b
630	b	b	0.78	1.39	0.78	0.83	2.47	1.58
800	0.51	0.50	0.81	0.89	b	0.64	0.81	b
1000	0.76	0.29	0.71	1.39	0.47	0.70	1.59	0.49
1250	0.33	a	0.45	0.89	1.60	0.41	0.84	0.22
1600	0.81	0.36	a	1.76	0.58	0.18	0.14	0.39
2000	0.78	0.46	0.81	0.46	0.59	0.53	0.54	0.39

a = one or more values below 40 dB.
b = direction of acoustic energy changes during measurement.

Table 5.6 continued **STATIONARITY RESULTS FOR BEAM I USING 1/4" MICROPHONE PAIR**

Freq. (Hz)	0,2	2,2	4,2	6,2	8,2	10,2	12,2	14,2
	Standard Deviation (dB) at different grid locations							
100	a	a	ab	1.87	3.38	b	b	b
125	1.07	b	b	1.60	1.35	1.27	1.14	ab
160	1.43	3.42	b	1.45	1.21	1.20	1.98	2.20
200	2.05	ab	ab	b	b	ab	1.58	0.85
250	2.35	b	ab	b	ab	1.60	0.88	0.97
315	1.68	ab	2.01	1.16	1.81	b	0.98	1.02
400	1.36	2.21	3.42	b	0.63	2.67	ab	b
500	2.08	1.13	1.17	b	1.42	1.57	b	3.46
630	0.50	0.58	1.20	0.76	0.96	1.42	0.80	1.01
800	0.74	0.47	3.43	0.70	b	0.58	0.73	1.92
1000	1.38	0.67	0.77	2.14	0.56	0.87	0.71	0.57
1250	0.40	ab	1.71	1.12	0.93	1.23	b	0.43
1600	0.29	0.48	a	1.10	a	0.61	0.44	0.36
2000	0.60	0.81	1.29	0.86	0.91	0.79	0.34	0.47
Freq. (Hz)	0,3	2,3	4,3	6,3	8,3	10,3	12,3	14,3
	Standard Deviation (dB) at different grid locations							
100	a	ab	ab	4.02	b	ab	b	b
125	1.02	ab	1.17	1.36	0.91	1.40	1.79	ab
160	0.91	3.25	1.15	1.12	1.16	1.38	2.49	b
200	3.30	ab	b	ab	ab	a	1.62	2.41
250	2.81	b	ab	b	ab	1.52	0.85	b
315	2.53	4.65	1.58	1.88	1.70	ab	1.80	2.78
400	1.34	b	b	2.08	1.47	a	ab	2.21
500	1.40	1.10	0.69	4.40	1.78	1.72	b	3.93
630	1.19	0.70	1.21	1.06	1.11	1.41	0.81	1.14
800	a	0.65	1.61	0.76	b	0.63	0.60	0.84
1000	1.20	1.08	3.08	1.09	0.36	0.79	1.57	b
1250	0.27	a	0.72	1.22	1.06	1.65	ab	b
1600	0.36	1.07	0.66	0.88	1.28	0.57	0.57	b
2000	0.60	0.97	a	0.62	a	a	0.86	b

a = one or more values below 40 dB.
b = direction of acoustic energy changes during measurement.

(L_p). The beam was excited using 1 kHz bandwidth random noise. The reactivity of the sound field (L_K) was determined and the phase change across the microphone spacers was calculated from this (Table 5.7). It is observed that the phase differences were quite high at the clamp locations and at the excitation points, near the ends of the plates. At 315 Hz, measurements at positions (x,1) and (x,2) are close to the node. There is therefore little energy flow in the z-direction and the phase is small. For the remaining frequencies between 160 Hz and 2000 Hz, the phase differences were considered acceptable when compared with the system phase errors. It should be noted that phase change data gives a measure of the reactivity only in the direction of the probe axis.

In addition to the single point reactivity measurements, the swept reactivity was measured. This was done by using a sufficiently long averaging time and sweeping the probe across the surface of the specimen during the data acquisition. Two passes were made, one each for intensity and pressure, and the phase change across the microphone spacer was calculated from the reactivity index (Table 5.8).

5.4.3 Spectrum Measurements

Spectrum measurements were made at location 4,1 (see Figure 4.13). The beam was excited using 1 kHz bandwidth random noise and the pressure and intensity were measured using two 1/4" microphones in the side-by-side configuration with a spacing of 12 mm. An attenuation of 40 dB was set on the analyzer, and 4 second linear averaging was used. Four spectra were collected. In all of the figures showing

Table 5.7 SINGLE POINT REACTIVITY (L_q) MEASUREMENTS (PHASE DIFFERENCE ONLY) USING 1/4" MICROPHONE PAIR ON BEAM I

Freq	Phase Difference (Deg.) at each Grid Location							
(Hz)	0,0	2,0	4,0	6,0	8,0	10,0	12,0	14,0
100	3.22	0.77	17.27	1.50	3.00	3.22	2.08	4.05
125	2.60	0.18	10.33	0.73	0.48	0.04	0.24	5.06
160	3.48	2.96	9.36	1.66	2.10	1.00	3.10	5.64
200	0.05	0.50	6.58	0.22	0.76	2.50	0.13	0.95
250	3.20	0.53	5.19	1.01	1.97	0.34	2.37	2.21
315	2.12	0.41	2.66	0.80	2.37	2.79	1.50	1.61
400	1.05	0.47	1.07	0.05	7.07	1.20	0.68	0.68
500	0.18	0.24	2.73	1.72	1.68	2.32	2.79	0.82
630	0.03	0.17	5.01	2.40	2.35	5.01	2.29	2.46
800	1.32	3.09	2.82	1.38	0.76	3.31	2.69	1.91
1000	1.54	4.87	0.20	1.34	1.89	1.57	0.52	0.77
1250	7.48	2.66	1.39	3.84	1.21	1.80	0.40	2.48
1600	2.58	2.83	1.45	0.85	4.18	2.30	3.10	7.44
2000	7.91	2.87	2.81	2.81	3.01	3.62	6.14	5.35
Freq	Phase Difference (Deg.) at each Grid Location							
(Hz)	0,1	2,1	4,1	6,1	8,1	10,1	12,1	14,1
100	3.87	0.87	0.31	0.18	0.97	0.09	0.00	0.46
125	1.46	1.39	0.90	0.40	0.44	0.51	0.68	1.03
160	0.45	2.05	0.98	0.83	0.74	1.35	2.89	0.62
200	0.20	0.55	0.39	2.13	4.35	11.44	5.73	3.62
250	0.17	0.68	1.37	3.35	4.22	4.03	5.43	7.16
315	0.43	0.07	0.29	1.61	5.57	1.89	1.04	2.27
400	0.45	0.40	0.62	1.15	30.85	2.57	0.62	1.86
500	0.22	0.12	0.84	2.32	3.77	3.68	0.34	0.39
630	0.26	0.10	0.74	5.76	5.25	8.51	1.23	5.01
800	2.40	3.02	4.79	3.89	2.46	10.97	6.77	0.48
1000	0.59	5.34	2.55	6.13	5.59	4.44	3.45	2.55
1250	6.83	0.57	1.03	12.14	5.06	2.16	0.55	6.23
1600	4.80	2.14	1.55	1.48	7.61	7.27	8.94	18.68
2000	5.35	2.33	1.85	6.43	8.48	6.43	14.73	14.73

Table 5.7 Cont'd. **SINGLE POINT REACTIVITY (L_t) MEASUREMENTS (PHASE DIFFERENCE ONLY) USING 1/4" MICROPHONE PAIR ON BEAM I**

Freq	Phase Difference (Deg.) at each Grid Location							
(Hz)	0,2	2,2	4,2	6,2	8,2	10,2	12,2	14,2
100	2.12	0.67	1.54	0.85	0.61	0.29	0.29	0.12
125	2.48	0.90	1.03	0.67	0.55	1.21	1.71	1.01
160	2.89	1.21	1.38	1.07	1.70	2.25	2.89	3.10
200	0.89	1.28	0.87	1.54	3.15	1.14	5.23	3.70
250	0.77	1.22	1.33	1.97	0.35	6.39	5.07	5.43
315	1.14	0.04	0.47	1.93	3.35	0.01	2.73	1.76
400	2.45	1.41	1.12	0.54	17.75	1.86	0.2	0.39
500	0.03	1.14	1.85	0.70	2.55	2.99	0.11	0.36
630	0.76	2.14	1.86	4.27	4.57	5.13	2.35	4.47
800	5.63	7.25	1.26	3.63	1.15	12.89	7.59	2.35
1000	3.37	9.05	3.45	2.80	9.71	5.10	3.37	2.93
1250	14.59	1.60	5.42	8.40	5.81	4.31	0.07	5.18
1600	15.54	6.63	4.18	1.74	1.32	7.79	9.80	15.90
2000	15.43	9.08	9.30	7.73	7.56	7.91	11.70	12.54
Freq	Phase Difference (Deg.) at each Grid Location							
(Hz)	0,3	2,3	4,3	6,3	8,3	10,3	12,3	14,3
100	1.57	0.07	0.64	0.08	0.20	0.56	0.56	1.37
125	1.46	0.41	0.92	0.90	1.21	1.56	2.01	3.12
160	1.42	1.18	1.38	2.41	1.66	3.10	4.38	6.19
200	2.68	0.48	0.89	2.81	2.68	0.51	5.73	3.53
250	1.97	1.01	0.44	0.52	3.51	6.39	5.69	5.43
315	1.30	1.28	2.49	4.52	5.44	0.54	4.96	7.01
400	1.95	0.26	1.38	0.05	13.78	1.44	1.05	3.88
500	3.36	1.65	3.68	0.33	4.85	3.21	1.85	2.38
630	4.37	3.02	3.72	5.63	7.77	5.63	6.03	7.08
800	7.77	7.25	8.13	5.25	0.81	13.50	7.95	7.25
1000	5.72	5.99	2.61	3.69	12.51	7.71	3.78	3.87
1250	12.42	4.02	5.81	5.30	5.68	4.31	0.40	6.52
1600	17.84	7.44	10.27	2.25	1.67	9.58	12.06	15.54
2000	17.31	9.96	10.43	9.96	10.67	11.44	11.44	11.70

Table 5.8 SWEPT REACTIVITY MEASUREMENTS FOR BEAM I USING 1/4" MICROPHONE PAIR

Freq (Hz)	L_P (dB)	L_I (dB)	L_K (dB)	Phase Diff. ϕ
100	60.8	40.0(+)	-20.8	0.01°
125	68.6	64.6(+)	-4.0	0.65°
160	72.1	69.9(+)	-2.2	1.26°
200	61.0	52.0(-)	-9.0	0.33°
250	60.7	56.8(+)	-3.9	1.33°
315	63.6	55.2(-)	-8.4	0.60°
400	71.5	61.4(-)	-10.1	0.51°
500	61.3	53.3(+)	-8.0	1.04°
630	67.9	59.7(+)	-8.2	1.29°
800	59.7	64.7(+)	-5.0	3.31°
1000	59.9	55.6(+)	-4.3	4.87°
1250	58.7	55.2(+)	-3.5	7.31°
1600	55.4	54.2(+)	-1.2	15.90°
2000	50.9	48.3(+)	-2.6	14.40°

spectral measurements, the frequency for each frequency slot is given in Table 4.1. The numbers at the spectral peaks refer to the Mode Numbers given in Table 5.9. Figures 5.5 and 5.6 show the 1/12-octave pressure and intensity spectra over the frequency range 1 to 1600 Hz Figures 5.7 and 5.8 show the 1/3-octave pressure and intensity spectra in the same frequency range 100 to 1600 Hz.

The 1/12-octave pressure and intensity spectra were also measured at location 8,2 and are displayed in Figures 5.9 and 5.10 respectively.

Inspection of the 1/3- and 1/12-octave pressure and intensity spectra of Figures 5.5 to 5.10 reveal some of the actual modal frequencies; these values are listed in Table 5.9 for comparison. Note that the mode shapes are not determined from the spectra and these have been identified from the subsequent intensity mapping. The difference between the modal frequencies determined from the theoretical analyses and the measured spectra increases with frequency and the variation is interpreted as being due to the non-ideal boundary conditions (flexibility of support) imposed by the actual test set-up as well as the finite element idealization.

It is also interesting to note that the amplitudes of acoustic pressure and intensity of the second and fourth frequencies are much higher than the other frequencies in all of the spectra.

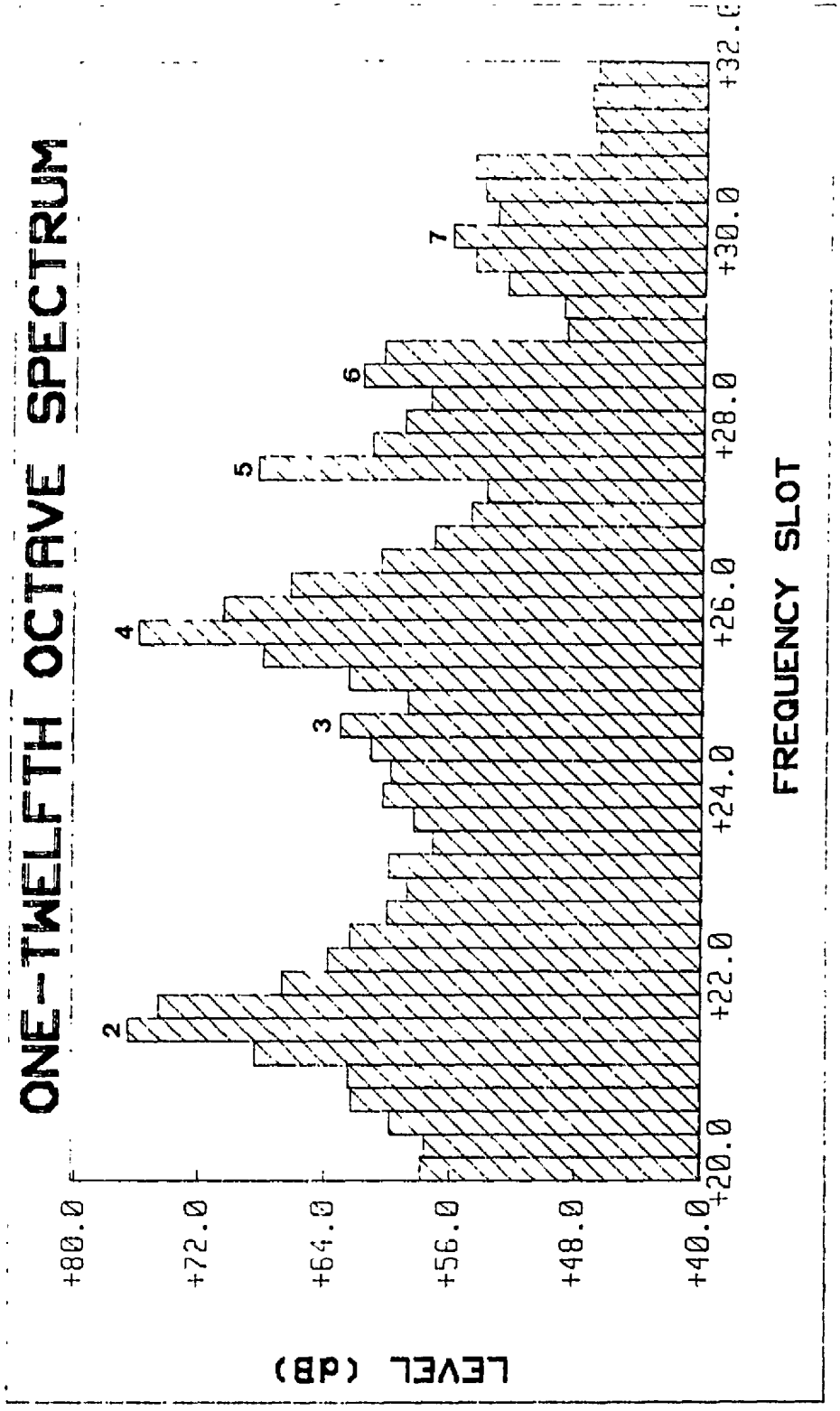

Figure 5.5 1/12th Octave Pressure Spectrum on Beam I at Location 4,1

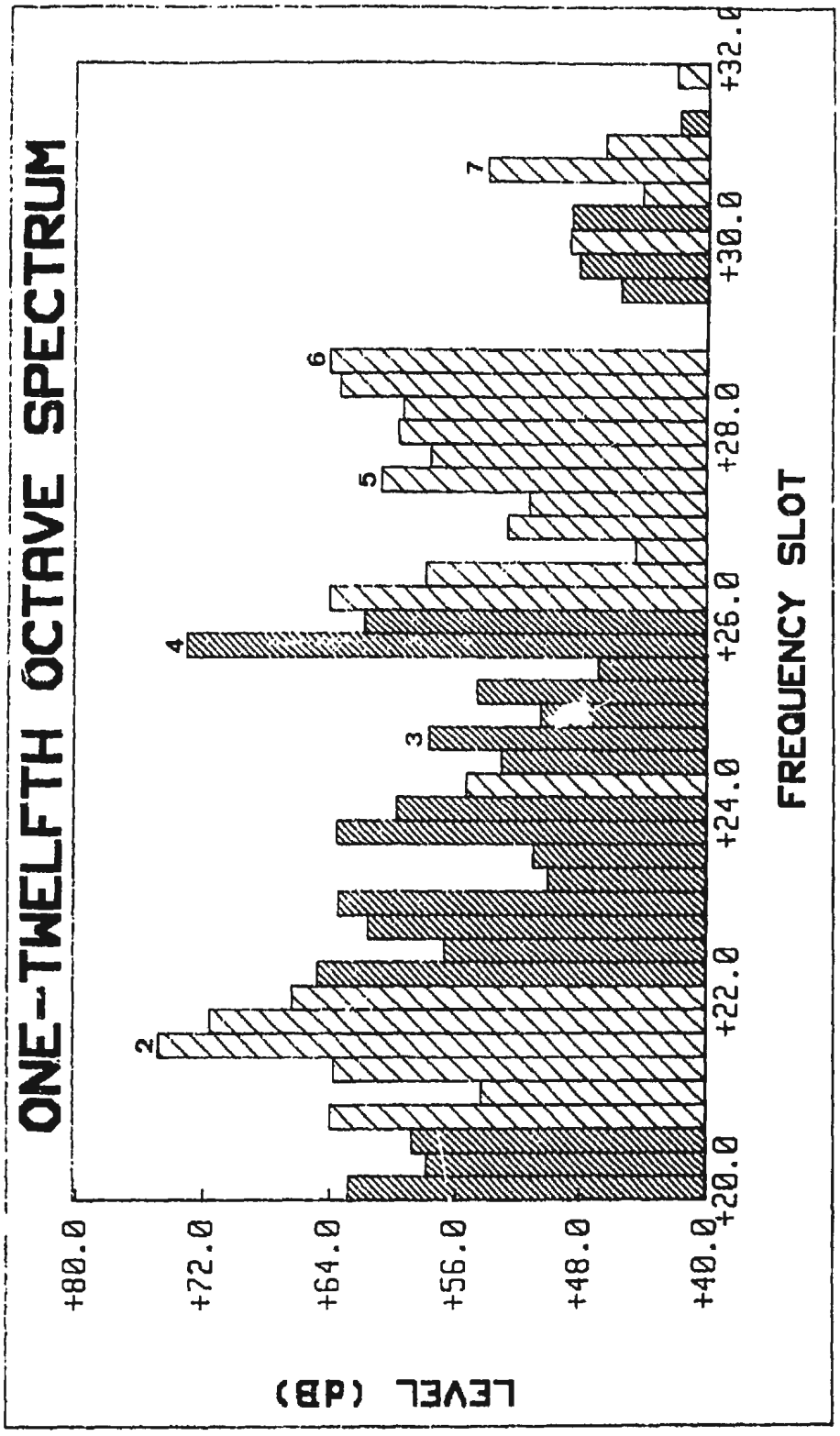

Figure 5.6 1/12th Octave Intensity Spectrum on Beam I at Location 4,1

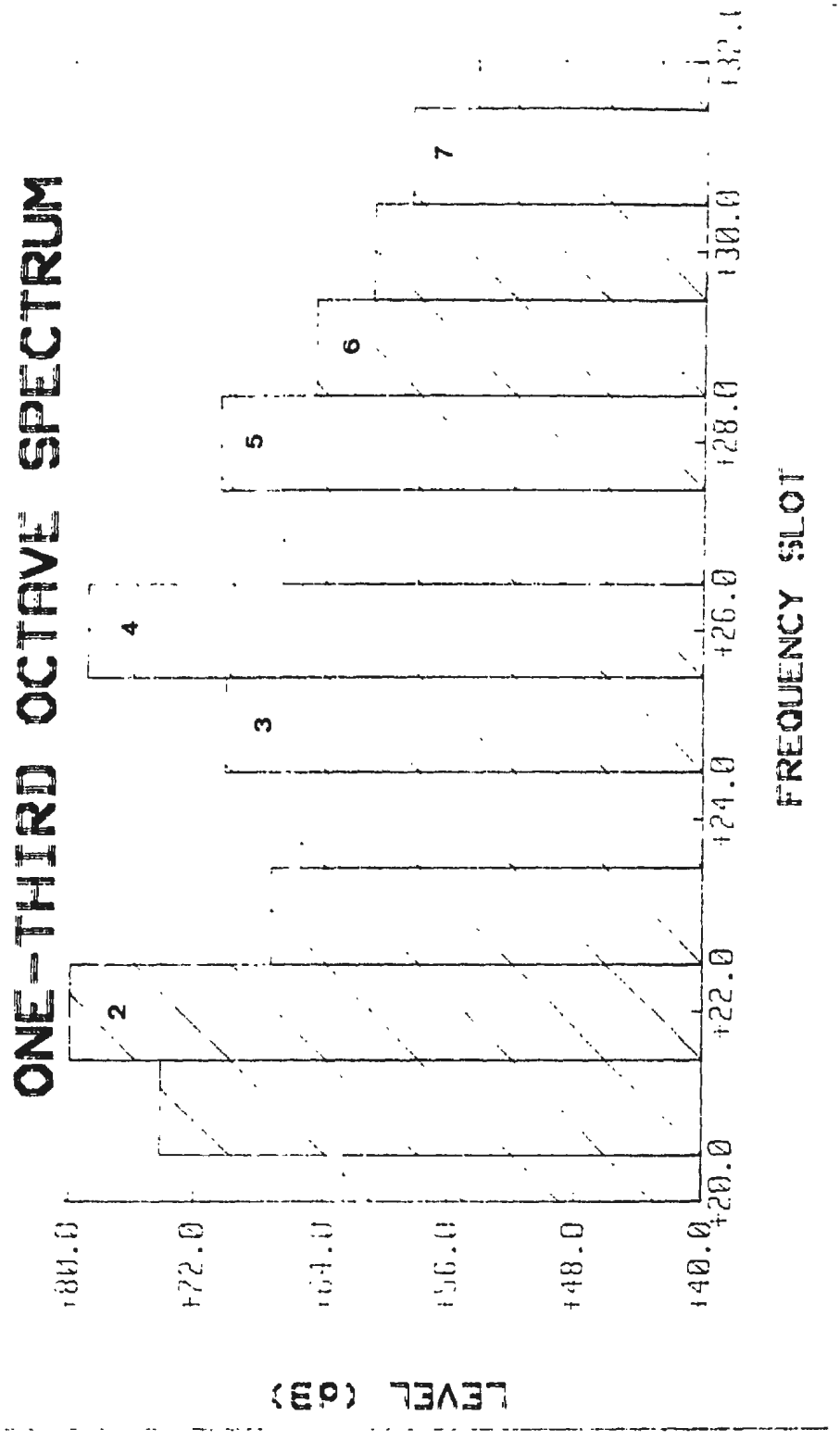

Figure 5.7 1/3rd Octave Pressure Spectrum on Beam I at Location 4,1

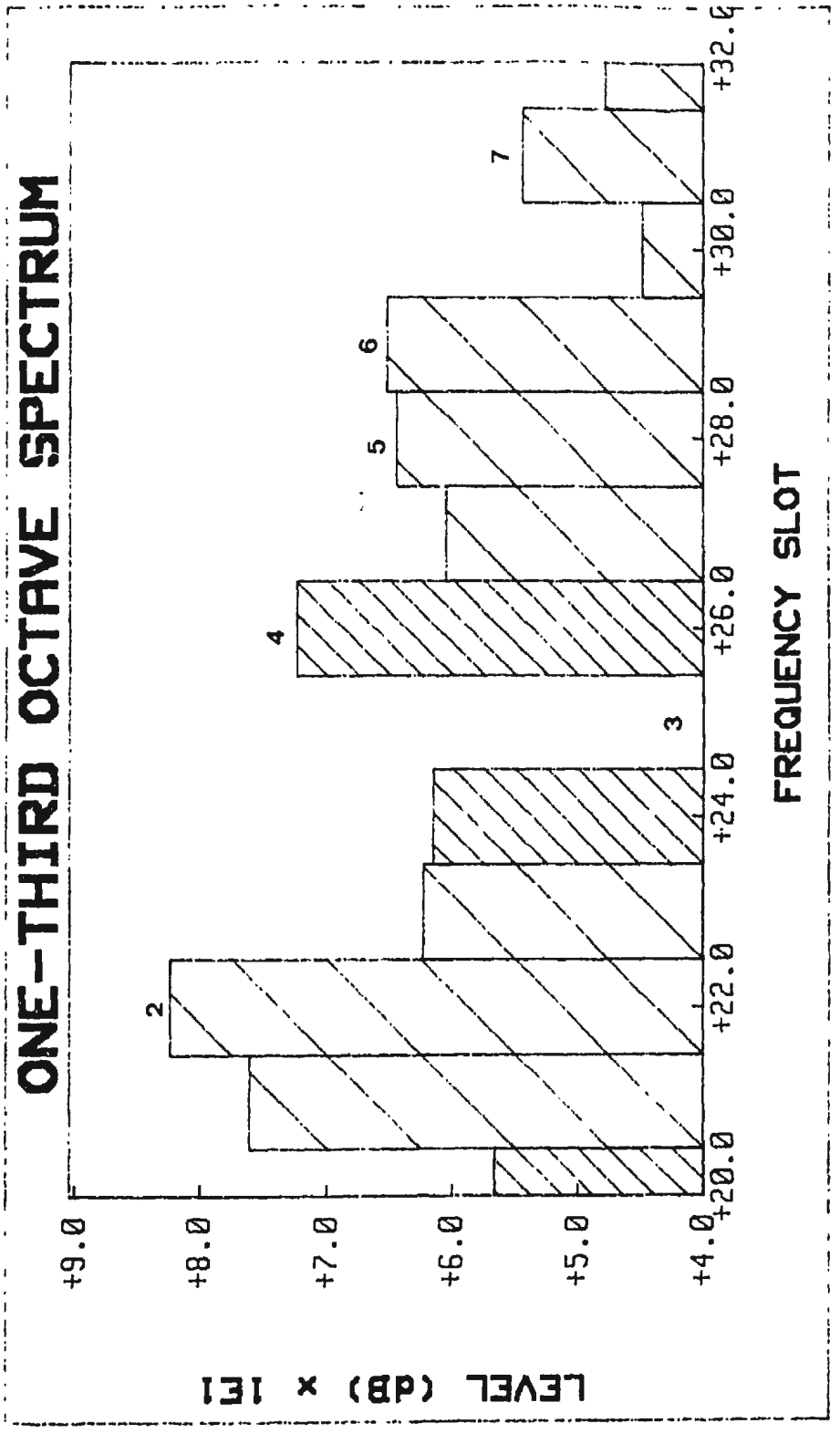

Figure 5.8 1/3rd Octave Intensity Spectrum on Beam I at Location 4,1

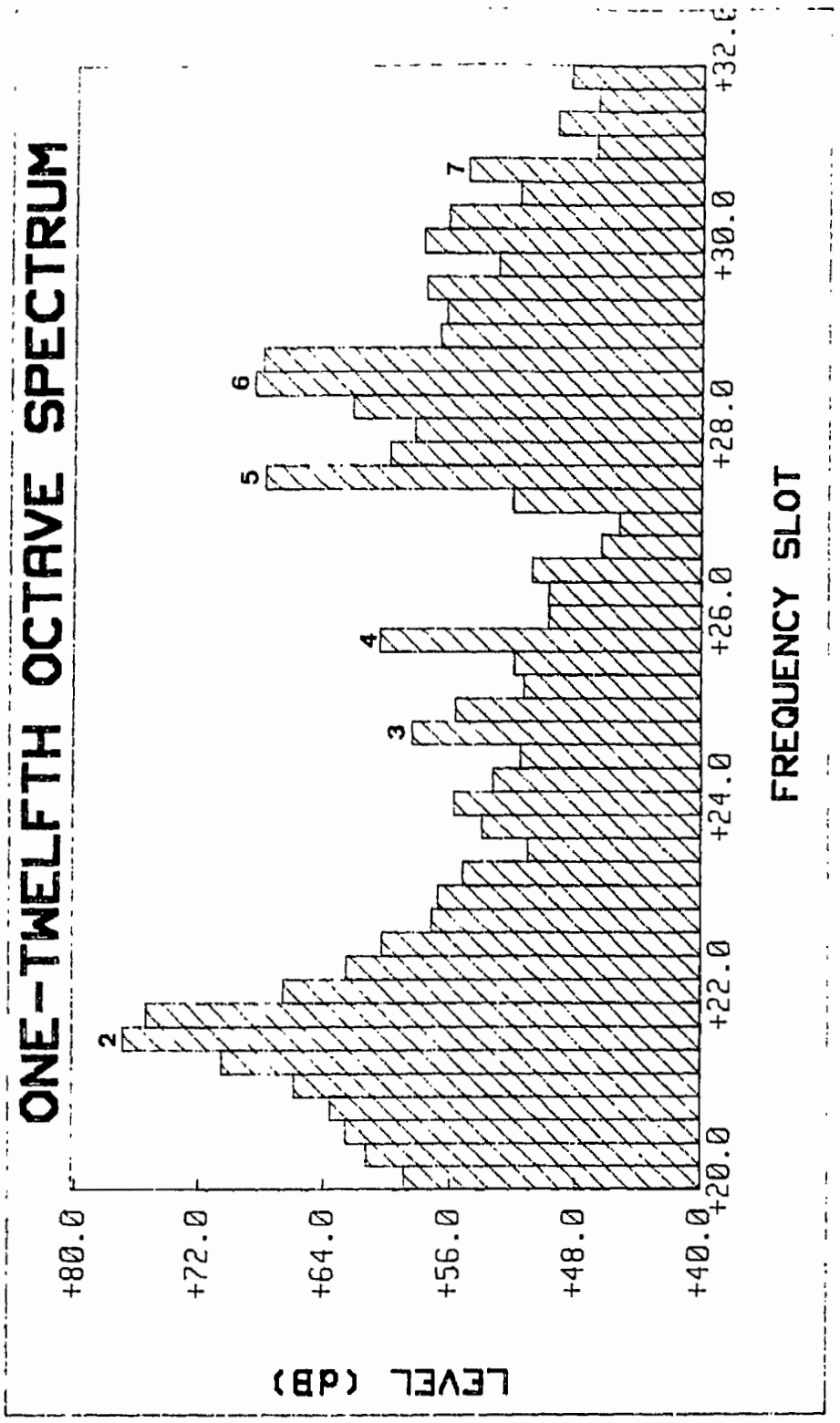

Figure 5.9 1/12th Octave Pressure Spectrum on Beam I at Location 8,2

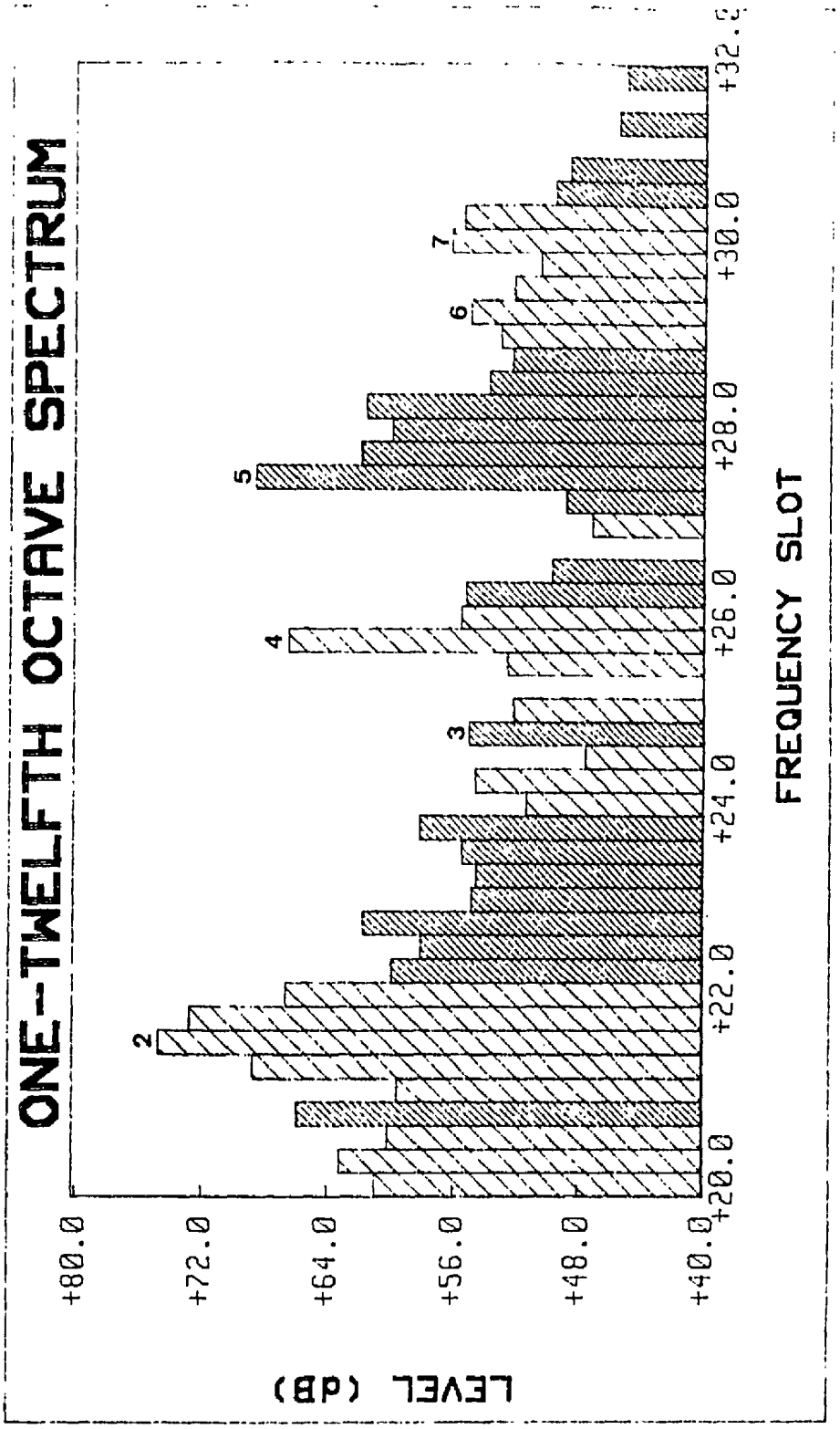

Figure 5.10 1/12th Octave Intensity Spectrum on Beam I at Location 8,2

Table 5.9 COMPARISON OF THEORETICALLY AND EXPERIMENTALLY DETERMINED MODAL FREQUENCIES FOR BEAM I

Mode Number	Mode Shape	Frequency (Hz) for different techniques 1	2	3	4	5
1	Bending	26.6	27.5	30.0	N/A	27.5
2	Bending	166.2	171.4	150.0	160.0	145.0
3	Torsional	N/A	283.0	310.0	_	302.4
4	Bending	466.0	479.6	395.0	400.0	389.6
5	Torsional	N/A	864.2	600.0	_	582.3
6	Bending	N/A	940.2	-	800.0	823.4
7	Torsional	N/A	1489.0	-	-	1155.0
8	Bending	N/A	1550.0	-	_	_

1 = Beam Theory Analysis

2 = Finite Element Analysis (SAP86)

3 = Experimental Values

4 = 1/3 Octave Intensity Spectrum

5 = 1/12 Octave Intensity Spectrum

It can be seen that both the pressure and the intensity spectra must be looked at in order to determine the modal frequencies, and this is because the sound field in the direction chosen may be reactive. From Table 5.8 we can see that at 630 Hz the phase difference is 0.74° at location 4,1 and 4.57° when measured at location 8,2. The 1/3-octave spectra, while still revealing the modal frequencies, do so with a much lower frequency resolution, and with much less clarity. It is also apparent that the frequency resolution of the system is important. Hence it is seen that a better identification of modal frequencies could be obtained if a filter much higher than 1/12th octave is used in both pressure and intensity measurements.

5.4.4 Pressure Mapping

An 8 column by 4 row rectangular grid with cell length 50 mm and width 20 mm was used to map the variation in the pressure over the surface of the beam. A one-third octave spectrum with linear averaging over a period of 1 second was measured at each grid location while the beam was excited using 1 kHz bandwidth white noise. The one-third octave frequency band maps are shown in Figures 5.11 (a) to 5.11 (l) for the frequencies 100 to 1250 Hz. Refer to Appendix B for an explanation of the contour map. The 1/3-octave pressure variation given in these do not reveal any clear information regarding modal behaviour. It could be surmised from these figures that there are modal frequencies around 160 Hz, 400 Hz and 800 Hz but the mode shapes are nor revealed with any clarity.

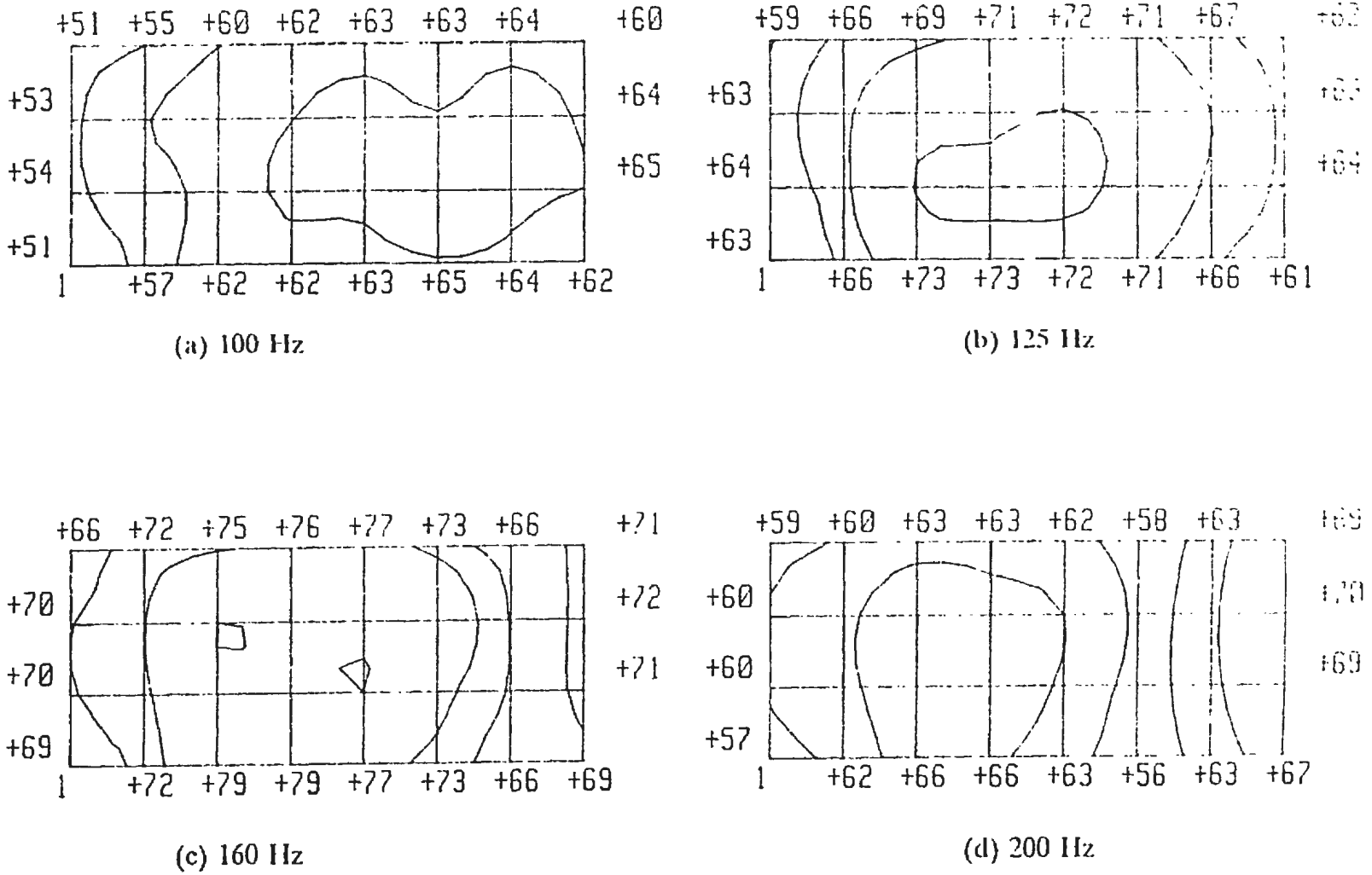

(a) 100 Hz

(b) 125 Hz

(c) 160 Hz

(d) 200 Hz

Figure 5.11 Pressure Contour Maps in 1/3 Octave Bands over Beam I. Contour Lines at 5 dB intervals. Excitation: 1 kHz White Noise

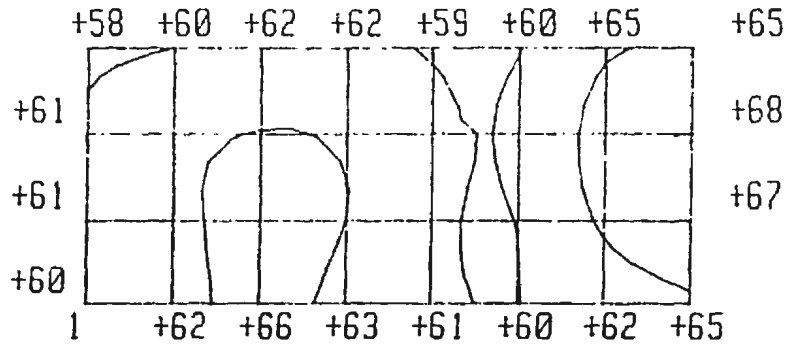

(e) 250 Hz

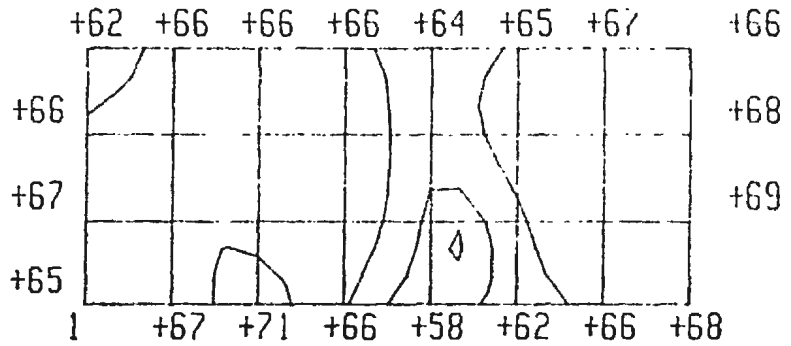

(f) 315 Hz

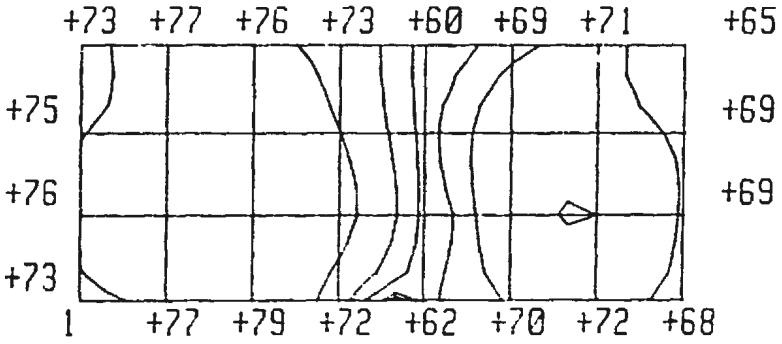

(g) 400 Hz

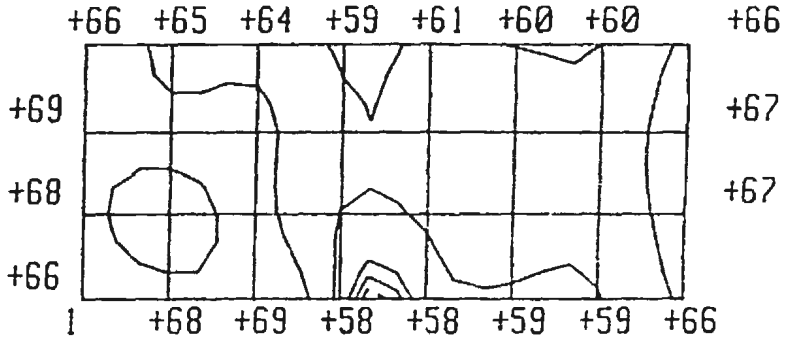

(h) 500 Hz

Figure 5.11 Continued...

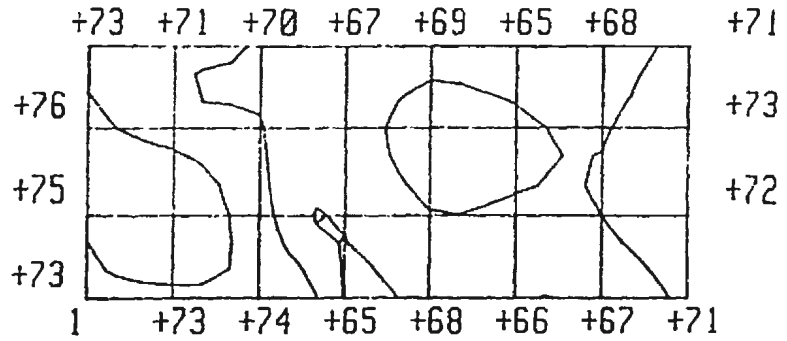

(i) 630 Hz

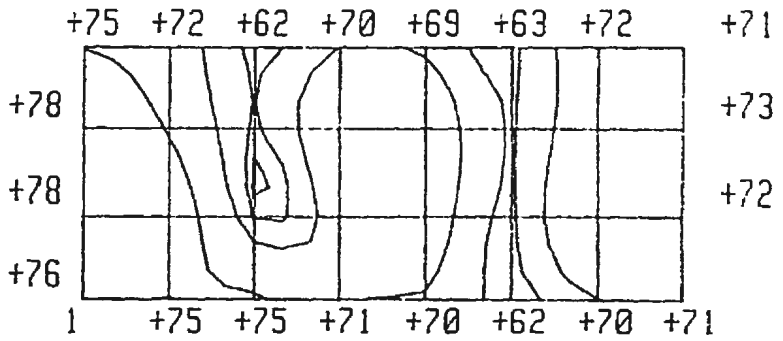

(j) 800 Hz

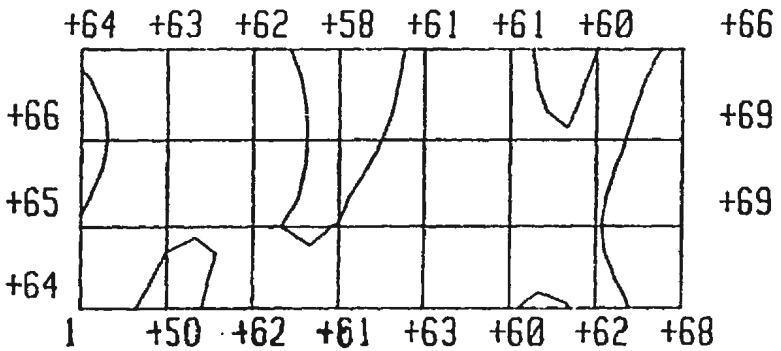

(k) 1000 Hz

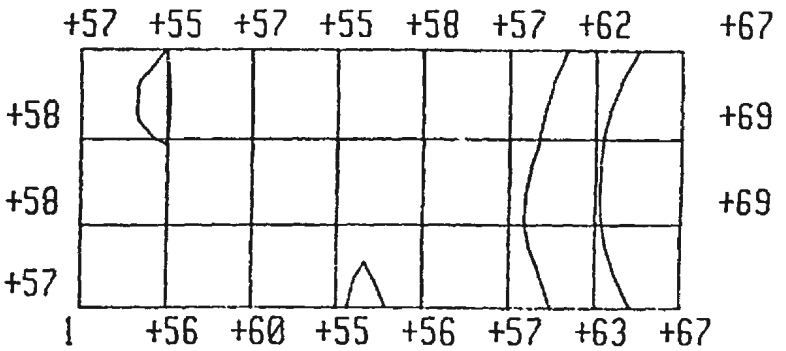

(l) 1250 Hz

Figure 5.11 Continued...

5.4.5 Intensity Mapping

The grid described in Figure 4.13 was used for the following measurements of the intensity variation over the plate. The intensity component normal to the plate was measured using two 1/4" microphones in the side-by-side configuration with a 12 mm spacing. The probe was held manually so that the acoustic centre was 12 mm from the surface of the beam. The spectra were measured with a 40 dB attenuation setting and 1 second linear averaging. Refer to Appendix B for an explanation of the contour map.

The first scan was performed with the beam excited by 1 kHz bandwidth white noise, and the intensity contour maps for the 1/3-octave bands from 100 to 3150 Hz are shown in Figure 5.12.

The next scan was done with the beam excited by 10 kHz bandwidth white noise and the intensity contour maps for the 1/3-octave bands from 100 to 3150 Hz are shown in Figure 5.13.

A number of comparisons between the Figures 5.12 and 5.13 for the same centre frequency are in order and, where relevant, comments on the relevant pressure maps of Figure 5.11 are also made.

<u>100 Hz.</u> This is not a modal frequency and the energy flow is therefore expected to be random and non-stationary. Although the pressure map is reasonably uniform, the

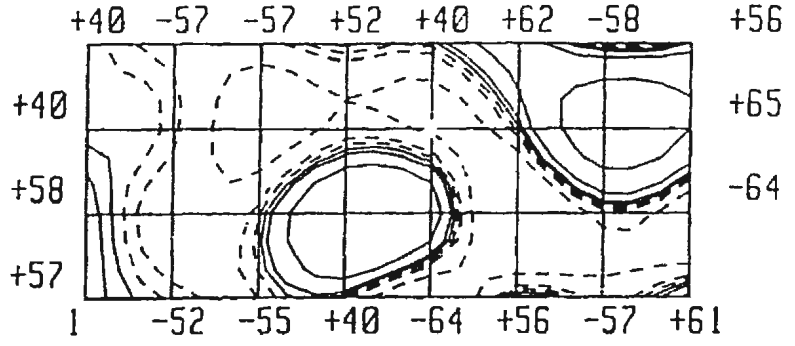

(a) 100 Hz

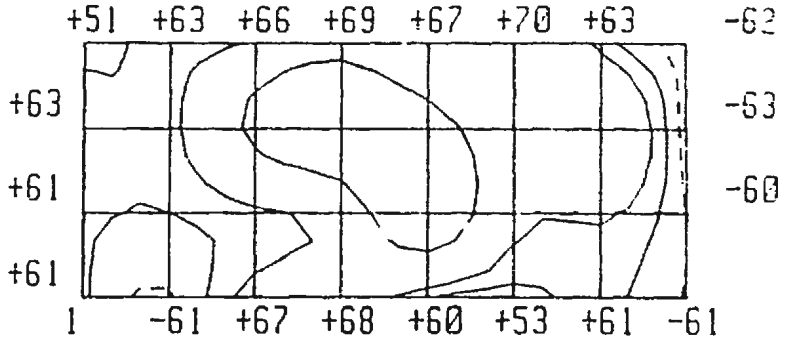

(b) 125 Hz

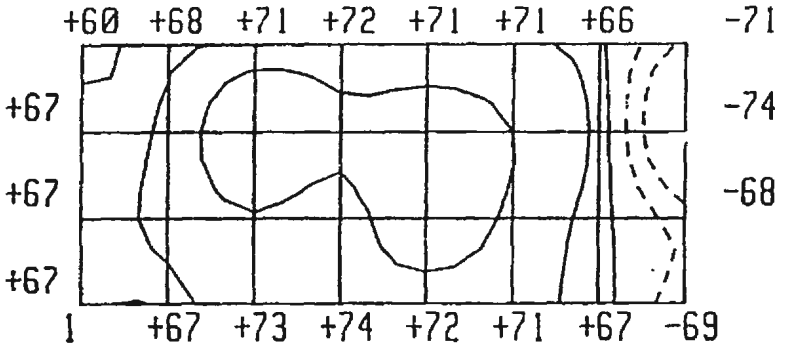

(c) 160 Hz

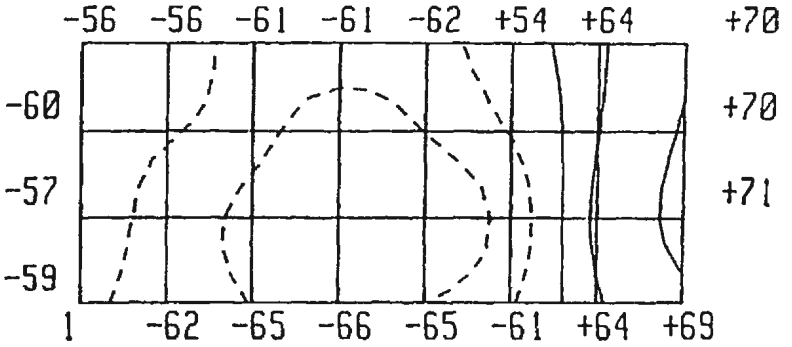

(d) 200 Hz

Figure 5.12 1/3 Octave Contour Maps of Normal Intensity Component over Beam 1. Contour Lines at 5 dB intervals. Excitation: 1 kHz White Noise

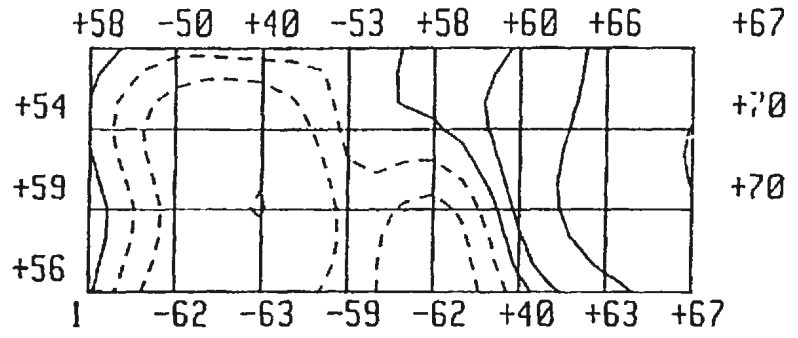

(e) 250 Hz

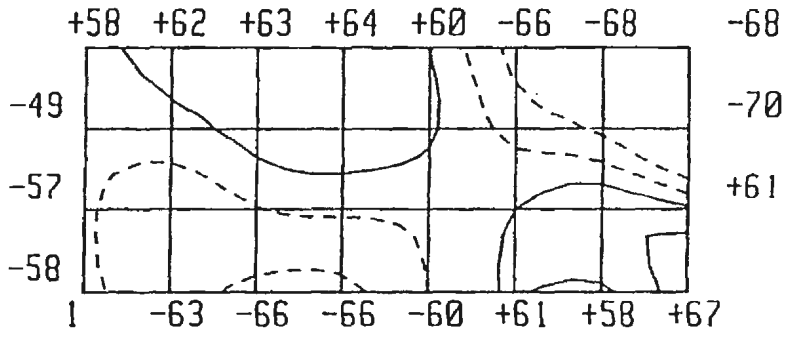

(f) 315 Hz

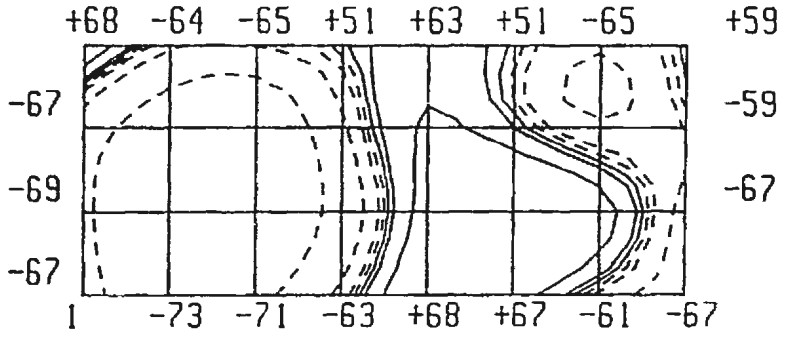

(g) 400 Hz

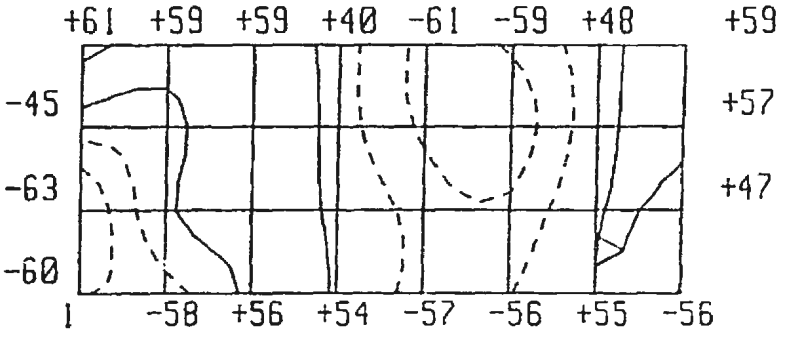

(h) 500 Hz

Figure 5.12 Continued...

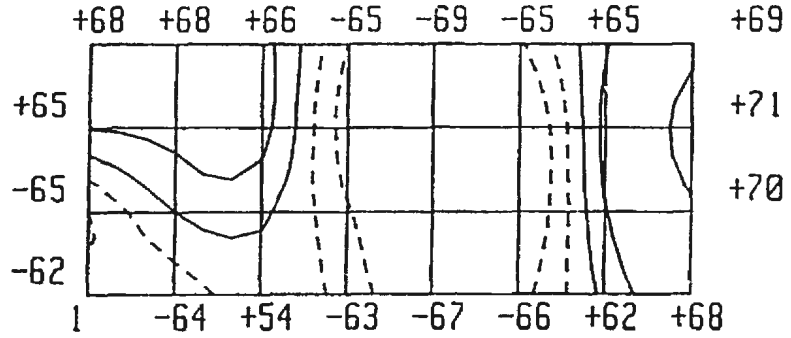

(i) 630 Hz

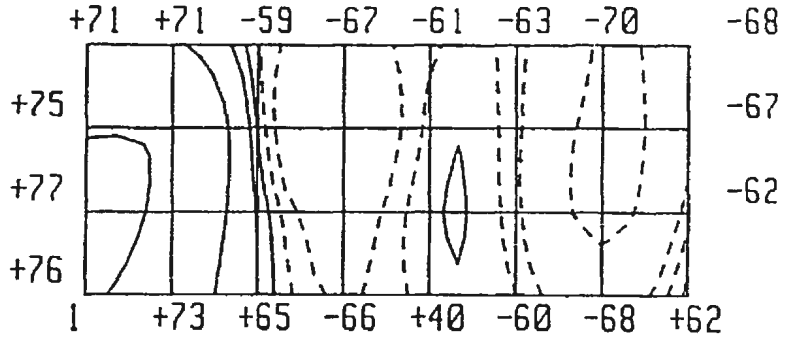

(j) 800 Hz

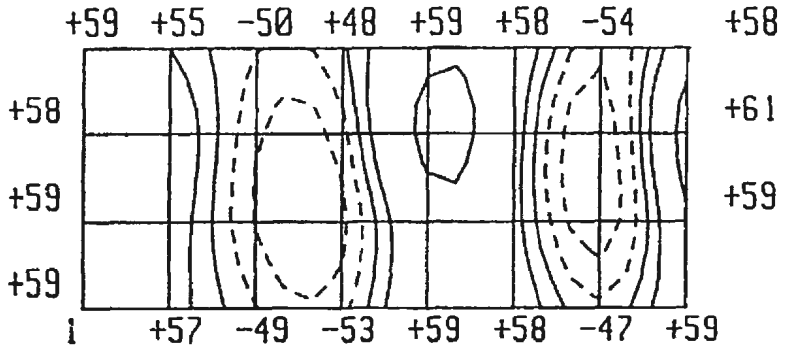

(k) 1000 Hz

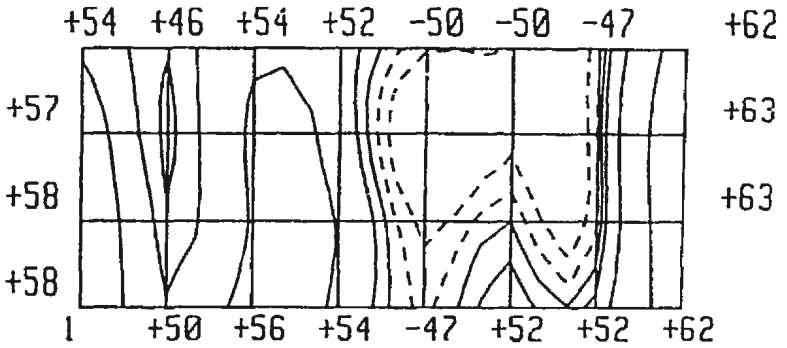

(l) 1250 Hz

Figure 5.12 Continued...

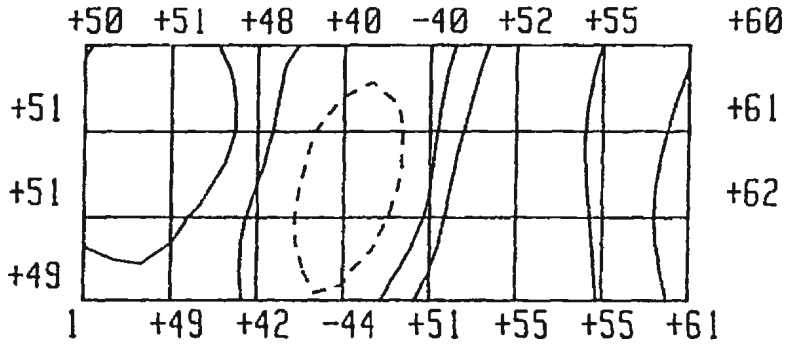

(m) 1600 Hz

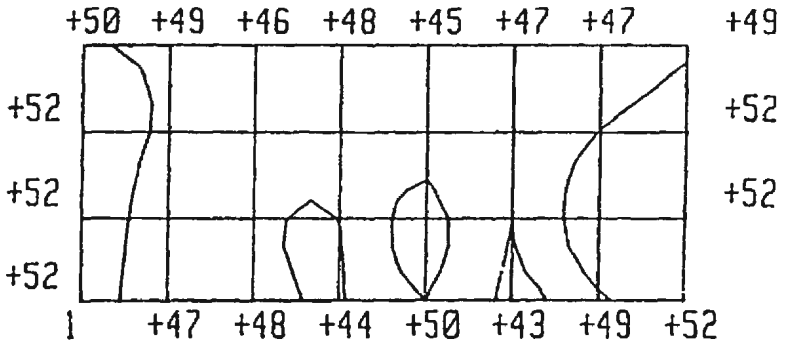

(n) 2000 Hz

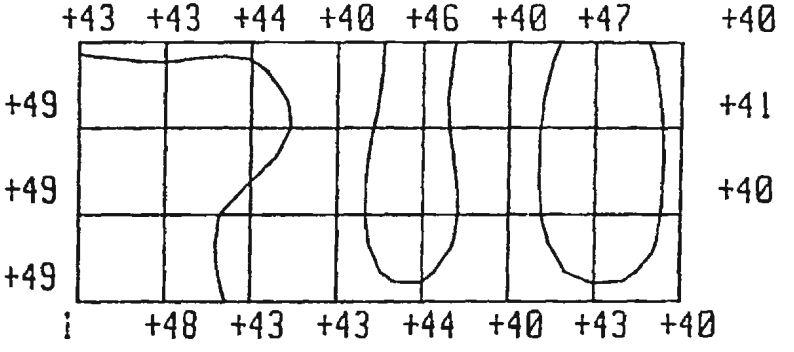

(o) 2500 Hz

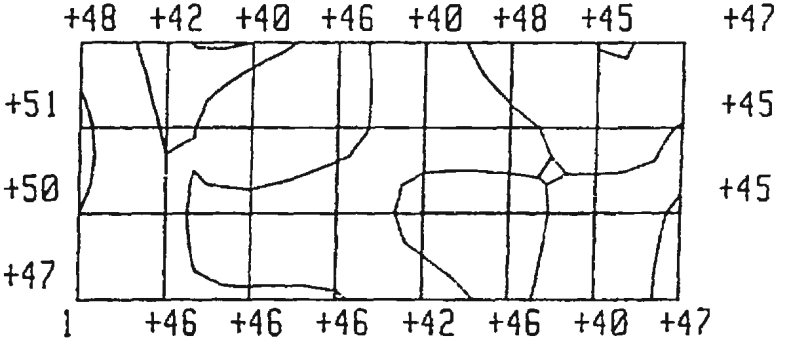

(p) 3150 Hz

Figure 5.12 Continued...

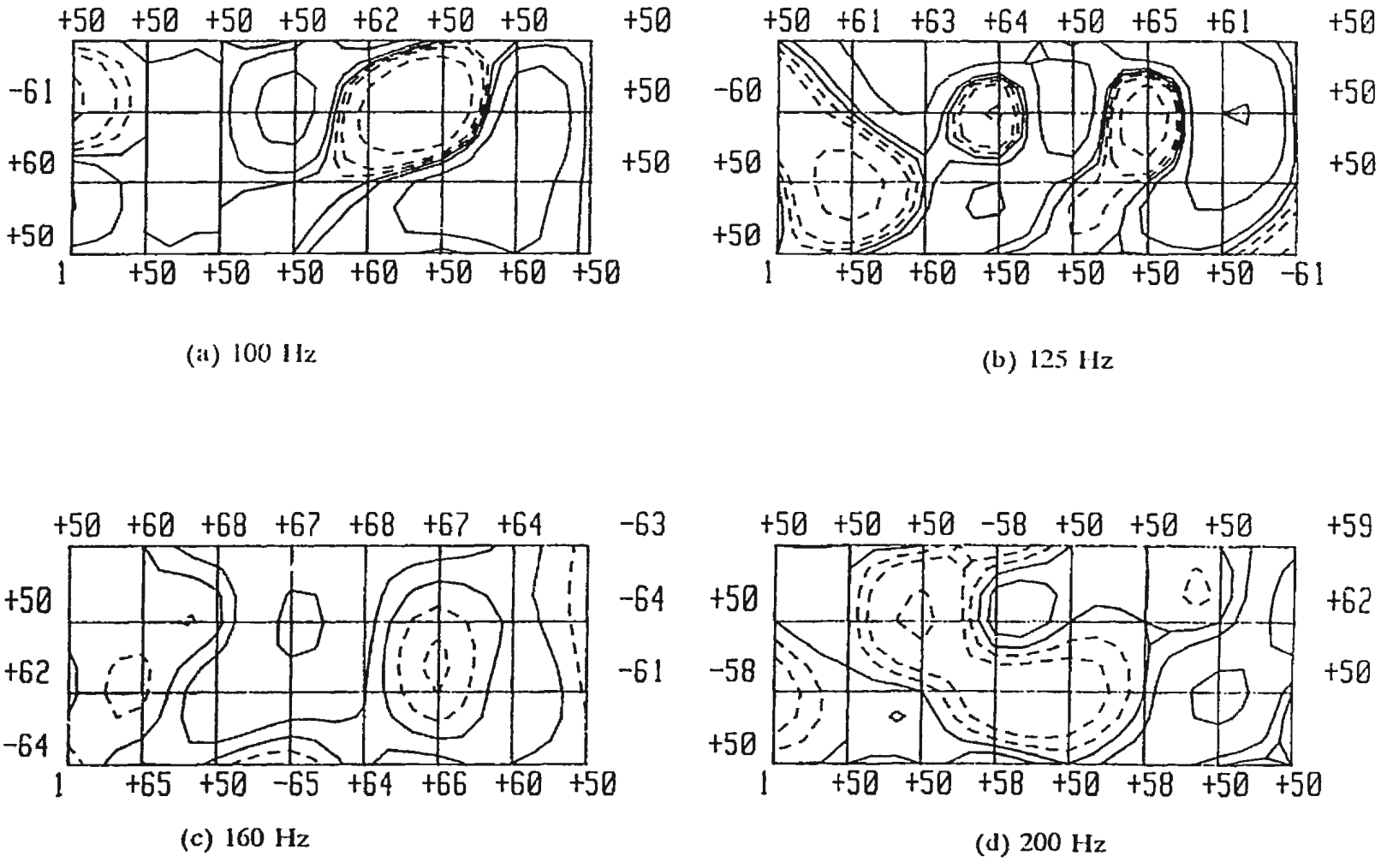

(a) 100 Hz

(b) 125 Hz

(c) 160 Hz

(d) 200 Hz

Figure 5.13 1/3 Octave Contour Maps of Normal Intensity Component over Beam I.
Contour Lines at 5 dB intervals. Excitation: 10 kHz White Noise

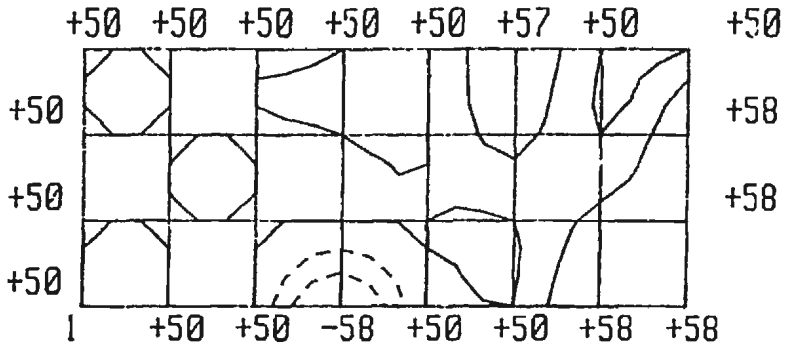

(e) 250 Hz

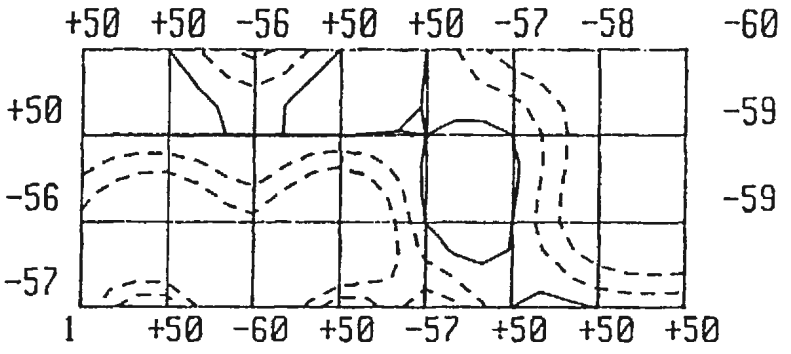

(f) 315 Hz

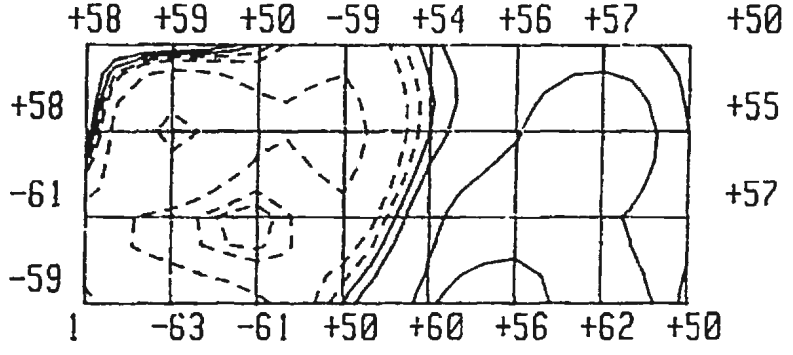

(g) 400 Hz

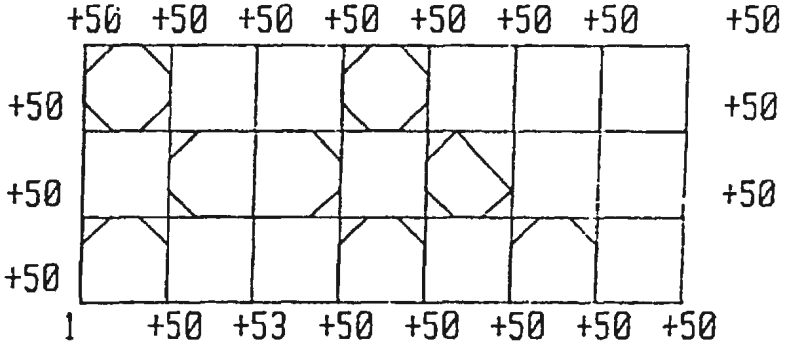

(h) 500 Hz

Figure 5.13 Continued...

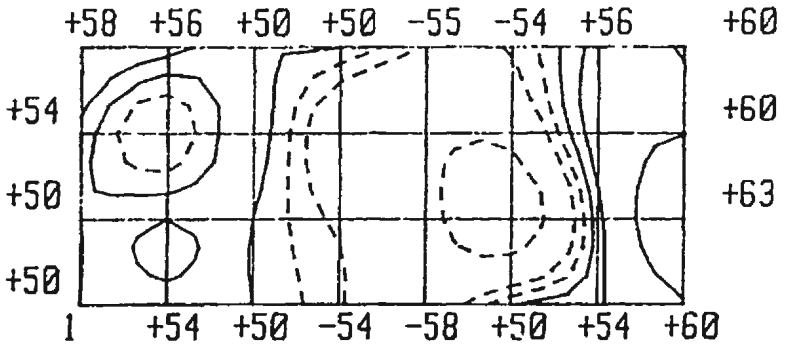

(i) 630 Hz

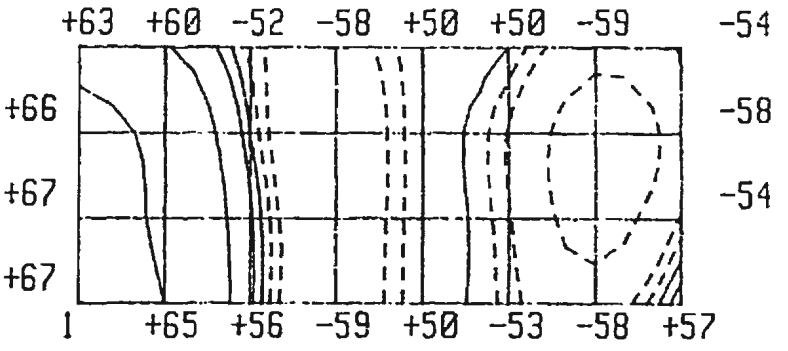

(j) 800 Hz

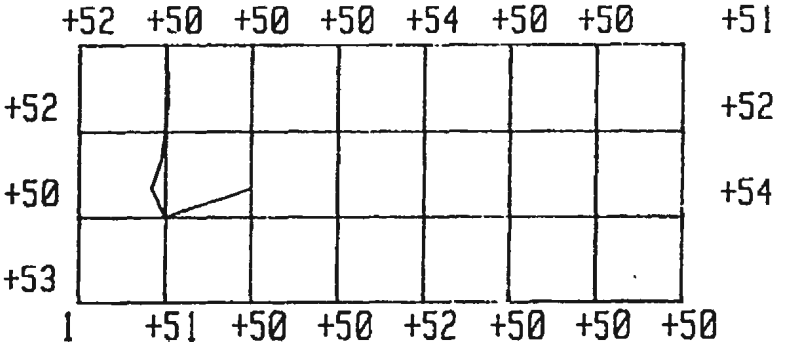

(k) 1000 Hz

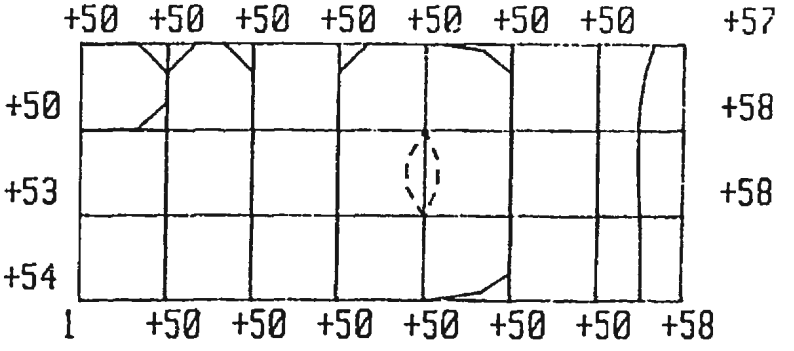

(l) 1250 Hz

Figure 5.13 Continued...

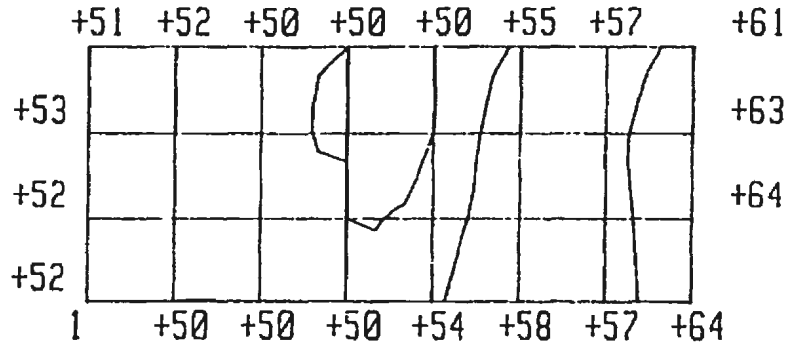

(m) 1600 Hz

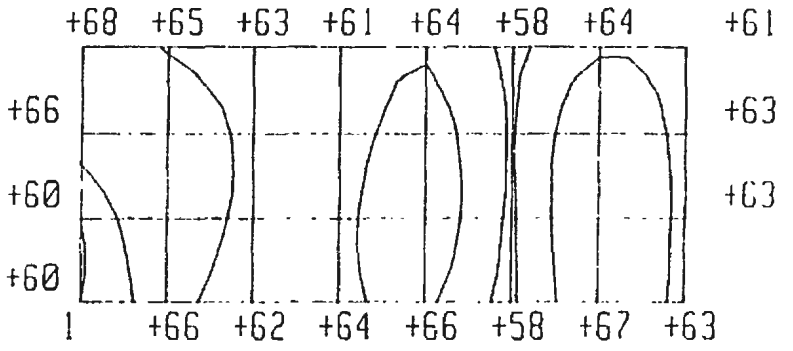

(n) 2000 Hz

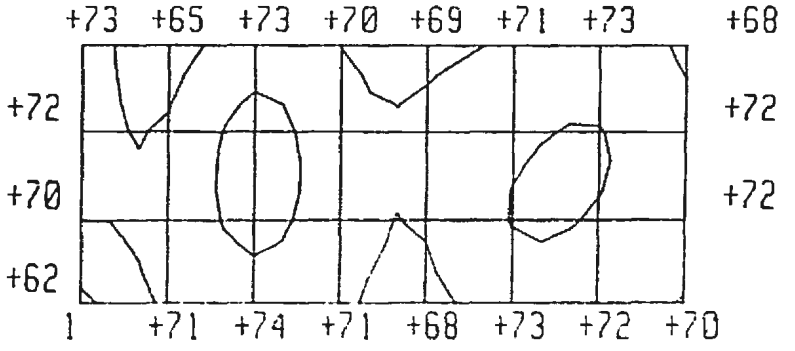

(o) 2500 Hz

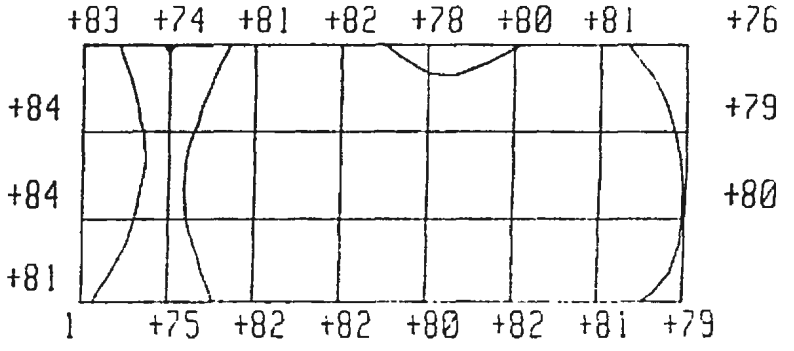

(p) 3150 Hz

Figure 5.13 Continued...

intensity maps are incoherent. When an unknown structure is being analyzed, this incoherence may conversely be used to indicate that the particular frequency is not a modal frequency.

125 Hz and 160 Hz. These two frequency bands lie either side of the modal frequency at 145.0 Hz and the patterns in both the pressure maps and the 1 kHz bandwidth-excited intensity maps show coherent patterns. However, only the intensity map identifies the node location near the end of the beam. It is not immediately apparent as to why the intensity pattern measured under 10 kHz bandwidth excitation appears incoherent but inspection of the data show that at a number of the measurement locations, the intensity levels were below the cut-off levels set on the analyzer. This suggests that under 10 kHz bandwidth excitation the energy input at this frequency was lower than under 1 kHz bandwidth excitation. This may arise because of the power and frequency response of the shaker and amplifier system.

200 Hz and 250 Hz. Although these frequencies do not appear to be modal frequencies, both pressure and intensity maps show coherent patterns in both frequency bands under 1 kHz B.W. excitation. The patterns for intensity measurements under 10 kHz B.W. excitation again show confused patterns and this is understood to be due to similar factors as described previously.

315 Hz. This is a particularly interesting frequency to examine as the data reveal a

number of significant points. The intensity map for this frequency shows the first torsional vibration mode of the beam with the node running along the length of the structure. While the corresponding pressure map does show a coherent pattern, no information regarding the mode shape is given. The pattern determined during excitation under 10 kHz B.W. excitation is still indistinct but can be seen to contain some of the information revealed under 1 kHz bandwidth loading.

A significant feature of this frequency band is that none of the measured intensity spectra (Figures 5.6, 5.8 and 5.10) give a clear indication that this is a modal frequency. Examining the probe locations during the spectral measurements does give us some insight into this as it shows that it was close to a (torsional mode) nodal location where there was very little energy flow normal to the plate. In fact, because the 1/12 octave pressure spectrum ignores the directionality it gives a clearer indication of the modal frequency and in particular, Figure 5.6 has quite an apparent peak at 315 Hz. Because of the lower energy flow in the torsional mode compared to the bending modes, in the 1/3-octave pressure spectrum the torsional mode in the 315 Hz frequency slot is overshadowed by the stronger energy output by the bending mode in the 400 Hz frequency slot.

The conclusion to be drawn from this is that in many cases, performing a swept measurement to give an averaged spectrum over the structure may be necessary in order to get a good indication of the modal frequencies. In addition, both intensity and pressure

spectra need to be analyzed to identify the modes.

Analysis of the intensity maps made up to this point reveal that there is a bending mode in the frequency band defined by the 160 Hz centre frequency. In order to more fully investigate this mode shape, the beam was excited with 1 kHz white noise and a mapping done using the 1/12-octave bandwidth. The intensity contour maps for the four frequencies 145, 155, 165 and 175 Hz are shown in Figure 5.14.

In order to compare the intensity map data obtained using a 1/12-octave bandwidth on a beam excited by random noise, with that obtained from a 1/3-octave intensity map of a beam excited at a single frequency, the following measurements were made. The beam was excited at 145, 155, 170 and 175 Hz and a mapping done using the 1/3-octave bandwidth. The intensity contour maps for the 160 Hz centre band are plotted in Figure 5.15.

Both the 1/12 octave band and 1/3 octave band results of Figures 5.14 and 5.15 show that the natural frequency is around 145 Hz since the acoustic intensity levels are very high at this frequency and the acoustic map indicates the modal pattern.

Analysis of the 1/3 octave intensity maps for 1 kHz white noise excitation and excitation at the centre frequency of each band reveal some interesting features. For example, the energy flow pattern in the 160 Hz frequency band remains the same

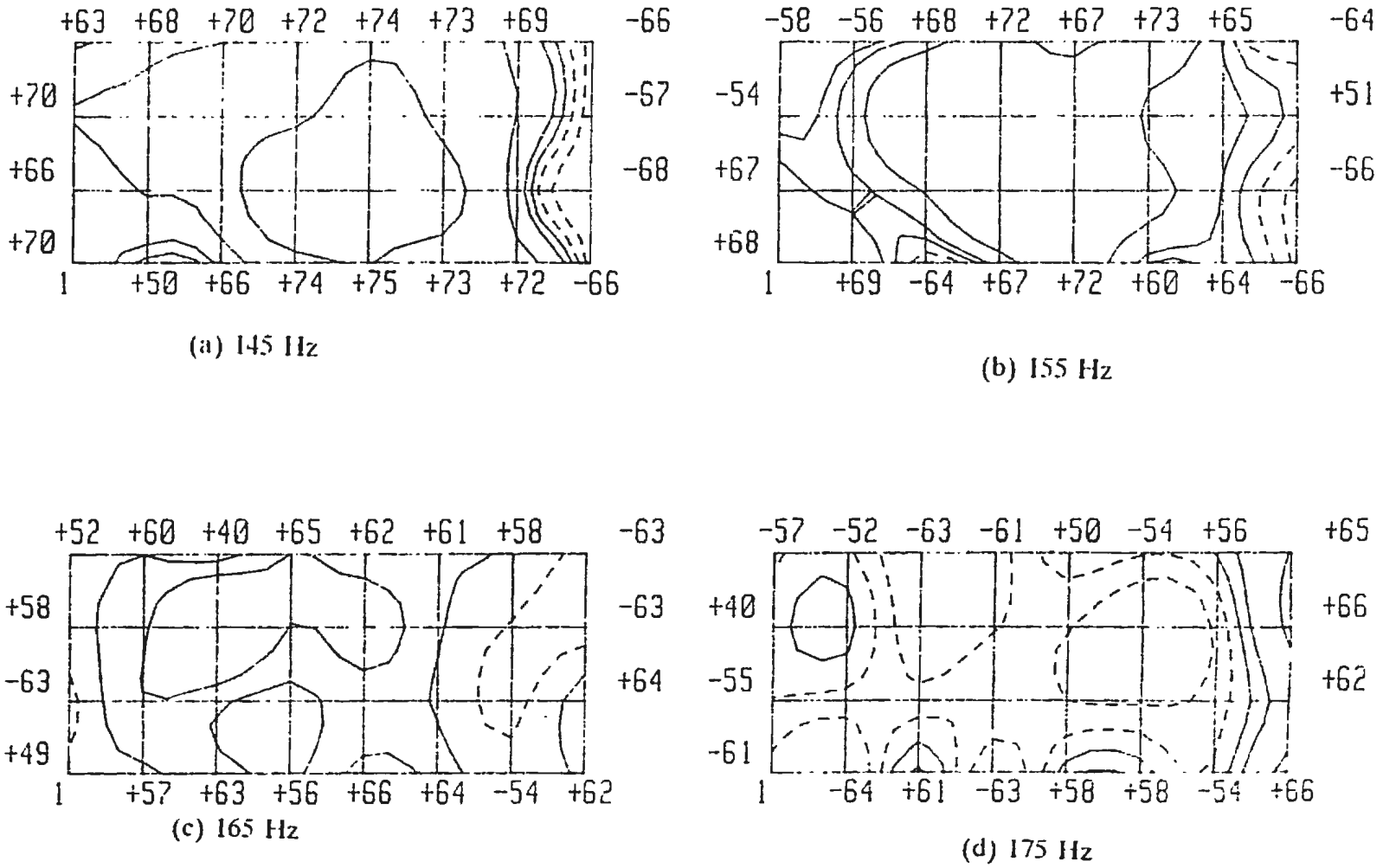

Figure 5.14 1/12 Octave Contour Maps of Normal Intensity Component over Beam 1. Contour Lines at 5 dB intervals. Excitation: 1 kHz White Noise

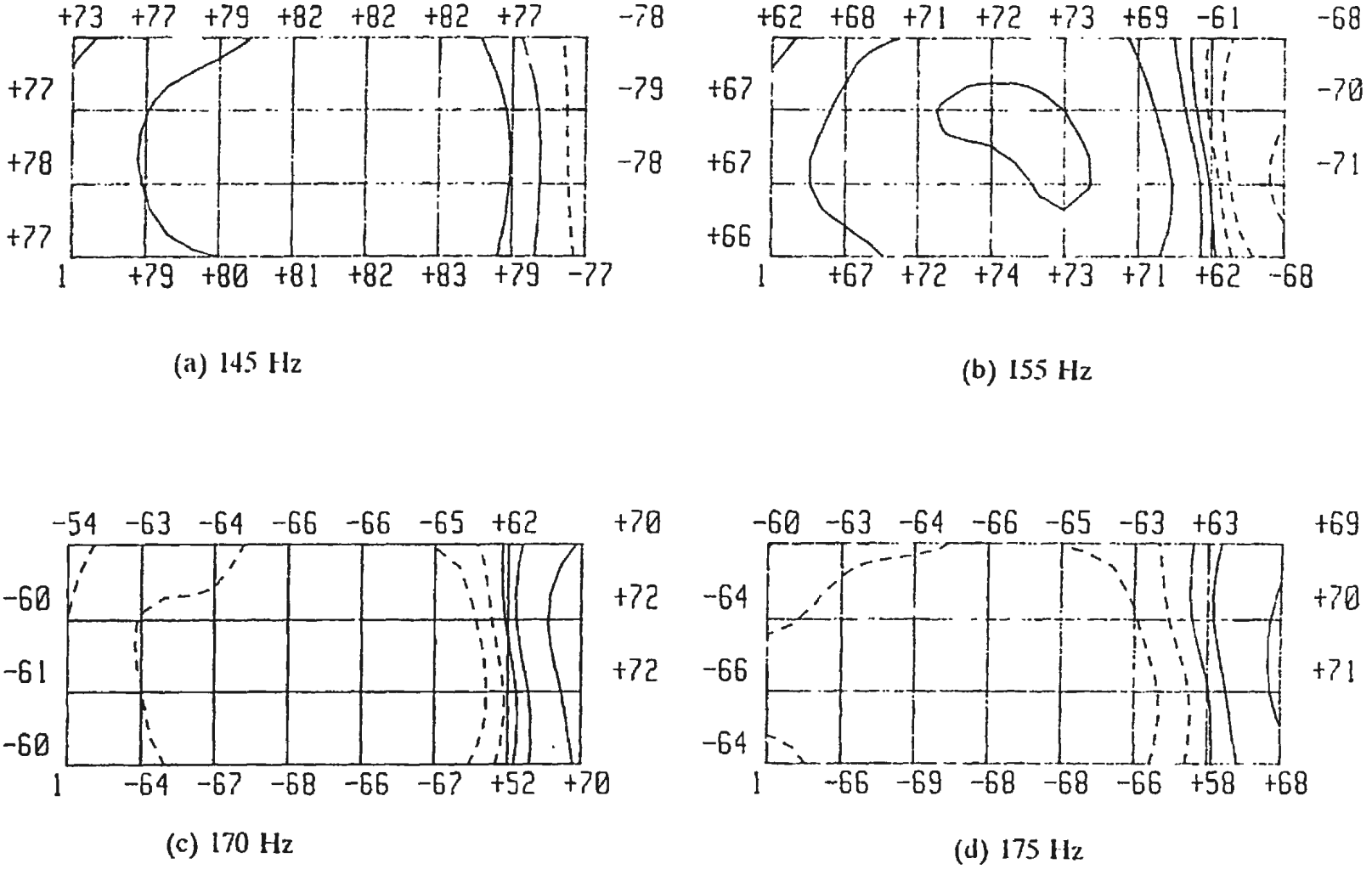

Figure 5.15 Contour Maps of Normal Intensity Component over Beam 1 in 160 Hz Centre Frequency 1/3 Octave Band. Contour Lines at 5 dB intervals. Excitation: 145, 155, 170, 175 Hz.

under white noise excitation and both the 145 Hz and 155 Hz (single frequency) excitations (Figures 5.12 (c) and 5.15 (a) and (b)). However, if the beam is excited at 170 Hz and at 175 Hz, then the two energy flow patterns show a reversal in energy flow (Figures 5.15 (c) and (d)). Under white noise excitation the 145 Hz modal frequency, and hence the energy flow at this frequency, dominates. If the excitation frequency is changed to 175 Hz then a different energy flow pattern is revealed. The use of the 1/12-octave filters to perform the analysis shows that these two energy flow patterns can be discriminated (Figure 5.14) under white noise excitation using a narrower bandwidth filter.

A torsional mode is also revealed by the one-third octave intensity maps. Further investigation revealed this to be at the frequency of 302 Hz. A one-third octave intensity map was plotted out with the beam excited at this frequency as shown in Figure 5.16. In addition, four scans were carried out over a grid normal to the plane of the specimen. The intensity vector component normal to the specimen was still measured. The four grids were selected so that they cut across a node; these measurements were intended to give a measure of the distance from the specimen at which the mode shape information becomes indistinct. (See figures 5.16 (b) - (d)). It is observed that beyond a distance of 100 mm the modal information becomes less clear. Hence the microphone pair must be kept within 50-100 mm of the surface in order for the correct modal information to be obtained.

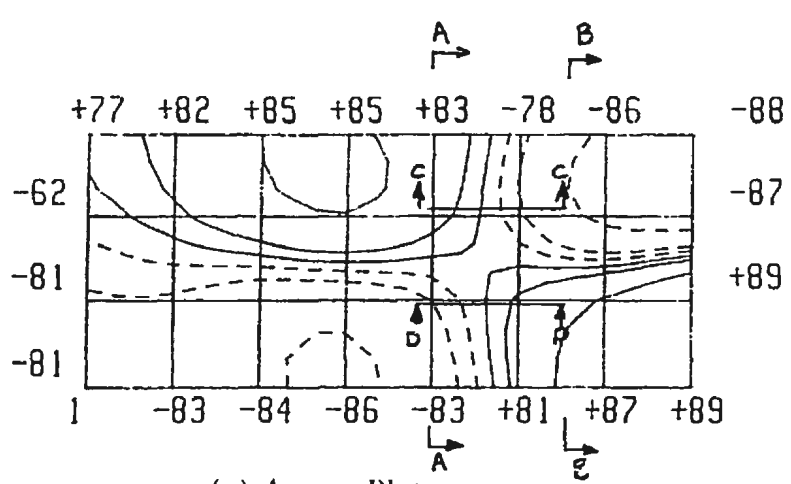

(a) Across Plate

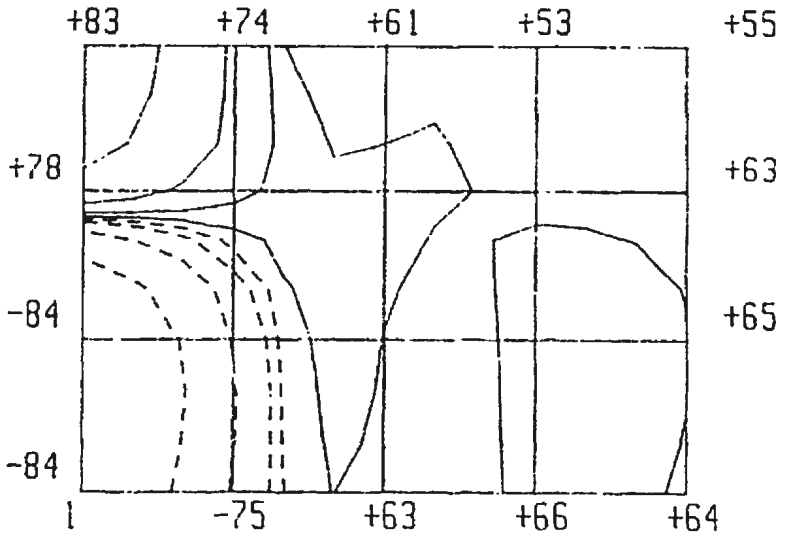

(b) Section A-A

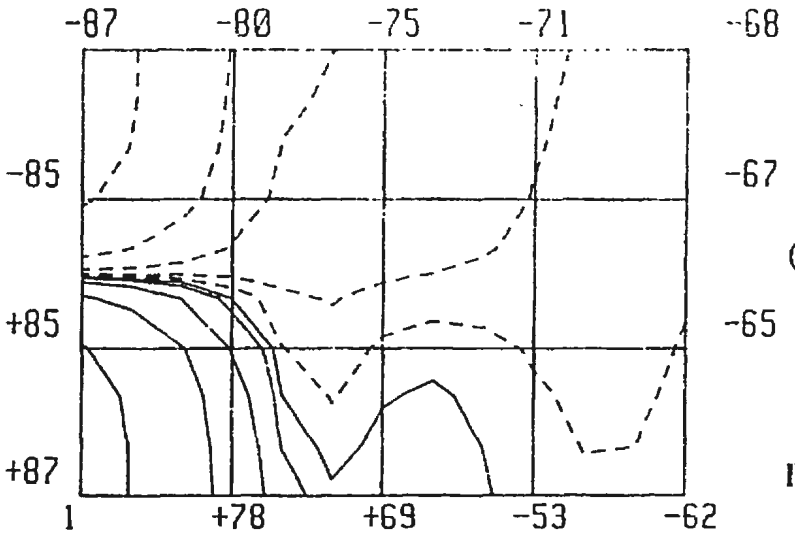

(c) Section B-B

Figure 5.16 Vertical Sections showing Normal Intensity Component over Beam I. 302 Hz. Excitation.

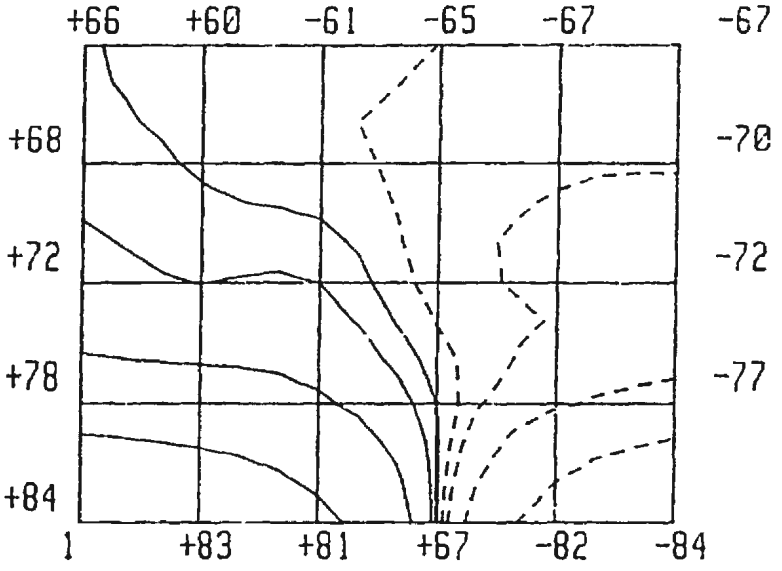

(d) Section C-C

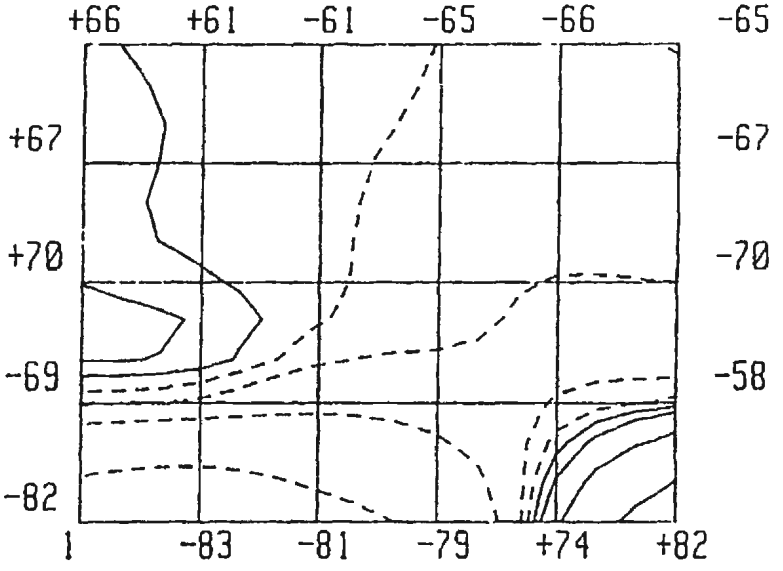

(b) Section D-D

Figure 5.16 Continued...

5.4.6 Full Vector Acoustic Intensity Scanning

In order to determine whether there are any advantages in measuring all three components of the acoustic intensity simultaneously, the six microphone array described in Section 3.5.2 was used to carry out some measurements on Beam I.

The stationarity and reactivity for each microphone pair were determined at grid location 4,2 and the results are given in Tables 5.10. and 5.11 respectively. Table 5.10 shows that the phase changes in the vertical direction are largest indicating that this is the principal direction of energy flow. At 315 Hz the phase changes of between 0.82° and 1.09° for the three components show that the energy flow is roughly at an equal angle to all three axes. The reactivity in the x-direction at 800 Hz appears to be an anomalous value. From Eqn. 3.17, we can calculate the maximum phase difference for a given microphone spacing and signal frequency; at 800 Hz and with a 12 mm spacing the maximum phase difference should be 10°. It is unclear why we should get such an anomaly since the stationarity measurements at 800 Hz in the x-axis reveal that the intensity level does not vary with time, as would be expected for a modal frequency. The anomaly therefore highlights the problem of not being able to determine reactivity through a single measurement. The requirement to take separate pressure and intensity measurements leads to a possible source of error in the reactivity measurements.

It can be seen from the design of the six element array that the acoustic centre

Table 5.10 ACOUSTIC INTENSITY REACTIVITY MEASUREMENTS FOR 6-ELEMENT PROBE OVER BEAM I AT GRID LOCATION 4,2

Freq. (Hz.)	Phase Change (x-axis)	Phase Change (y-axis)	Phase Change (z-axis)
100	0.97	0.02	2.44
125	0.20	0.04	0.78
160	0.12	0.43	0.55
200	0.01	0.02	4.25
250	0.97	0.13	0.43
315	1.09	1.46	0.82
400	0.76	0.56	1.09
500	0.03	0.31	1.19
630	3.80	0.59	2.00
800	67.66	2.89	8.13
1000	3.29	1.73	0.97
1250	2.06	0.71	6.37

Table 5.11 ACOUSTIC INTENSITY STATIONARITY MEASUREMENTS FOR 6-ELEMENT PROBE OVER BEAM I AT GRID LOCATION 4,2

Freq. (Hz.)	Standard Deviation (x-axis)	Standard Deviation (y-axis)	Standard Deviation (z-axis)
100	ab	ab	b
125	ab	ab	ab
160	b	1.56	4.82
200	ab	ab	1.55
250	2.05	a	2.49
315	1.35	1.32	2.10
400	1.23	1.24	1.51
500	ab	ab	0.70
630	0.38	4.11	0.75
800	0.63	0.74	0.84
1000	0.36	1.43	ab
1250	0.58	a	0.47

a = one or more values below 40 dB.
b = direction of acoustic energy changes during measurement.

of the probe cannot be held as close to the surface as is done for the two element side-by-side configuration. In order to measure the effect of this, two intensity scans were carried out. In the first, the face-to-face microphone pair was removed to allow the measurement of the x- and y-components of the intensity vector with the acoustic centre at the same height above the surface as the side-by-side configuration. These x- and y-components of the intensity vector are represented in Figure 5.17 by vectors for the four modal frequencies 160 Hz, 315 Hz, 400 Hz and 800 Hz. See Appendix B for an explanation of the vector maps.

When all three microphone pairs were used, this moved the acoustic centre of the probe to 35 mm above the surface of the beam. These intensity scans are shown in Figure 5.18. The x- and y-components of the intensity vector are represented by vectors whilst the normal (z-) component is shown by a contour map. Only the four modal frequencies (160 Hz, 315 Hz, 400 Hz and 800 Hz) are shown. It can be seen that the increased height reduced the clarity of both the vector and contour maps, with the 315 Hz modal pattern becoming much more difficult to interpret.

It was concluded that while the vector maps themselves offered interesting information regarding the in-plane energy flow - for example, the anti-clockwise energy circulation at 315 Hz, the information does not facilitate the recognition of modal shapes in this particular structure. In fact, the increased height above the surface reduces the clarity of the contour maps and these are the patterns which provide the clearest

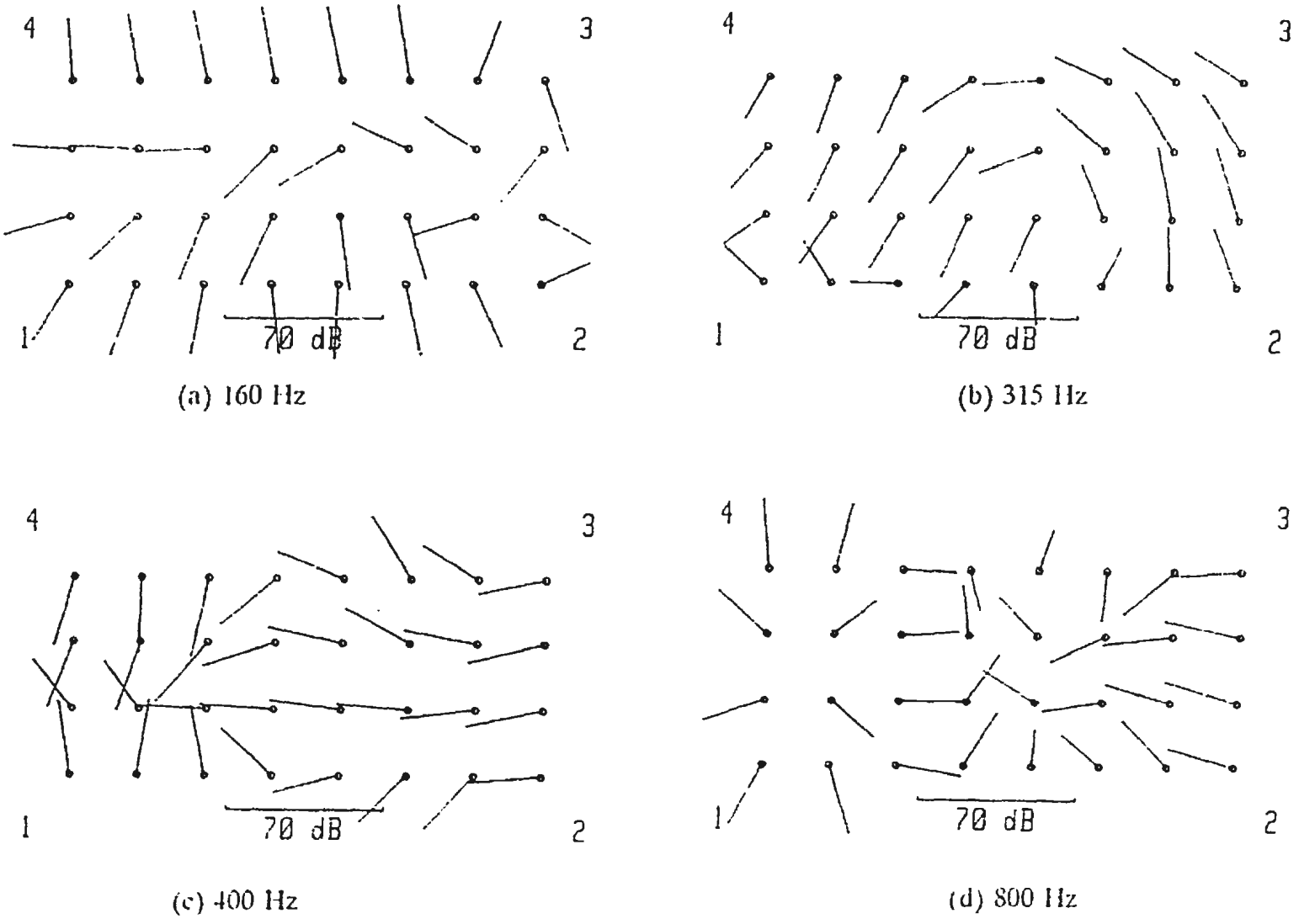

(a) 160 Hz

(b) 315 Hz

(c) 400 Hz

(d) 800 Hz

Figure 5.17 1/3 Octave Vector Maps of In-Plane Intensity Components over Beam I.
Excitation: 1 kHz White Noise

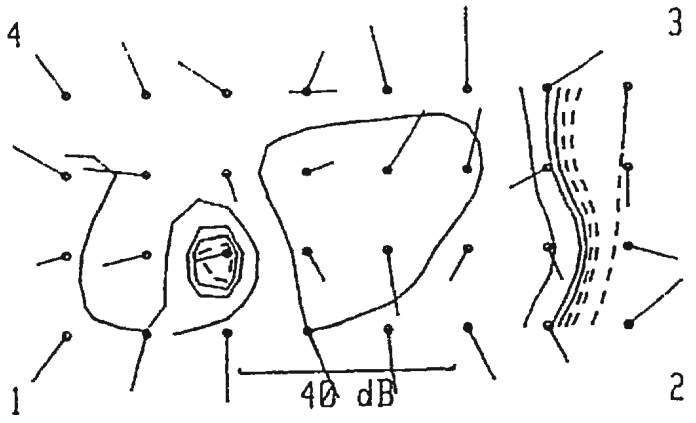

(a) 160 Hz

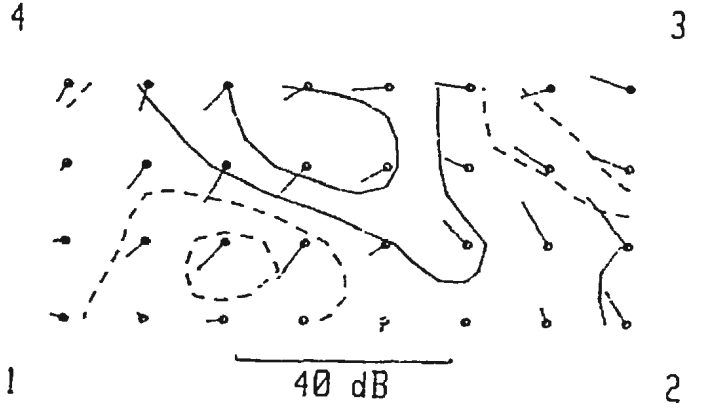

(b) 315 Hz

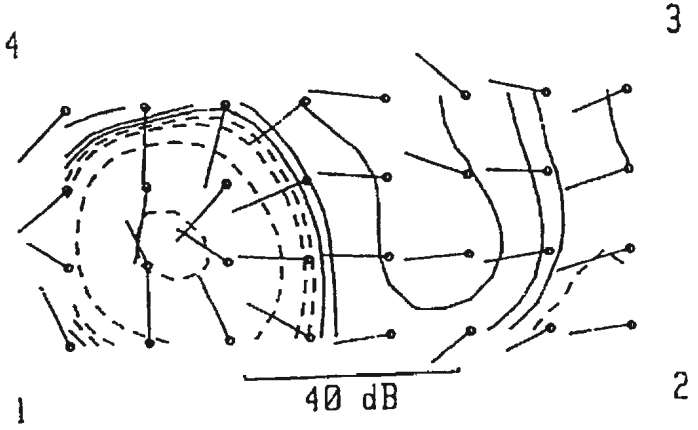

(c) 400 Hz

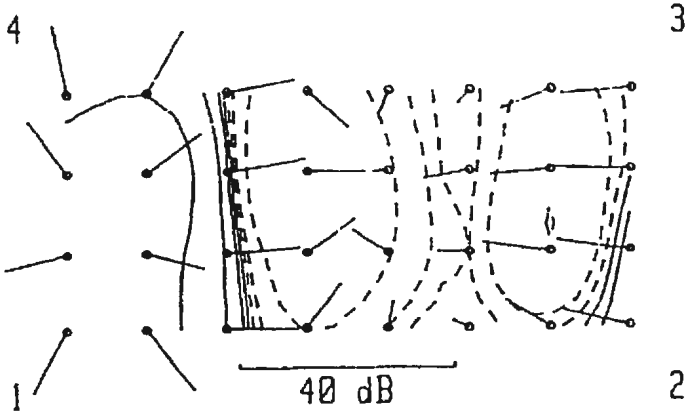

(d) 800 Hz

Figure 5.18 1/3 Octave Combine Contour and Vector Maps of Intensity Vector over Beam 1. Contour Lines at 5 dB Intervals; Excitation: 1 kHz White Noise

correlation with the modal shapes. It should be noted, however, from the in-plane energy flow measured at the torsional mode that this information may of use in more complex structures.

5.4.7 Measurements made on Beam I after Notching

In order to investigate the change in the modal behaviour of Beam I, a notch was cut into it using a band-saw. The following measurements were then made with the beam excited by 1 kHz bandwidth random noise (all measurements were made with the 1/4" microphone pair in side-by-side configuration for intensity unless otherwise stated):

a) Single point reactivity at two grid points (4,1 and 12,1) as well as swept reactivity. These data are given in Table 5.12. As stated earlier, the phase changes across the microphone pair indicate that the principal energy flow is in the direction measured and that the values are sufficient to minimize any phase error.

b) Stationarity measurements at grid points 4,1 and 12,1. These data are listed in Table 5.13. The measurements indicate that the readings in most frequency bands are stationary and that valid intensity scans can be made on the notched beam.

Table 5.12 SINGLE POINT AND SWEPT REACTIVITY MEASUREMENTS FOR BEAM I AFTER NOTCHING

Freq. (Hz.)	Phase Change (4,1)	Phase Change (12,1)	Phase Change (Swept)
100	0.79	0.03	0.01
125	0.73	0.32	1.03
160	0.76	0.62	1.23
200	2.81	3.70	1.12
250	1.76	6.24	1.88
315	1.61	1.61	0.12
400	2.57	1.78	0.62
500	2.99	0.29	1.37
630	9.12	0.34	2.57
800	12.31	8.92	4.08
1000	7.37	3.29	4.34
1250	9.64	3.34	8.59

Table 5.13 STATIONARITY MEASUREMENTS FOR BEAM I AFTER NOTCHING

Frequency (Hz.)	Standard Deviation 4,1	Standard Deviation 12,1
100	ab	b
125	2.18	1.84
160	0.93	3.82
200	1.60	0.75
250	1.77	1.09
315	1.16	1.90
400	1.40	b
500	0.41	ab
630	0.57	b
800	0.93	0.77
1000	2.00	1.08
1250	0.77	0.53

a = one or more values below 40 dB.
b = direction of acoustic energy changes during measurement.

c) 1/12-octave accelerometer spectra at grid point 4,1. The spectrum is displayed in Figure 5.19. Comparison with Figure 5.6 (Intensity spectrum at the same location on the un-notched specimen) reveals that notching has caused a clear downward shift in modal frequency from 307 Hz to 290 Hz for the first torsional mode and from 387 Hz to 365 Hz for the third bending mode.

d) Intensity maps of the intensity vector component normal to the surface of the beam. These data are given as contour maps in Figure 5.20 for the frequency range 100 Hz to 1250 Hz. Comparing these maps with Figure 5.12 it is observed that the contour maps of all of the frequency values below 800 Hz are modified following notching. Looking at each resonant frequency, we find that intensity levels have increased in the frequencies below resonance while above the resonant frequency the intensity values have decreased.

5.5 ACOUSTIC AND ACCELEROMETER MEASUREMENTS FOR BEAM II

5.5.1 Single Component Acoustic Intensity Scans

With the beam excited using 1 kHz bandwidth random noise, the following acoustic measurements were made using a 1/4" microphone pair in the side by side configuration in order to measure pressure or the component of the acoustic intensity vector normal to the beam.

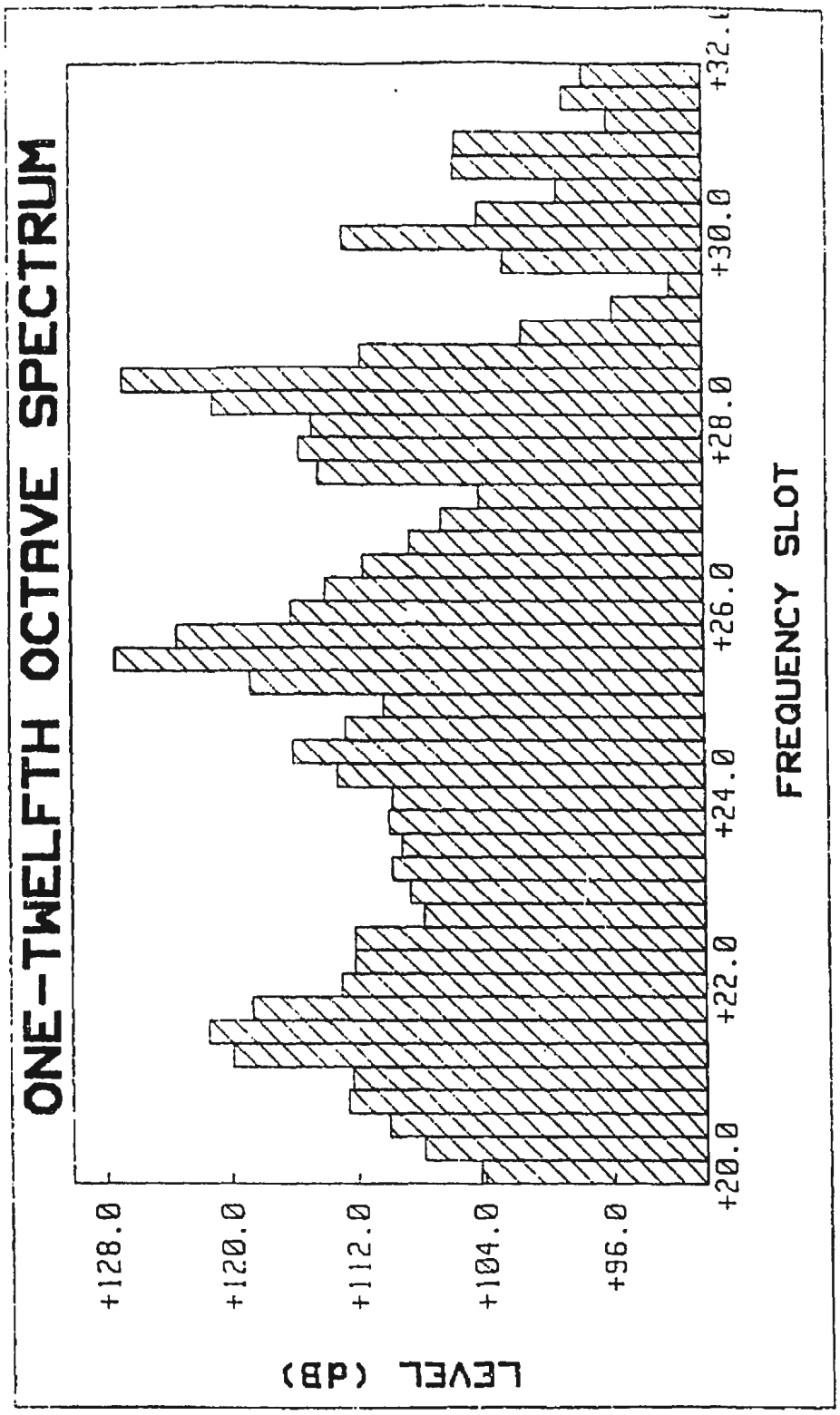

Figure 5.19 1/12 Octave Accelerometer Spectrum at Position 4,1 on Beam I after Notching

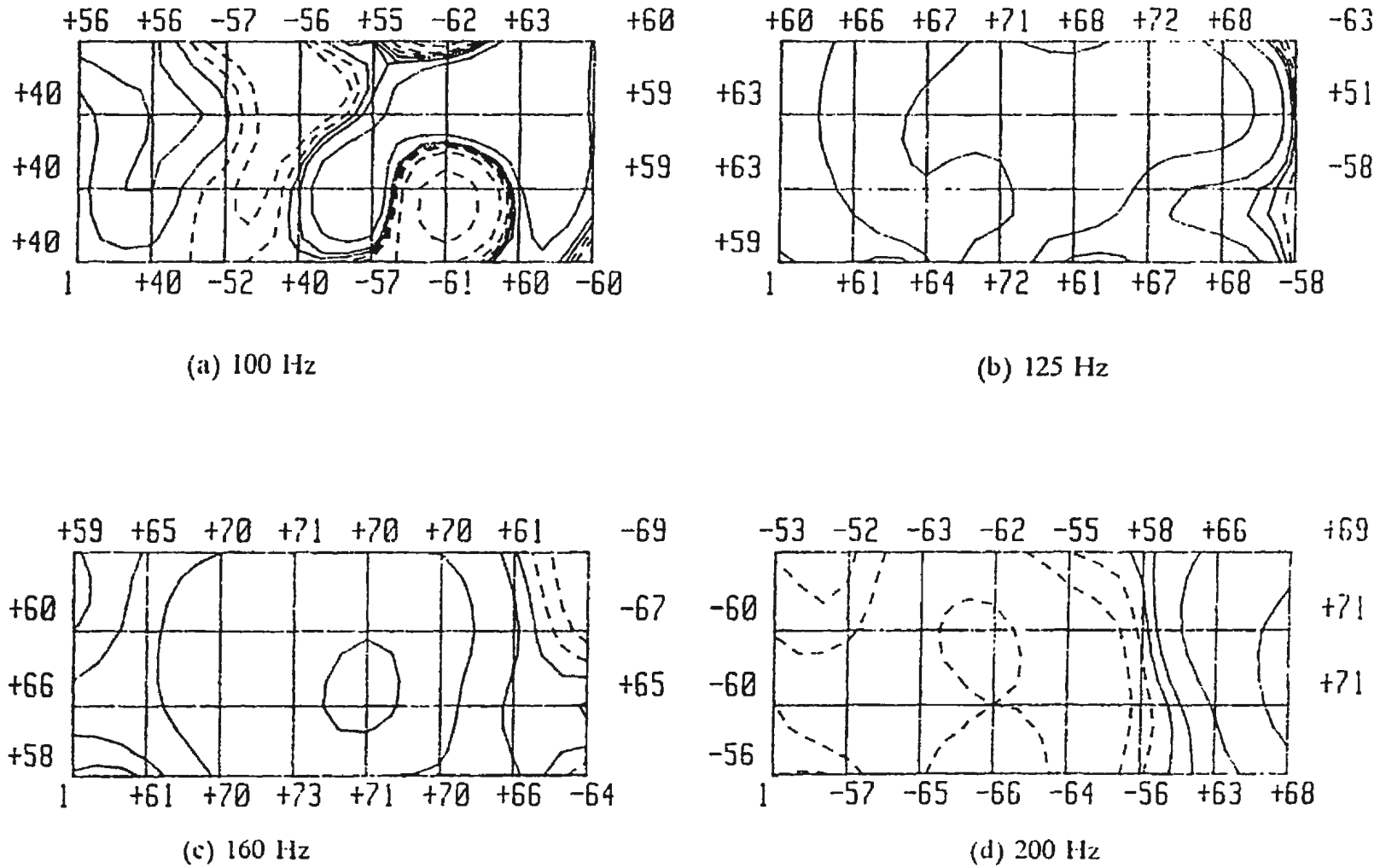

Figure 5.20 1/3 Octave Contour Maps of Normal Intensity Component over Beam 1 after Notching. Contour Lines at 5 dB intervals. Excitation: 1 kHz White Noise

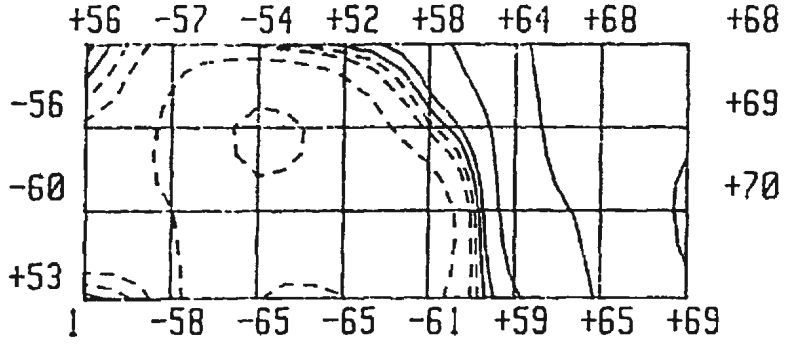

(e) 250 Hz

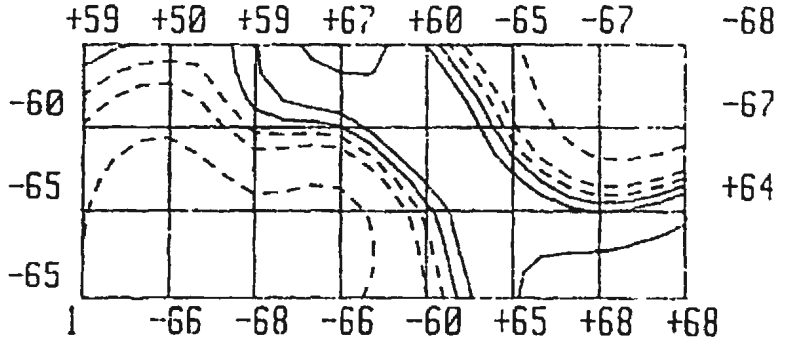

(f) 315 Hz

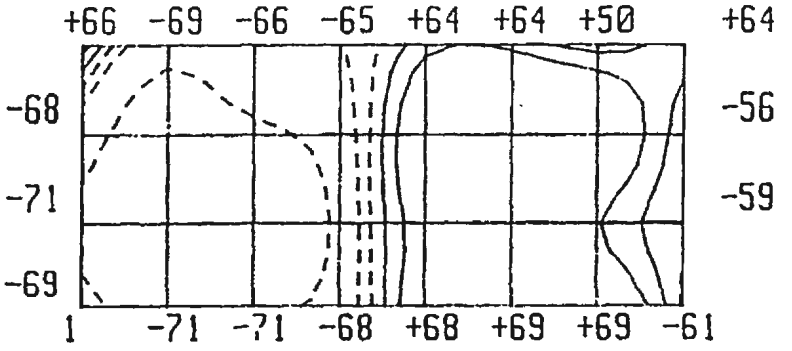

(g) 400 Hz

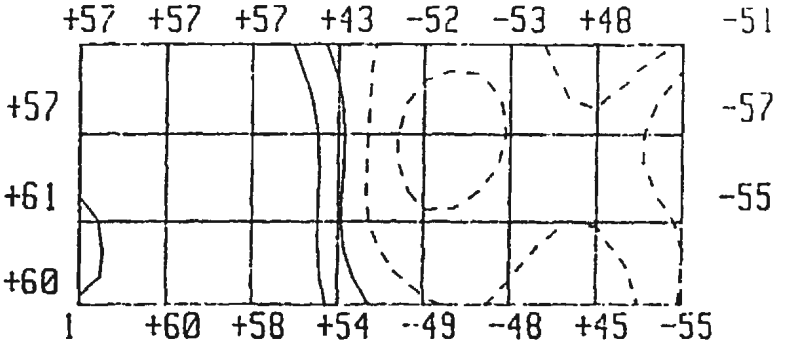

(h) 500 Hz

Figure 5.20 Continued...

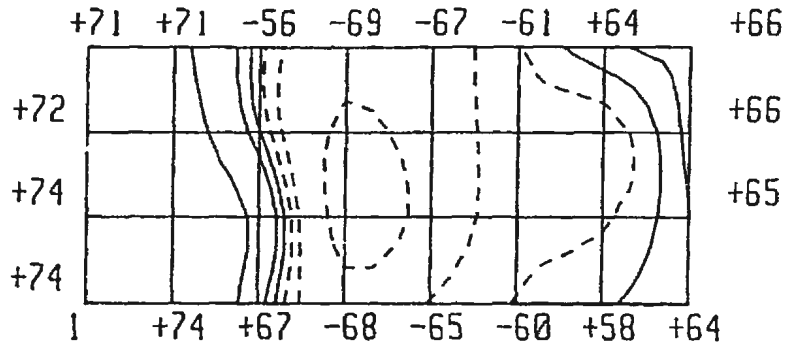

(i) 630 Hz

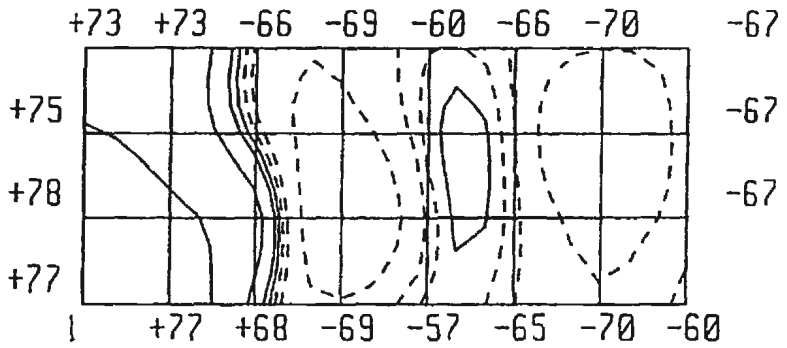

(j) 800 Hz

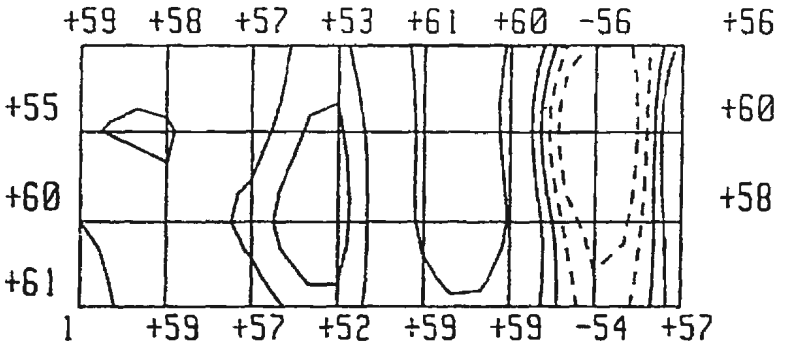

(k) 1000 Hz

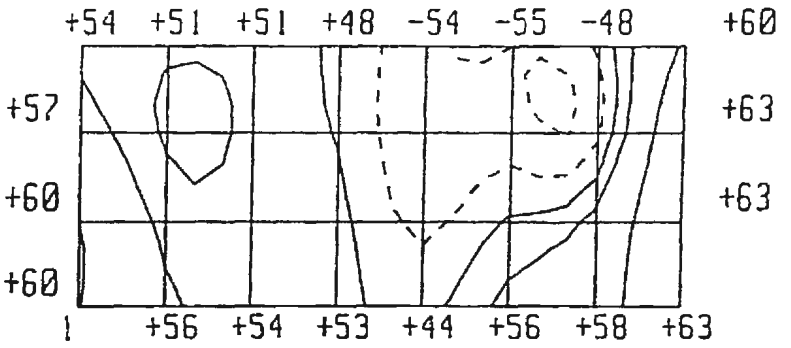

(l) 1250 Hz

Figure 5.20 Continued...

a) The experimentally identified modal frequencies using modal testing and the 1/12-octave intensity spectrum are compared with theoretically computed values in Table 5.14

b) Reactivity at the grid location 4,1 as well as the reactivity from sweeping the microphone over the surface (Table 5.15). Except at 630 Hz the swept and single point reactivities agree well.

c) Stationarity measurements at grid location 4,1 (Table 5.15). The values indicate that there is little variation in the sound field over time.

d) Acoustic Intensity scans over the frequency range 100 to 1600 Hz (Figure 5.21). The modal behaviour is exhibited most clearly at 500 Hz where the first torsional mode can be seen. This clarity probably arises from the narrow resonant response that can be seen in the accelerometer spectra shown in section 5.5.2. The intensity scans at the other frequencies do not show clear modal characteristics. However, when examined following identification of the modal frequencies, it is possible to recognize some of the modal pattern elements in the second bending mode at 400 Hz and in the second torsional mode at 1600 Hz.

Table 5.14 COMPARISON OF THEORETICALLY AND EXPERIMENTALLY DETERMINED MODAL FREQUENCIES FOR BEAM II

Mode Number	Mode Shape	Frequency (Hz) for different techniques 1	2	3	4
1	Bending	84.2	83.8	28.6	N/A
2	Bending	526.2	522.2	379.5	367
3	Torsional	N/A	663.9	504.6	550
4	Bending	1475.8	1460.0	1023.4	917
5	Torsional	N/A	2048.0	1461.0	1634
6	Bending	N/A	2861.0	N/A	N/A

1 = Beam Theory Analysis
2 = Finite Element Analysis (SAP86)
3 = Experimental Modal Analysis
4 = 1/12 Octave Intensity Spectrum

Table 5.15 ACOUSTIC INTENSITY REACTIVITY AND STATIONARITY MEASUREMENTS FOR BEAM II

	Reactivity	Stationarity	
Freq. (Hz.)	Phase Change (Swept)	Phase Change (4,1)	Standard Deviation (4,1)
100	0.79	0.11	ab
125	1.30	1.16	ab
160	0.09	1.23	ab
200	2.50	3.45	2.15
250	1.01	1.88	ab
315	0.73	0.62	1.09
400	0.14	0.08	1.62
500	1.31	3.52	1.99
630	1.82	0.87	1.73
800	4.57	2.04	0.81
1000	5.85	3.45	0.75
1250	7.66	6.37	0.56

a = one or more values below 40 dB.
b = direction of acoustic energy changes during measurement.

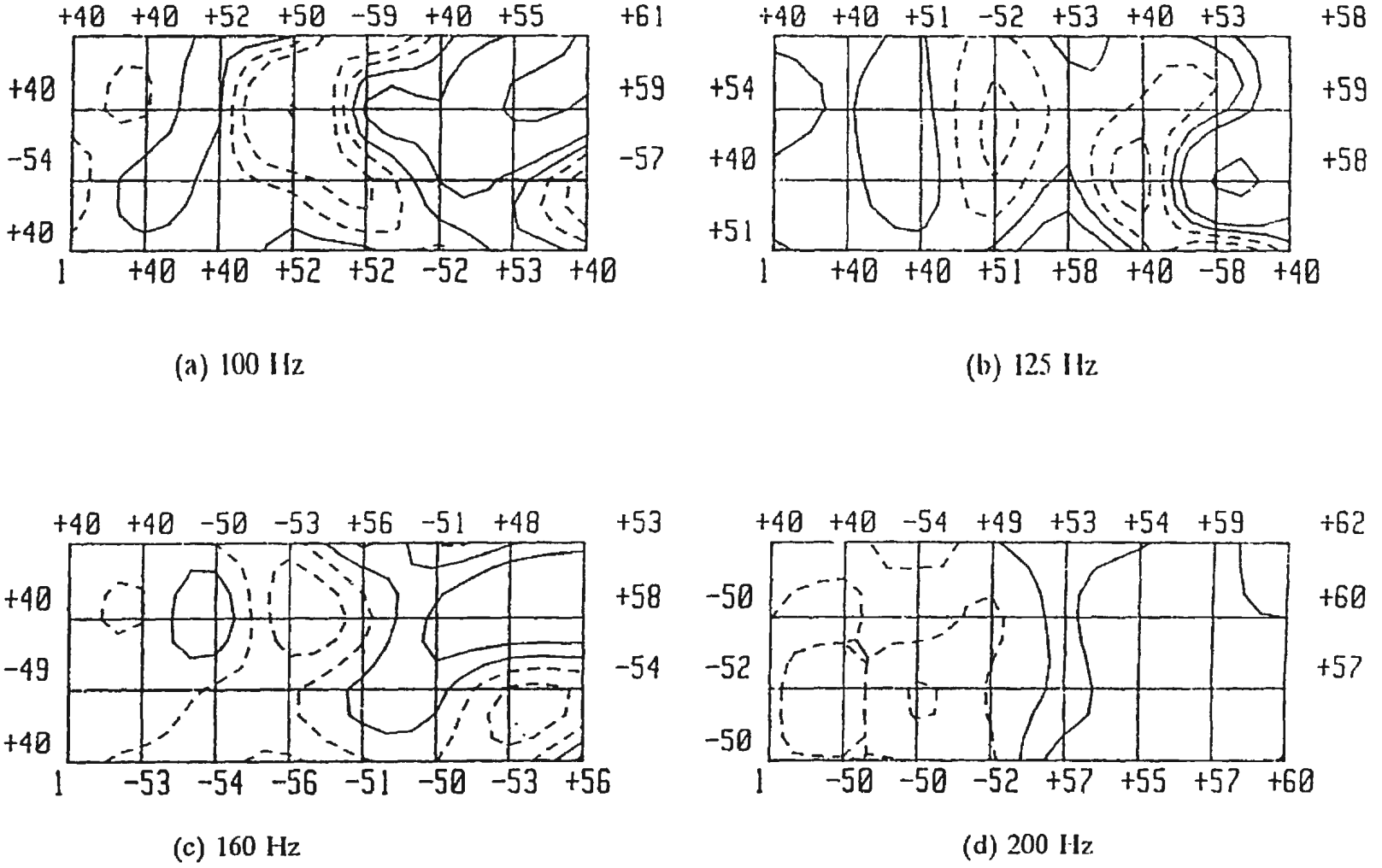

(a) 100 Hz

(b) 125 Hz

(c) 160 Hz

(d) 200 Hz

Figure 5.21 1/3 Octave Contour Maps of Normal Intensity Component over Beam II. Contour Lines at 5 dB intervals. Excitation: 1 kHz White Noise

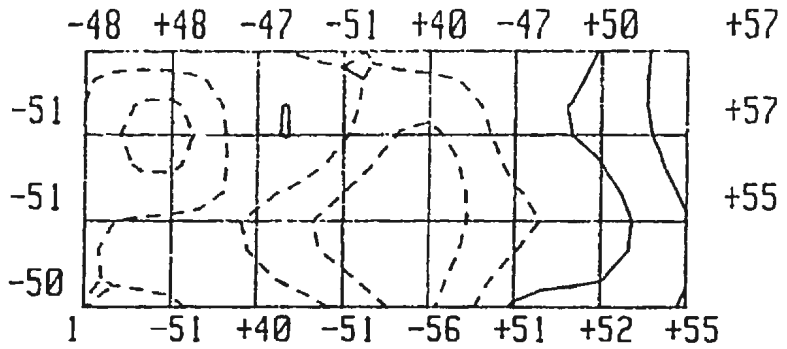

(e) 250 Hz

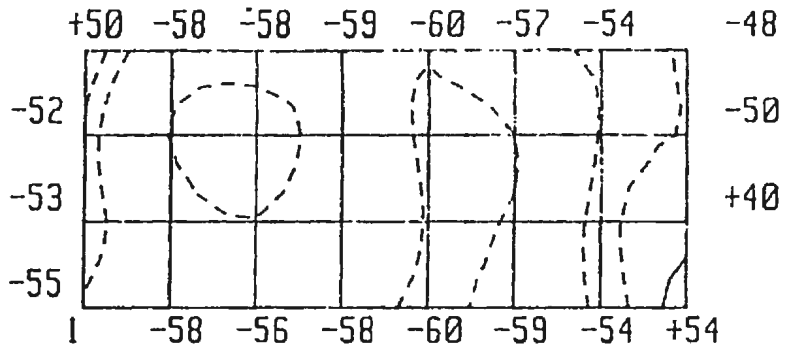

(f) 315 Hz

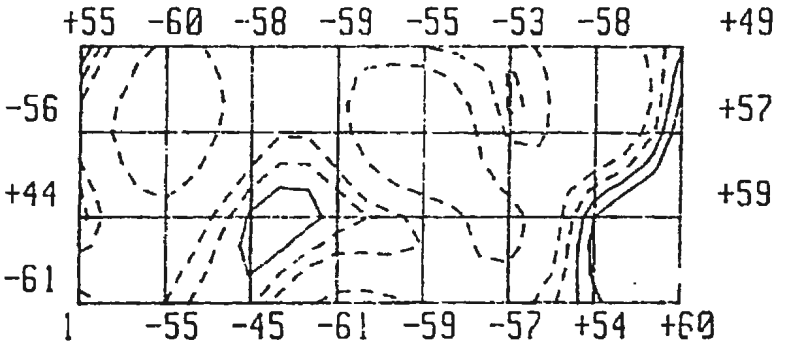

(g) 400 Hz

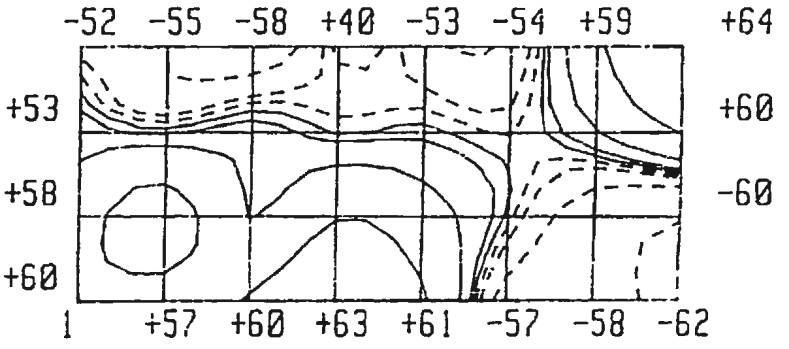

(h) 500 Hz

Figure 5.21 Continued...

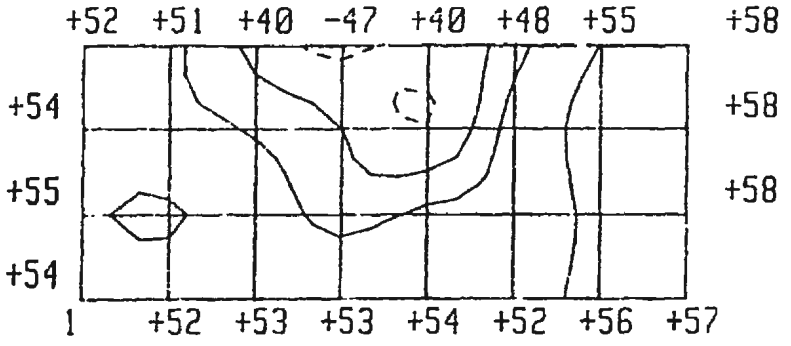

(i) 630 Hz

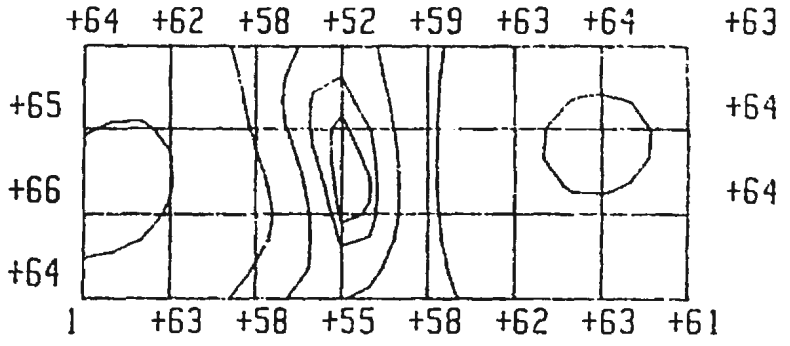

(j) 800 Hz

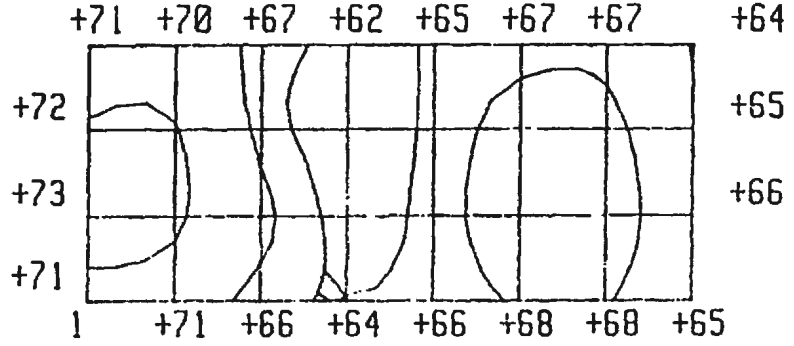

(k) 1000 Hz

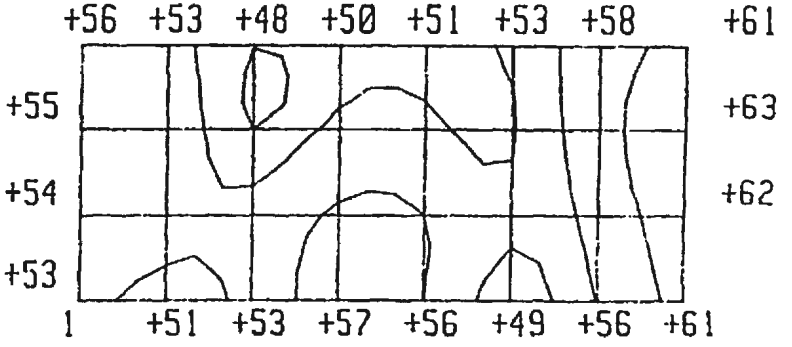

(l) 1250 Hz

Figure 5.21 Continued...

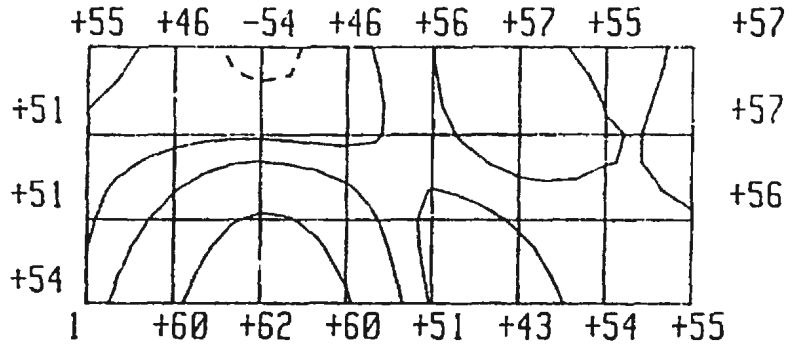

(m) 1600 Hz

Figure 5.21 Continued...

5.5.2 Accelerometer Measurements and Surface Intensity Scans

The accelerometer array was placed at grid location 3.5,0.5 and the acceleration, x-intensity and y-intensity spectra all measured using the 1/12-octave bandwidth. These spectra are shown in Figures 5.22 to 5.24. It is seen from all three of these figures that the four modal frequencies numbered 2 to 5 (see in Table 5.14 for frequencies) are clearly identified. The source of the two spurious peaks at 196 Hz and 250 Hz was considered to be unidentifiable. The surface intensity was then scanned, measuring the 1/3 octave bandwidth spectra. These data are given as vector maps over the frequency range 100 to 1600 Hz in Figure 5.25. As discussed with reference to Figure 5.21, modal behaviour is only clearly identified in the 500 Hz frequency band which encompasses the first torsional mode. In fact, it can be seen that the energy flow patterns for this mode affect the adjacent frequencies significantly, masking out any evidence of the bending mode in the 400 Hz band. The lack of clarity for the second torsional mode may arise from the fact that resolution of the measurement grid is insufficient to clearly define the energy flow.

5.5.3 Full Vector Acoustic Intensity Scanning

The six microphone array described in Section 3.5.2 was used to carry out some measurements on Beam II. As shown earlier, stationarity and reactivity measurements for each microphone pair were determined at grid location 4,2 and the results were found to be acceptable over the range of the frequency scans.

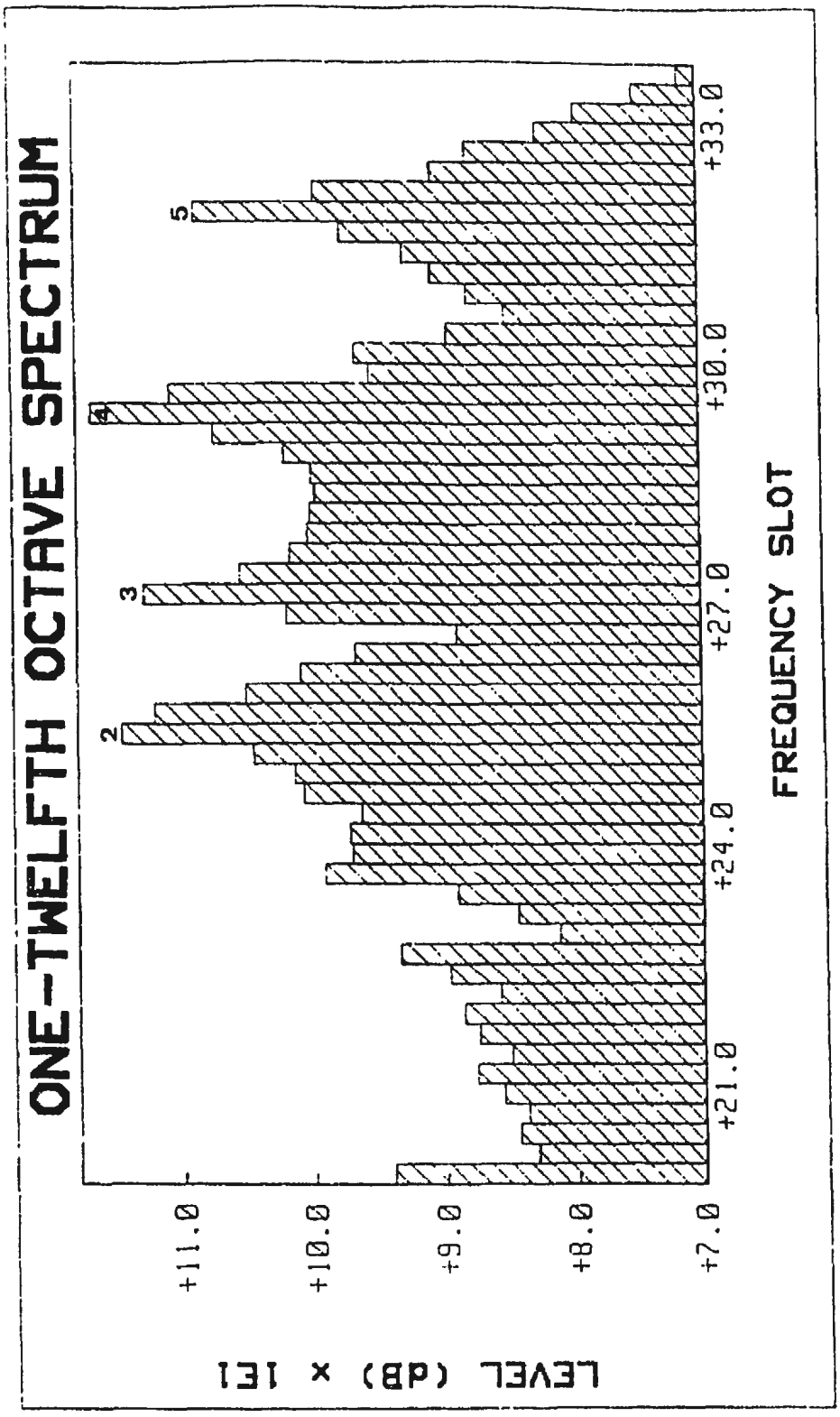

Figure 5.22 1/12 Octave Accelerometer Spectrum at Position 3.5,0.5 on Beam II

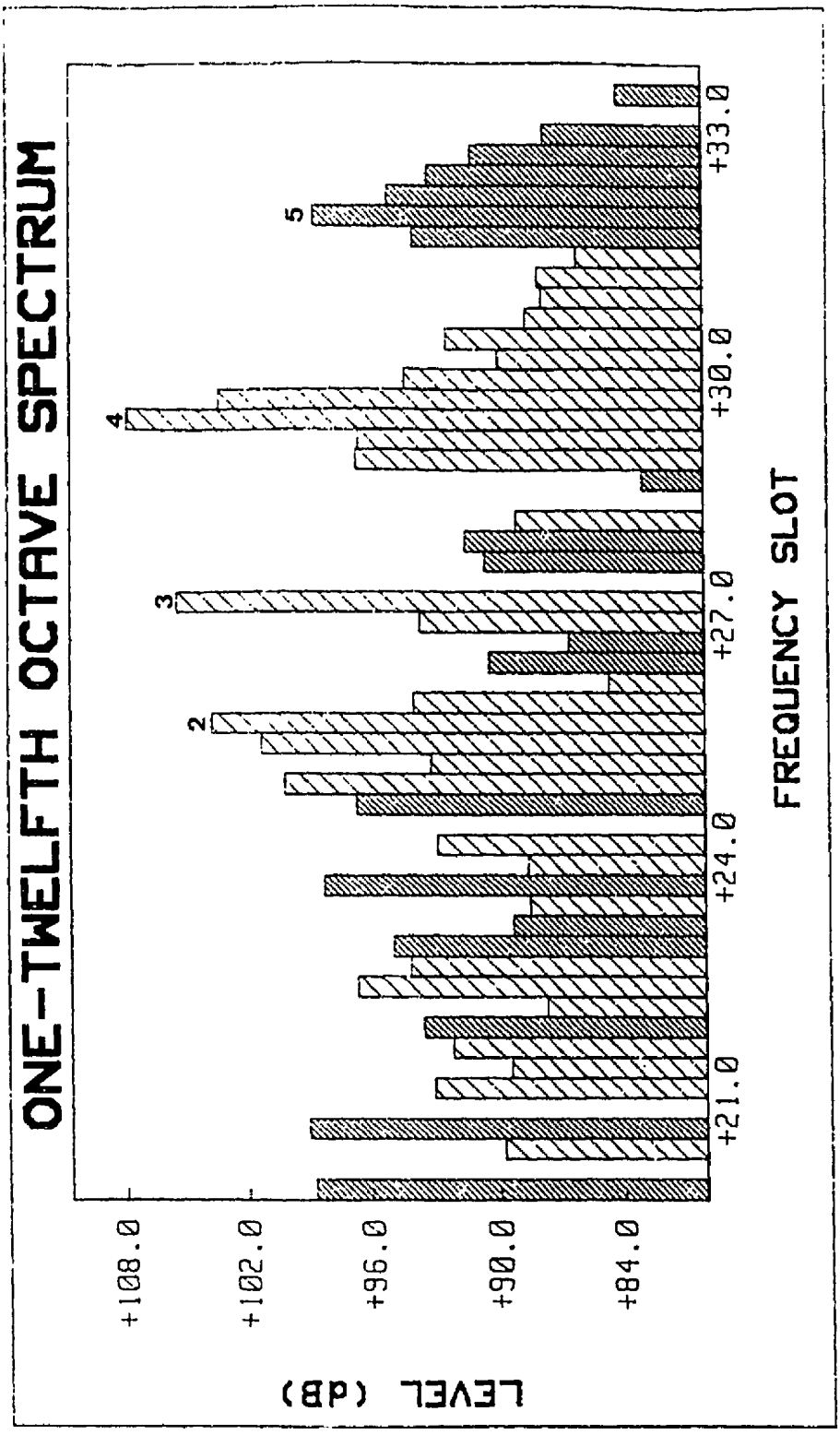

Figure 5.23 1/12 Octave Surface Intensity Spectrum (x-component) at Position 3.5,0.5 on Beam II

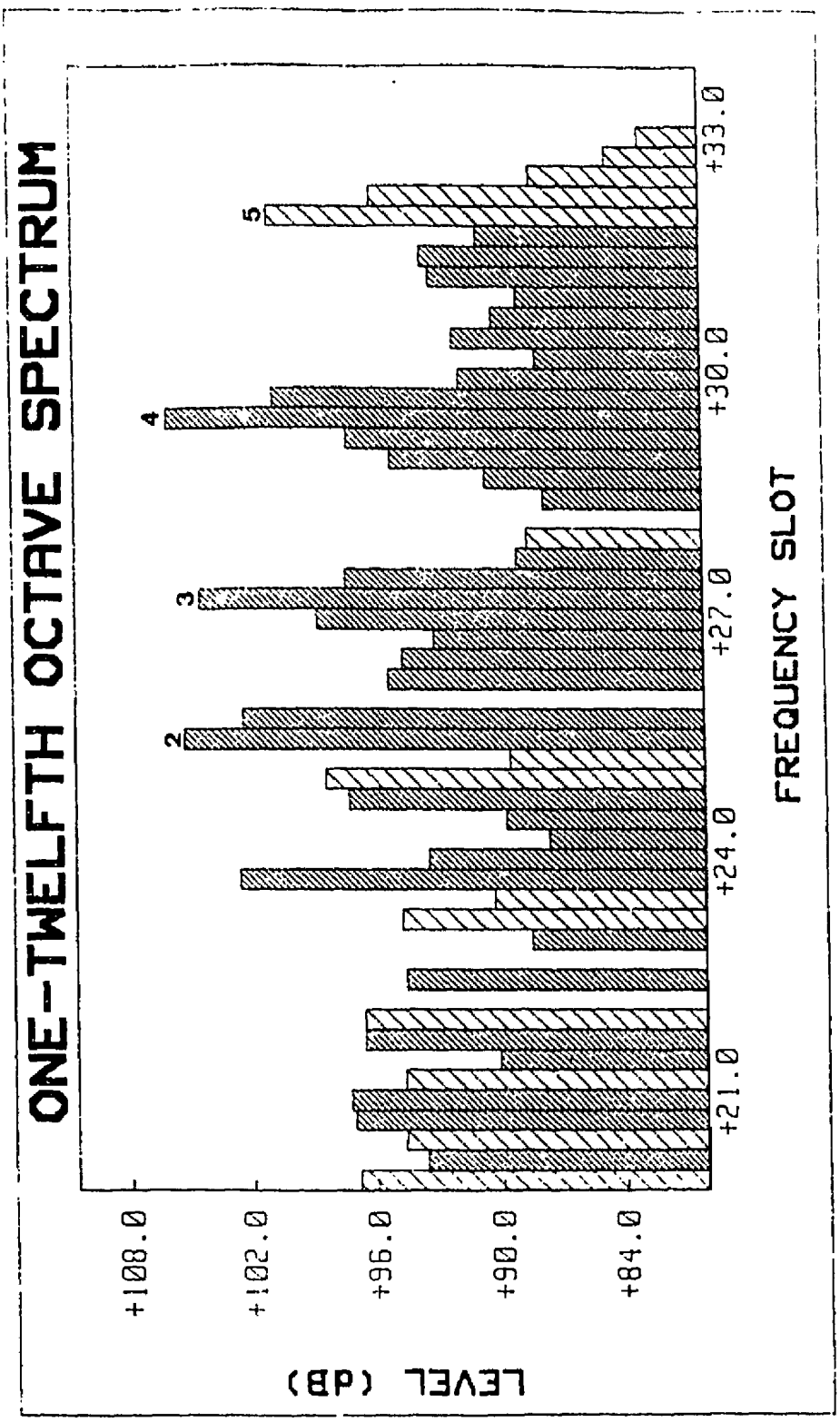

Figure 5.24 1/12 Octave Surface Intensity Spectrum (y-component) at Position 3.5,0.5 on Beam II

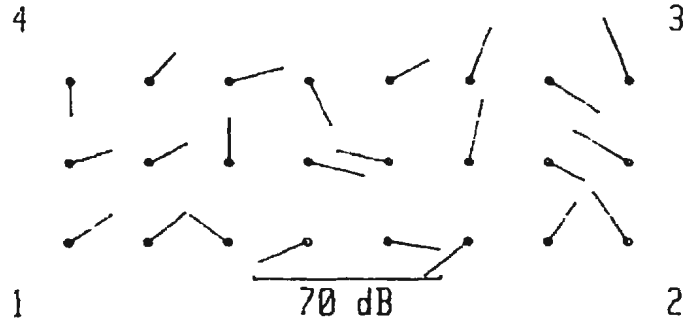

(a) 100 Hz

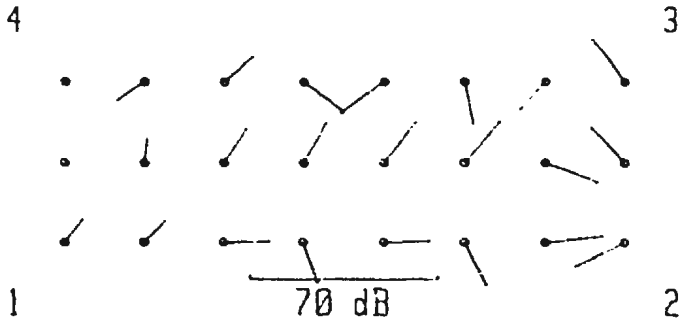

(b) 125 Hz

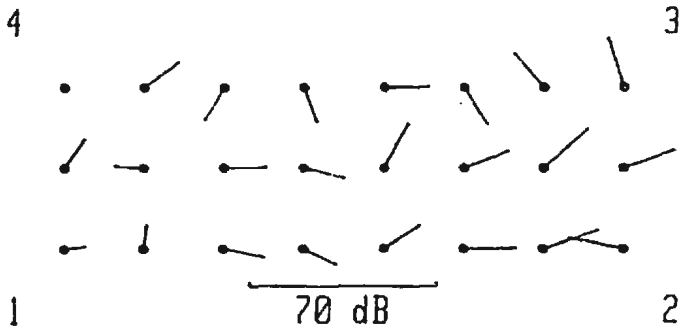

(c) 160 Hz

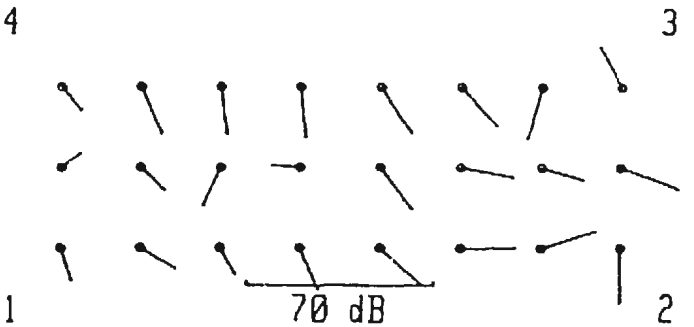

(d) 200 Hz

Figure 5.25 1/3 Octave Surface Intensity Maps of Beam II.
Excitation: 1 kHz White Noise

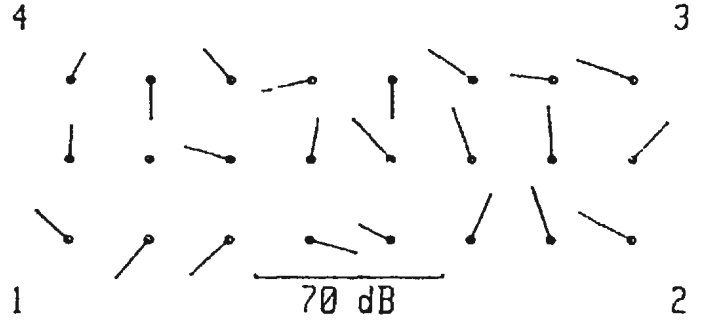

(e) 250 Hz

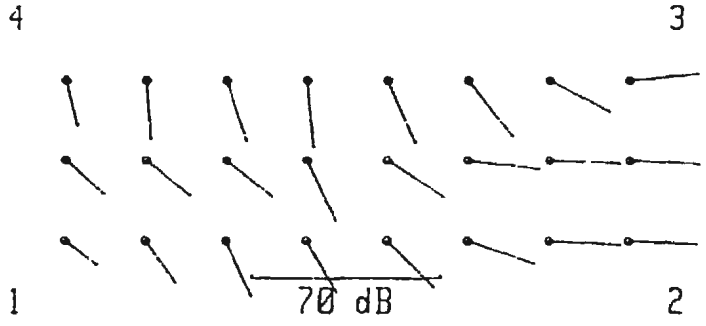

(f) 315 Hz

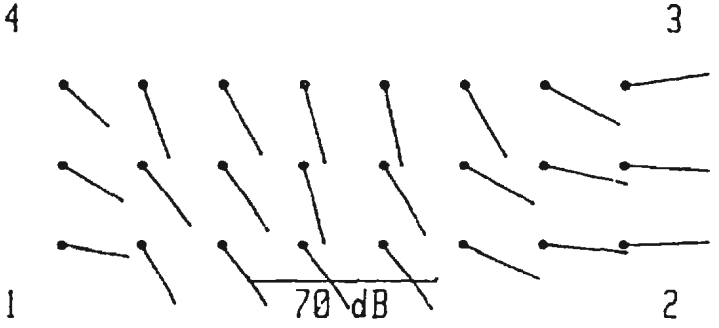

(g) 400 Hz

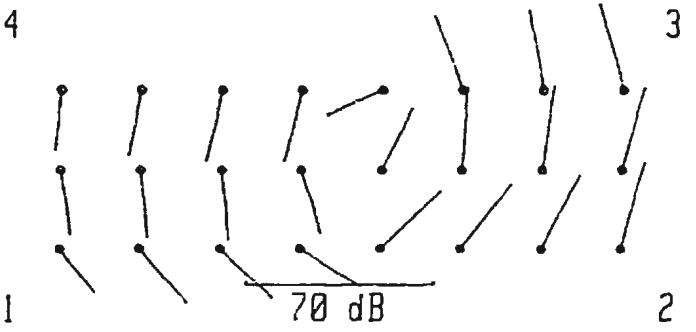

(h) 500 Hz

Figure 5.25 Continued...

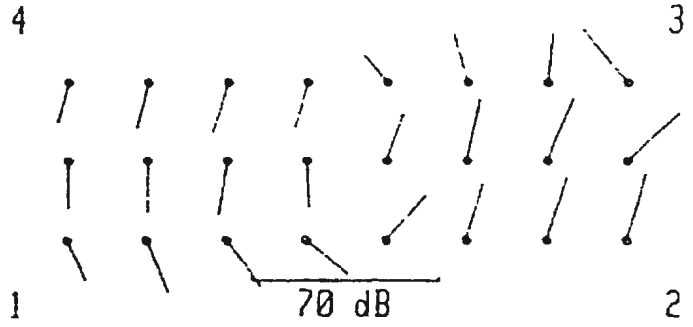

(i) 630 Hz

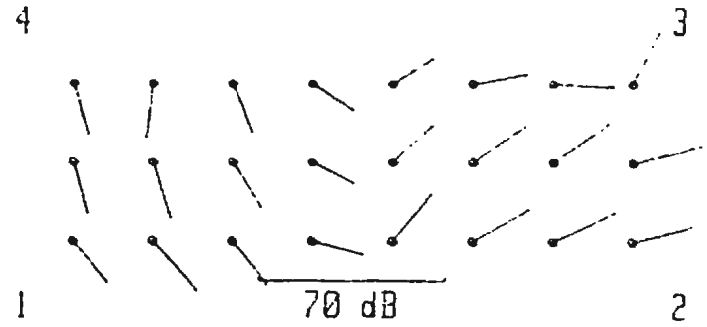

(j) 800 Hz

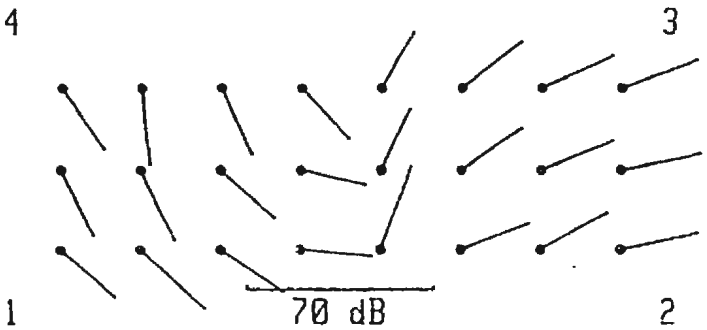

(k) 1000 Hz

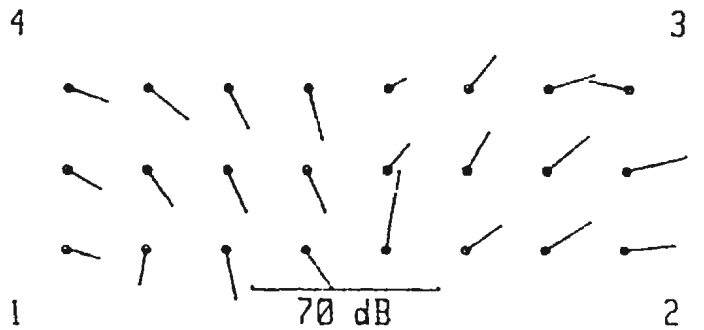

(l) 1250 Hz

Figure 5.25 Continued...

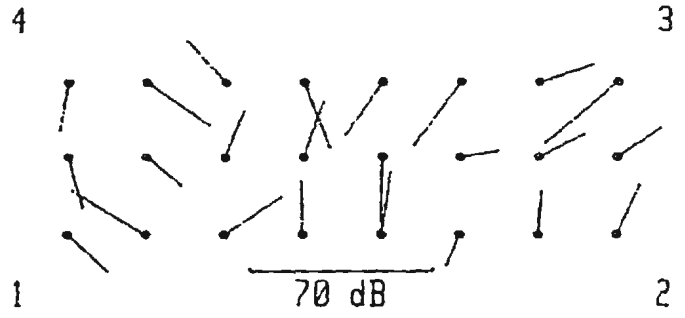

(m) 1600 Hz

Figure 5.25 Continued...

Two intensity scans were carried out. In the first, the face-to-face microphone pair was removed to allow the measurement of the x- and y-components of the intensity vector with the acoustic centre at the same height above the surface as the side-by-side configuration. These intensity scans are shown as vector maps in Figure 5.26 for the four frequency bands encompassing the 380 Hz, 405 Hz, 1023 Hz and 1461 Hz modal frequencies. In the second intensity mapping, all three microphone pairs were used. This moves the acoustic centre of the probe to 35 mm above the surface of the beam. These intensity scans are shown in Figure 5.27, again only for the four frequency bands encompassing the modal frequencies. The x- and y-components of the intensity vector are represented by vectors whilst the normal (z-) component is shown by a contour map. It is observed from Figures 5.26 and 5.27 that better modal information is obtained when the normal intensity component is included in the mapping. From Figure 5.27 the torsional behaviour at 500 Hz can be clearly identified and the modal response at 400 Hz is more clearly visualized.

5.5.4 Measurements on Beam II following Notching

Beam II was cut using a band-saw to give a 5 mm wide, 5 mm deep notch across the width of the beam on one face. Following confirmation of the reactivity and stationarity measurements, the following data were collected, using the 1/4" microphone pair in the side-by-side configuration for all acoustic measurements. The beam was excited using 1 kHz bandwidth random noise.

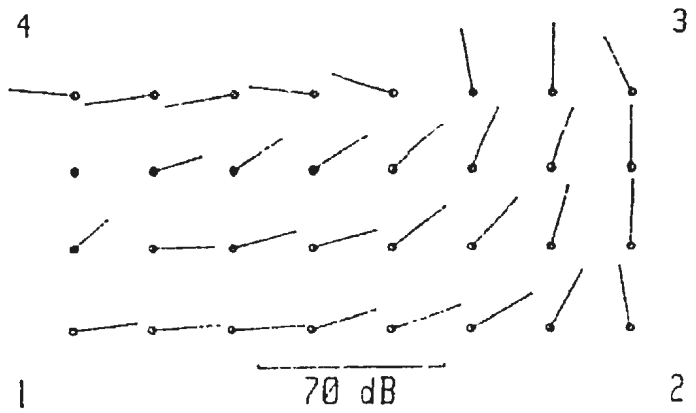

(a) 400 Hz

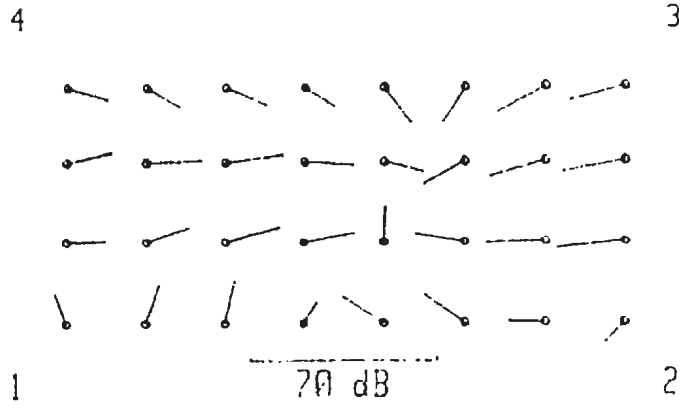

(b) 500 Hz

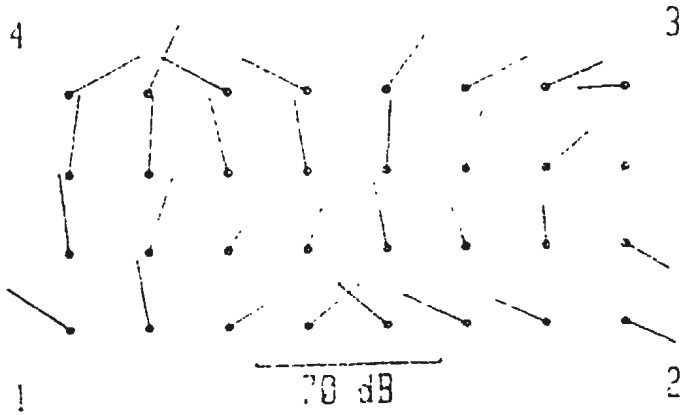

(c) 1000 Hz

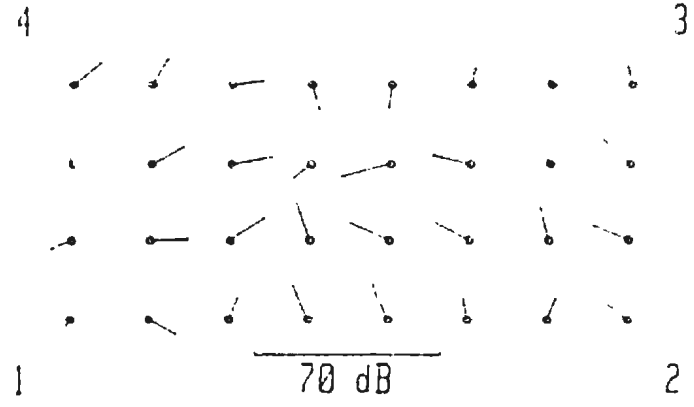

(d) 1600 Hz

Figure 5.26 1/3 Octave Vector Maps of In-Plane Intensity Components over Beam II. Excitation: 1 kHz White Noise

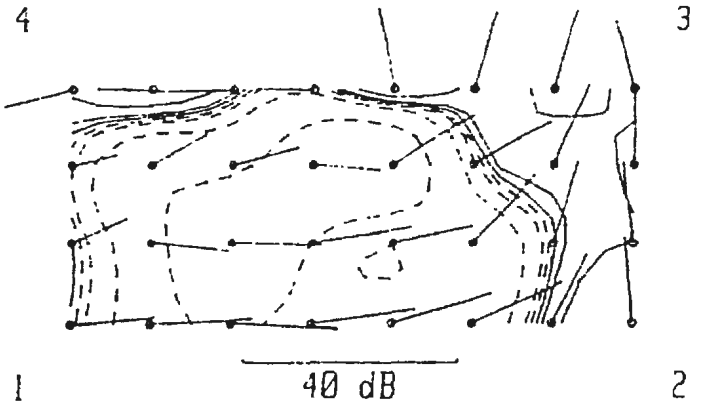

(a) 400 Hz

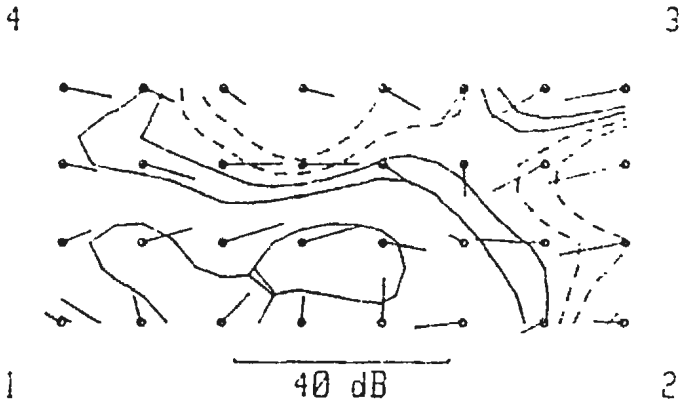

(b) 500 Hz

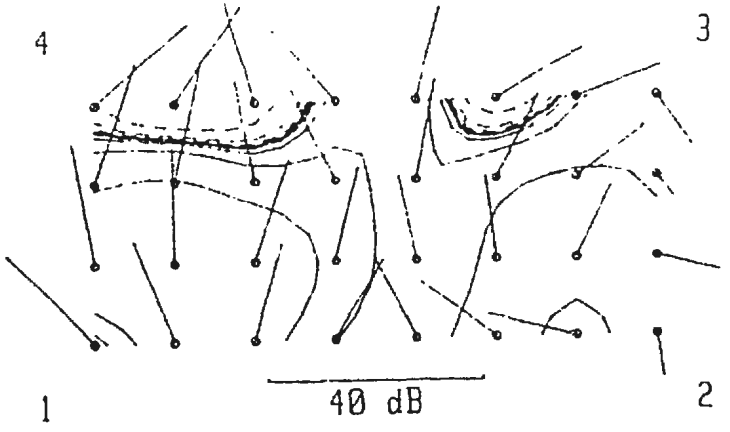

(c) 1000 Hz

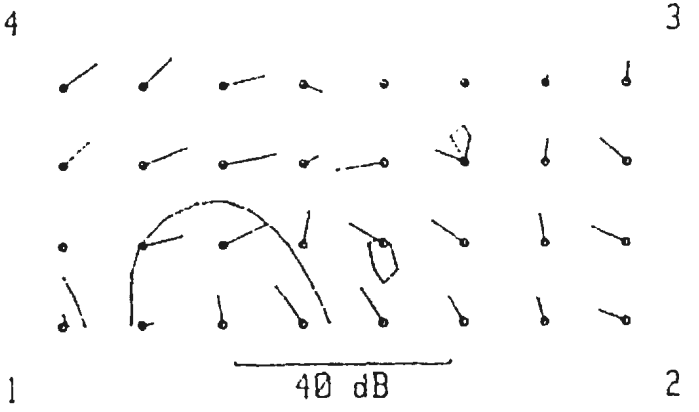

(d) 1600 Hz

Figure 5.27 1/3 Octave Combined Contour and Vector Maps of In-Plane Intensity Components over Beam II. Contour Lines at 5 dB Intervals; Excitation: 1 kHz White Noise

a) 1/12 octave accelerometer spectra at grid location 3.5,0.5, Figure 5.28. Comparison with Figure 5.22 shows that the four modal peaks can still be identified, but that the frequencies have shifted lower: Mode 2 has shifted from 365 Hz to 322 Hz; Mode 3 from 547 Hz to 488 Hz; Mode 4 from 921 Hz to 869 Hz; Mode 5 from 1640 to 1548 Hz. This would be expected as the stiffness of the beam has been reduced by the introduction of the notch.

b) Acoustic Intensity scans of the component of the intensity vector normal to the surface of the beam. These data are shown as contour maps in Figure 5.29 for the frequency bands 400 Hz, 500 Hz, 1000 Hz and 1600 Hz. The bending modes in the 400 and 1000 Hz maps and the torsional modes in the 500 and 1600 Hz maps could be visualized clearly. Comparison with Figures 5.21 and 5.27 showed that there were very clear differences in the maps for the two bending modes. In particular, looking at Figures 5.27 (a) and 5.29 (a) we can see a reversal in the direction of energy flow and this is directly comparable with the effect seen in beam I in Figures 5.15 (c) and (d). The two torsional mode patterns appear to remain unchanged following notching. A few variations between Figures 5.21 and 5.29 are noted, in particular the reduction in the intensity levels at 500 Hz following notching while the 1600 Hz band shows no change in intensity levels following notching.

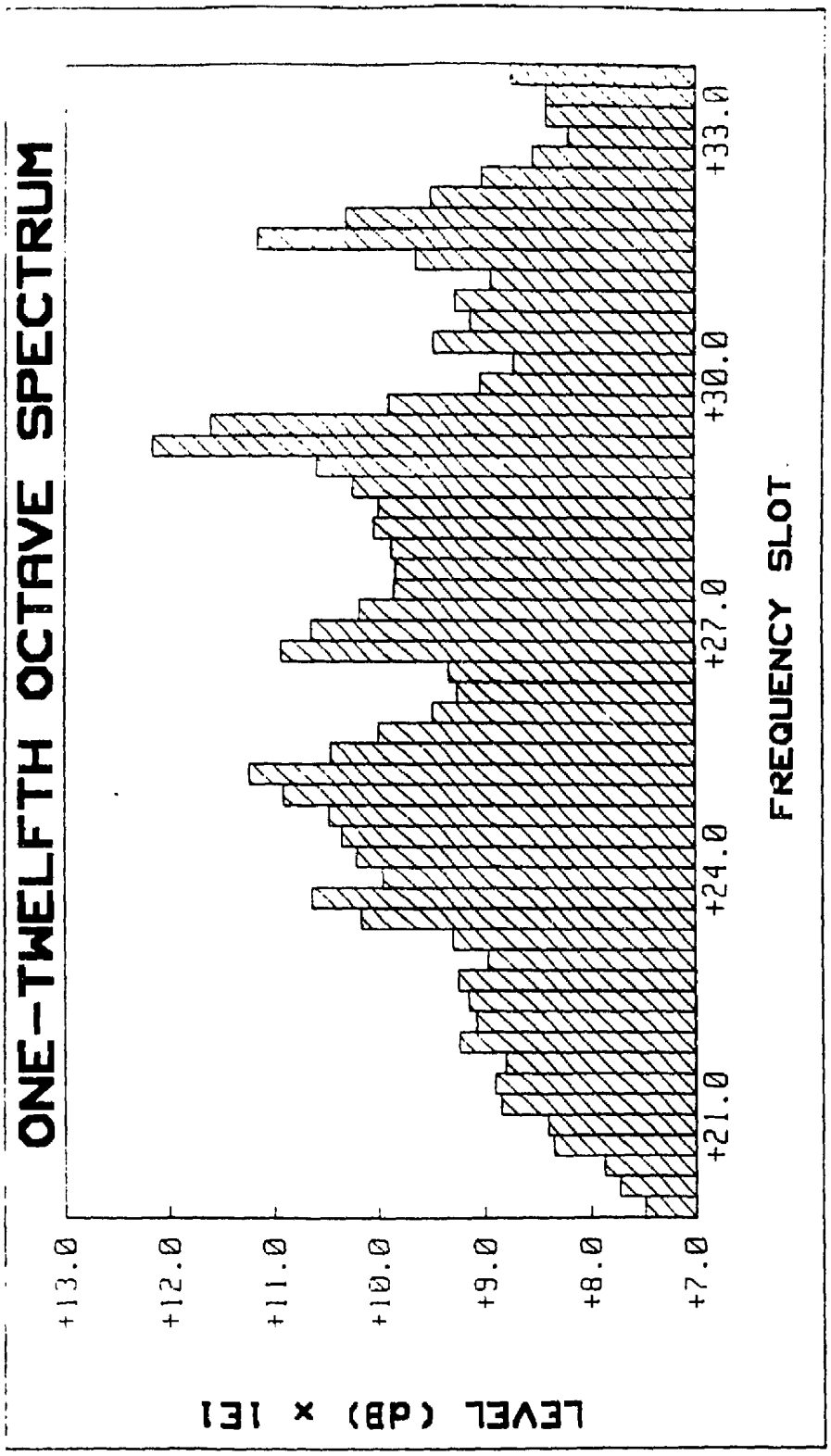

Figure 5.28 1/12 Octave Accelerometer Spectrum at Position 3.5,0.5 on Beam II after Notching.

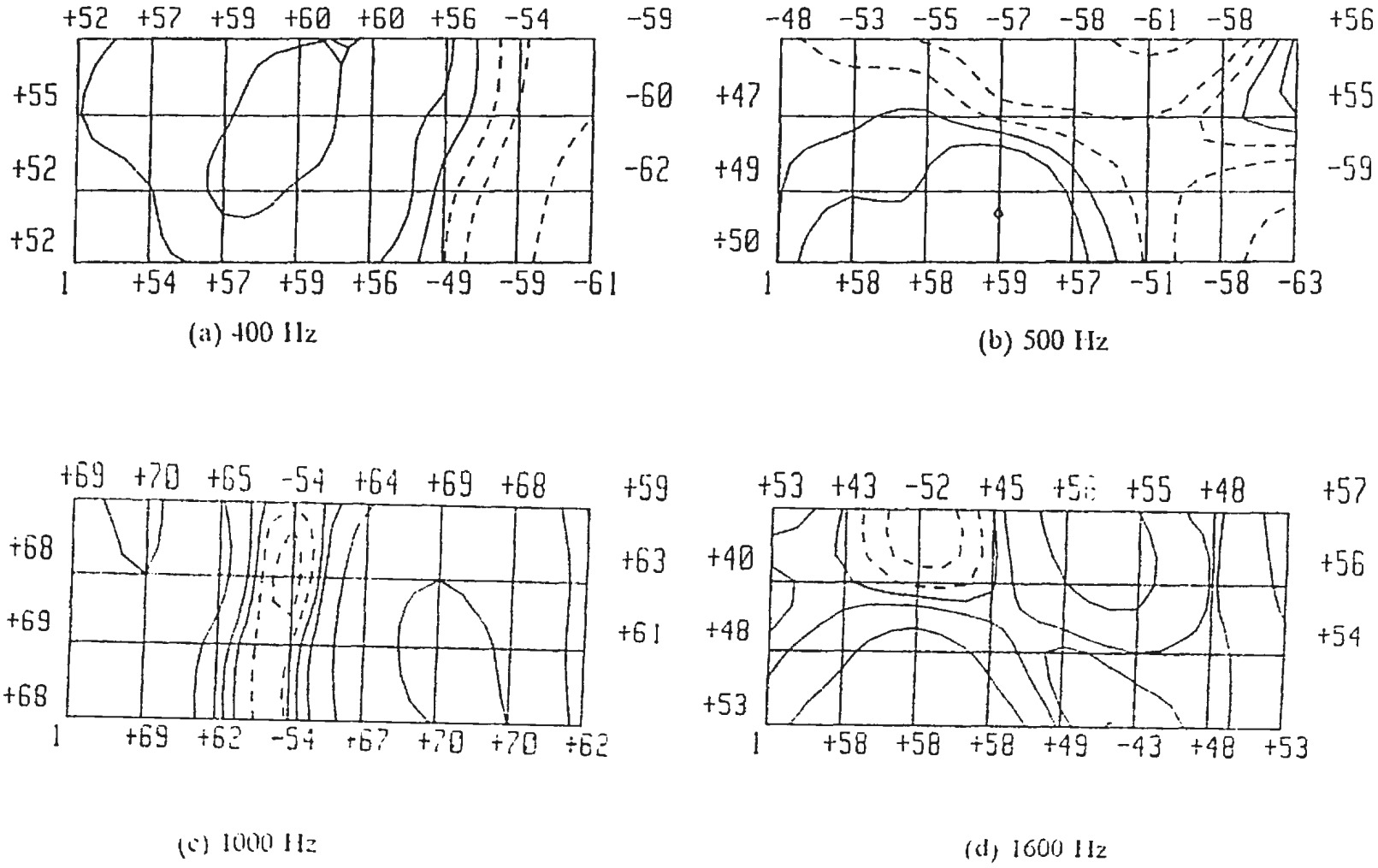

Figure 5.29 1/3 Octave Combined Contour Maps of Normal Intensity over Beam II Following Notching. Contour Lines at 5 dB Intervals; Excitation: 1 kHz White Noise

5.7 UNDERWATER ACOUSTIC PROBE MEASUREMENTS

Experiments were carried out in order to evaluate the acoustic scanning technique in an underwater environment. Beam II was suspended from a servo-hydraulic actuator so that it hung freely in a large cylindrical water tank having a depth of 1.0 m and a radius of 0.5 m. The specimen was vibrated using a pseudo-random excitation with a bandwidth of 10 kHz. Although the displacement of the specimen was negligible, significant acoustical energy was produced. The transducers used in the measurements were a pair of omni-directional hydrophones. Phase matching of the hydrophone pair had been carried out as described in Section 4.2.

The transducers mounted side-by-side in a bracket which was then suspended from a bench support system which allowed accurate and repeatable positioning of the array. The system configuration is shown in Figure 5.30. The acoustic centre of the hydrophone array was kept at 100 mm from the specimen surface and two intensity scans were carried out. The first measured the intensity component normal to the plate (z-component) and the second scan measured the intensity component across the plate (y-component). The acoustic energy flow for these two components in the 800 Hz frequency band are shown in Figures 5.31 and 5.32 in the form of contour maps and three-dimensional surface maps. The two scans were repeated in order to obtain visual confirmation of the repeatability of the measurements. It was clear that modal information could be obtained even when the beam was submerged in water.

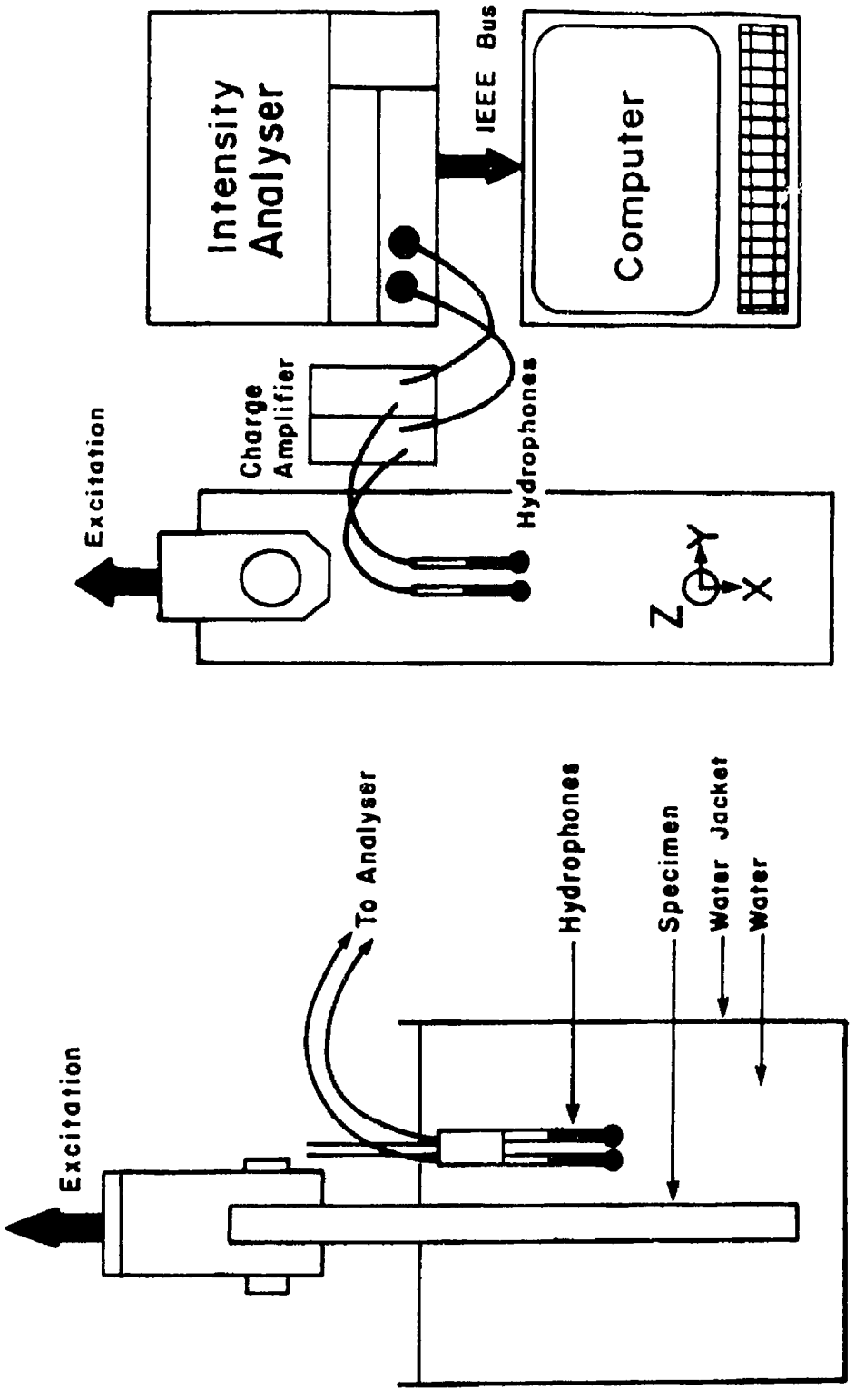

5.30 Underwater Acoustic Mapping

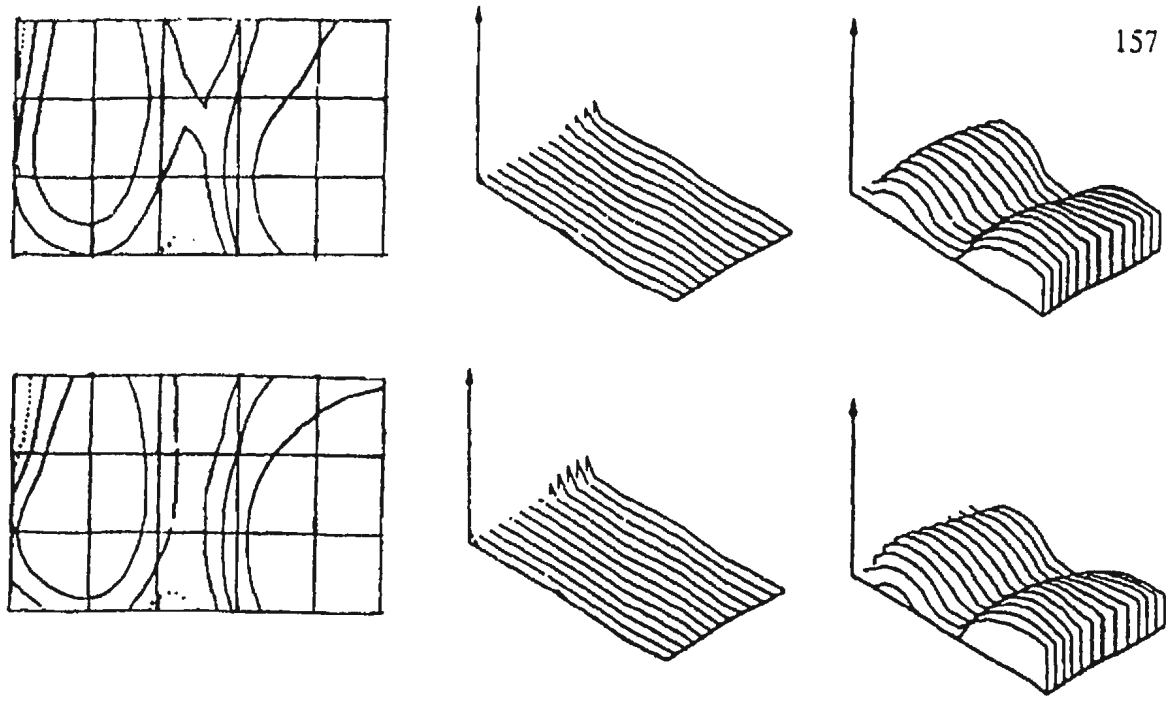

5.31 800 Hz. 1/3 Octave Contour and Surface Maps of Normal Intensity Components over Beam II. Contour Lines at 5 dB Intervals; Excitation : 1 kHz White Noise.

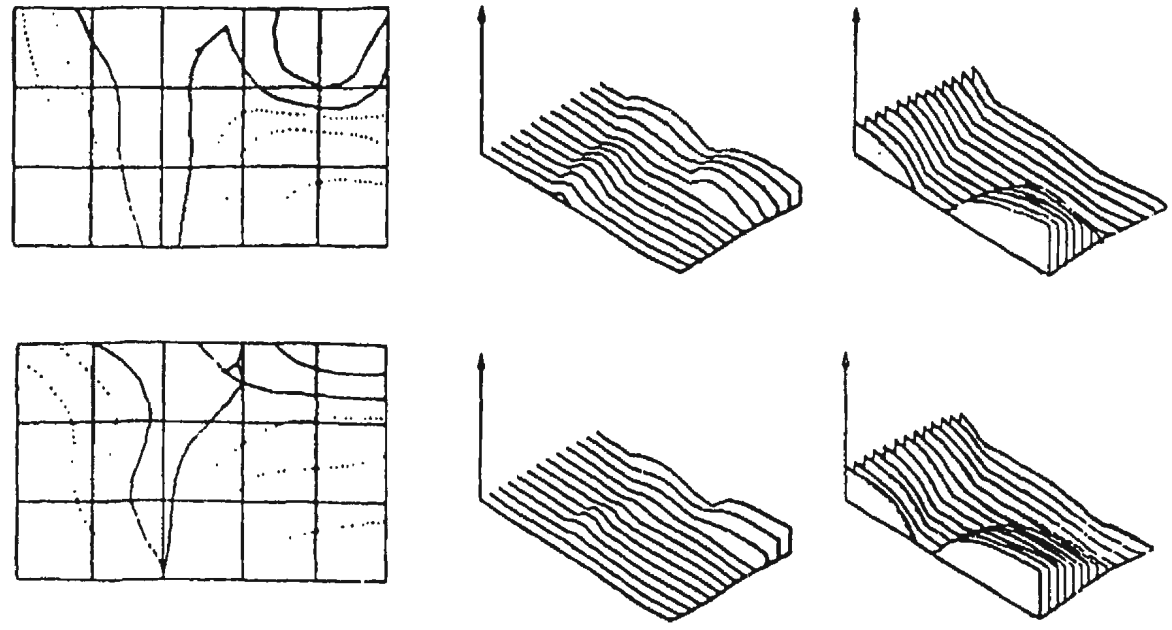

5.32 800 Hz. 1/3 Octave Contour and Surface Maps of Across-Plate Intensity Component over Beam II. Contour Lines at 5 dB Intervals; Excitation : 1 kHz White Noise.

5.9 SUMMARY

The use of a constant percentage bandwidth analyzer for determining acoustic intensity flow and relating it to modal deformation and changes in the modal frequencies due to structural change has been investigated. It has been shown that acoustic techniques can be used to identify mode shapes and modal frequencies, with a number of limitations. It has been demonstrated that the readings are stationary and that the technique adopted gives reasonably good results for both amplitude and phase. The modal frequency shift due to notching could be observed from the frequency spectra when taken at the 1/12-Octave bandwidth, but not with the 1/3-Octave spectra. Variations in the intensity patterns were noted using only the 1/3-Octave spectra. Although these were slight they did show that the analysis of the intensity maps was more sensitive than simple analysis of the 1/3-Octave spectra. It was possible to provide conclusive evidence of a shift in the modal frequency through a combined interpretation of the 1/12-Octave spectrum data and the 1/3-Octave intensity maps.

6.0 FURTHER DISCUSSION AND CONCLUSIONS

6.1 FURTHER DISCUSSIONS

The acoustic intensity scanning technique has been shown to be able to identify the modal information of a structure. The change of the energy flow with increasing distance from the surface has been determined in air and this variation showed that in order to successfully measure the modal deformation of a structure the measurements must be made in the near-field of the structure. The residual intensity index measurement as a method for determining data reliability have been evaluated and a new measurement, the stationarity of the measured intensity, has been developed. The stationarity measurements have been shown to improve the data analysis by identifying frequency bands in which variations in the energy flow occur over the measurement period and hence made these data unreliable.

Surface energy flow was also measured and shown to correlate well with both the acoustic energy flow and with the modal deformation of the structure.

In order for acoustic scanning to become widely applicable as a non-destructive testing technique it must be possible to transfer it to underwater applications. Because the acoustic theory is the same in both water and in air, the measurement techniques can be used in both media. The measurement transducers must be modified, and this was

accomplished with well established underwater technology. Hydrophones were evaluated for use as intensity probes and were shown to have phase matching and directional properties of the necessary sensitivity. Underwater intensity mapping was successfully carried out as a final test of the hydrophone intensity probe.

Since this work was carried out, research has moved on in some of the directions suggested by this work. Guigne et al 1992 investigated the use of an FFT analyser to obtain more detailed information regarding modal parameters, including intensity mapping. Klein et al (1994) look at the changes in modal parameters arising from fatigue cracking in cantilever beams. However, the work presented in this thesis is still considered to provide an important underpinning of the subsequent research.

6.2 CONCLUSIONS

The following can be stated as the more specific findings of this thesis investigation:

a) While the experimental natural frequencies of the thin plate correlated well with the analytically computed values, those of the thicker one are observed to be only 70-75% of the analytically computed values.

b) It is possible to correlate the natural frequencies of the vibrating plate with the

acoustic pressure and intensity spectra obtained from the microphone pair through the B & K 3360 intensity analyzer.

c) Since the spectral bands are rather wide, it is possible only to identify the natural frequencies within the bandwidth of the particular filter; hence the spectra generated by the intensity analyzer cannot be used as an exact tool to identify natural frequencies.

d) Mode shapes could be suitably identified by the 1/3 octave intensity contour maps carried out as specific frequency scans.

e) The in-plane acoustic intensity information obtained, while not being immediately applicable in this study, indicated that it could provide useful information in investigating torsional modes in more complex structures.

f) Surface measurements using accelerometers produced 1/3- and 1/12-octave intensity spectra from which the natural frequencies could be identified. Additionally, the surface intensity flow correlated well with the in-plane acoustic intensity.

g) Acoustic intensity spectral measurements made on notched beams indicate the shift in the natural frequencies (through the change in the spectral amplitudes) but

these shifts are not sufficiently precise to indicate the actual change in notch depth.

h) Acoustic intensity contour maps on notched beams did show variations in the energy flow patterns that could be attributed to the notching.

i) Studies similar to the above could be carried out in an underwater environment.

As a result of the above studies, the following recommendations are made for future studies in this area:

a) More studies need to be done to examine whether intensity scans and the intensity contour maps could be used more effectively to identify the mode shapes in structures. The use of narrower band measurements may clarify the intensity maps sufficiently to assist in mode shape identification. In addition the effects of spatial resolution need to be investigated at a higher frequencies where nodes are closer together.

b) Since one of the strengths lies in its non-contacting element, the technique would be ideally suited to glass and carbon fibre composite structures where accelerometers are more difficult to use. Such an investigation would be extremely informative.

REFERENCES

Angelo, M. (1987) "Vibration Monitoring of Machines", Bruel & Kjaer Technical Review No. 1.

Atarashi, M et al, (1988) "Application of Sound Intensity Methods for Turbo Machine Noise", Proc. 2nd Symposium on Acoustic Intensity, Tokyo.

Bathe, K.J. and Wilson, E.L. (1976) Numerical Methods in Finite Element Analysis. Publ. Englewood Cliffs, Prentice Hall.

Begg, R.D., Mackenzie, A.C., Dodds, C.J. and Loland, O, (1976) "Structural Integrity Monitoring using Digital Processing of Vibration Signals", Offshore Technology Conference, Dallas, Paper No. OTC 2549.

Bennet, I. (1987) "Acoustic Intensity Analysis Points to the Noisy Parts", Noise Control, CME November.

Bissinger, G. and Chowdhury, M.R. (1992) "Comparison of Hammer-Impact Modal Analysis Measurements with Cardioid and Omnidirectional Microphone in the Near- and Far-Field Regions", Proc. 10th Int'l Modal Analysis Conference, pp 394-399.

Bruel & Kjaer (1986) "Sound Intensity", Bruel & Kjaer Publication DK BR 0476-11, Publ. Bruel & Kjaer, Denmark.

Bruel & Kjaer, (1987) "Environmental Noise Measurement", Bruel & Kjaer publication DK BR0139-12. Bruel & Kjaer, Denmark.

Bruel & Kjaer "Operating manual for the 3360 Intensity Analyzer", Bruel & Kjaer, Denmark.

Bruel & Kjaer (1988) Intensity Measurements -The analysis technique of the Nineties, G. Rasmussen (Ed.) Publ. Bruel & Kjaer BA7196-14 (Publ. 1988)

Brughmans, M, Leuridan, J. and LMS International (1992) "Integrated Design Approach to BEM Acoustic Radiation Prediction", Proc. 10th Int'l Modal Analysis Conference, pp 390-393.

Castagna, J.P.E. (1992) "Acoustic Noise Reduction using Experimentally Determined Complex Mode Shapes", Proc. 10th Int'l Modal Analysis Conference, pp 91-96.

Cragg, A. (1972) "The use of Simple Three-Dimensional Acoustic Finite Elemnts for Determining the Natural Modes and Frequencies of Complex Shaped Enclosures", JSV 23 pp331- 339.

Desai, M. and Koval, L.R., (1988) "Rayleigh-Ritz Applied to Noise Measurement", Proc. 6th Int'l Modal Analysis Conference, pp 322-330.

Fahy, F.J. (1989) Sound Intensity. Publ. Elsevier Science Publishers Ltd.

Filipi, P.J.T. (1983) "Integral Equations in Acoustics", publ. for the Internbational Centre for Mechanical Science by Springer Venlag Wien, New York pp 1-50.

Forssen, B and Crocker, M.J. (1983) "Estimation of Acoustic Velocities and Radiation Efficiency by use of the Two Microphone Technique.", J. Acoust. Soc. Am. pp1047-1052

Fyfe, K.R., Coyette, J.P. and Wynendale, H. (1989) "Acoustic Modal Identification of Boundary Element Modelling". Proc. 7th Int'l Modal Analysis Conference, pp 276-280.

Fyfe, K.R. and Ismail, F. (1987) "Application of Modal Analysis to the Acoustic Modelling of Vibrating Cylinders", Proc. 5th Int'l Modal Analysis Conference, pp 336-342.

Gade, S. (1985) "The Validity of Intensity Measurements." Bruel and Kjaer Technical Review 4, pp 3-31.

Garibaldi, L. Liang, L.G. and Piombo, B. (1990) "Acoustical Emission Control of Metal Plates using Modal Analysis to Distribute Visco-elastic Materials", Proc. 8th Int'l Modal Analysis Conference, pp 275-278.

Grosveld, F.W., Sullivan, B.M. and Marulo, F., (1988) "Aircraft Interior Noise Prediction using a Structural-Acoustic analogy in NASTRAN Modal Synthesis", Proc. 6th Int'l Modal Analysis Conference, pp 1191-1198.

Guigne, J.Y., Williams, P.G. and Adams, J.G. (1990) Stationarity of Acoustic Intensity Measurements on Steel Plates", J. Acoust. Soc. Am. 87(6), pp 2773-2778

Guigne, J.Y., Klein, K., Swamidas, A.S.J. and Guzzwell, J (1992) "Modal Information from Acoustic Measurements for Fatigue Crack Detection Applications", Proc. 11th Int'l Conf. on Offshore Mechanics and Arctic Engineering, pp 585-593.

Hashimoto, M. and Tagawa, N. (1987) "Noise Radiation Reduction for High Speed Fully Formed Character Printer using Dynamic Design Analysis Approach", Proc. 5th Int'l Modal Analysis Conference, pp 356-363.

Kelly, J.K. (1988) "A Generalised Approach to Acoustic Intensity", J. Acous. Soc. Am. 83 (6).

Kenley, R,M, and Dodds, C.J. (1980) "West Sole WE Platform: Detection of Damage by Structural Response Measurements", Offshore Technology Conference, Texas, Paper No. OTC 3866.

Kinsler, L.E., Frey, A.R., Coppens, A.B. and Sanders, J.V. (1982) "Fundamentals of Acoustics.", Publ. John Wiley & Sons, 3rd Edition.

Klein, K., Guigne, J.Y. and Swamidas, A.S.J. (1994) "Monitoring Change in Modal Parameter with Fatigue", Proc. IMAC 1994, pp 1792-1800.

Lamancusa, J.S., and Koopmann, G.H. (1991) "Minimization of Radiated Sound Power from Structures using Shape Optimization Techniques", Proc. 9th Int'l Modal Analysis Conference, pp 945-948.

Leuridan, J., Aquilina, R. and Flandrin, J. (1989) "The Use of Coherence Functions for Calculating Mechano-Acoustical Impedances" Proc. 7th Int'l Modal Analysis Conference, pp 280-288.

Moore, T. and Reif, Z., (1987) "Modal Analysis as a Tool for Reducing Transmission Case Machining Noise", Proc. 5th Int'l Modal Analysis Conference, pp 350-356.

Nilles, P.E. and Dauby, P.H., (1976) "Control of the OBM/Q-BOP Process", Iron and Steel Engineer, March.

Noiseux, D.U. (1970) "Measurements of Power Flow in Uniform Beams and Plates", JASA, 47(1) p. 238-247.

Okubo, N. and Tajima, Y. (1988) "Prediction of Structural Born Noise based on the Modal Analysis", Proc. 6th Int'l Modal Analysis Conference, pp 309-314.

Park, Y. and Lee, H. (1990) "An Analytical Method of Acoustic Radiation from a Clamped Layered Circular Plate Contacting with Inviscid Fluid", Proc. 8th Int'l Modal Analysis Conference, pp 279-285.

Pascal, J.C. and Lu, J. (1985) "Advantage of the Vectorial Nature of Acoustic Intensity to Describe Sound Fields", Proc. Internoise '85, p1111-1114.

Pavic, G. (1976) "Measurement of Structure Born Wave Intensity, Part I: Formulation of the Method.", J. Sound and Vibration, 49(2), p. 221-230.

Petyt, M (1983) "Finite Element Techniques in Acoustics", publ. for the Internbational Centre for Mechanical Science by Springer Venlag Wien, New York pp 51-104.

Randall, R.B. (1977) "Application of B & K Equipment to Frequency Analysis.", Publ. Naerum Offset, Denmark.

Rasmsussen P. (1984) "Measuring Intensity", Intensity Measurements - the analysis technique of the nineties, G. Rasmussen (Ed.), Publ. Bruel & Kjaer No. BA 7196-14 (Publ. 1988), pp1-10.

Rasmussen, P. (1986) "SIRA Vibration Course, March 1986", Intensity Measurements - The analysis technique of the Nineties, G. Rasmussen (Ed.) Publ. Bruel & Kjaer BA7196-14 (Publ. 1988), pp 153-160.

Rasmussen, P. (1985) "Phase Errors in Intensity Measurements.", Intensity Measurements - the analysis technique of the nineties, G. Rasmussen (Ed.), Bruel & Kjaer No. BA 7196-11, B1-B10.

Rasmussen, G. (1988) "Report on Sky-Train Measurements, Vancouver Rapid Transit System".

Rasmussen, P. (1984) "Engine Testing using Noise Measurements", Intensity Measurements, Bruel and Kjaer publication 3/84.

Rasmussen, G., (1985) "Measurements of Intensity", Noise-Con 1985, Intensity Measurements, The Measurement technique of the Nineties, Bruel and Kjaer Publication BA7196-14, (Publ. 1988)

Rasmussen, G. and Rasmussen, P., (1988) "Identification of Energy Sources and Absorbers", Intensity Measurements, The Measurement technique of the Nineties, Bruel and Kjaer Publication BA7196-14, (Publ. 1988)

Rasmussen G., Rasmussen P. and Kjaergaard N (1985) "Intensity Measurements", Proc. Inter-Noise.

Rogers, L.M., Hansen, J.P. and Webborn, T.J.C. (1980) "Application of Acoustic Emission Analysis to the Integrity Monitoring of Offshore Steel Production Platforms.", Materials Evaluation, 38(8), p. 39-49.

Rossi, M. (1988) Acoustics and Electroacoustics, pp 32, Publ. Artech House, Inc.

Sen, S.N. (1990) Acoustics, Waves and Oscillators, Publ John Wiley and Sons, New York.

Seybert, A.F. and Khurana, R.(1988) "Calculation of the Sound Intensity and Sound Radiation Efficiency of Structures from Vibration Data"

Shultz, T.J., Smith, P.W. Jr. and Malne, C.T. (1975) "Measurement of Acoustic Intensity in a Reactive Sound Field", J.Acoustic Soc. Am. 57(6),pp 1263-1268.

Stephens, R.W.B. and Bate, A.E. (1966) Acoustics and Vibrational Physics, Publ. Edward Arnold Ltd London, 818p.

Sung, M.H., Kang, Y.J., Lee, J.M, Kim, S.H., Kim, J.H., and Jung, S.G. (1991) "A Study on the Interior Noise-Reduction of a Passenger Car", Proc. 9th Int'l Modal Analysis Conference, pp 956-961.

Technisch Physiche Dienst, (1983) "Determination of Propeller Noise Radiated Underwater with the Intensity Method.", Memorandum 208.725/1.

Thompson, J.K. and Tress, D.R. (1981) "Finite Difference Approximation Errors in Acoustic Intensity Measurements." J. Sound and Vibration 75, pp 229-238.

Thomson, W.T., (1981) "Theory of Vibrations with Applications." (2nd Edition), Publ. Prentice-Hall, New Jersey.

Tinti, F.C. (1992) "Passive Sound Insulation Package Experimental Development on Medium Truck Diesel Engine Based Sound Intensity Measurement Technique", Proc. 10th Int'l Modal Analysis Conference, pp 400-406.

Watkinson, P.S. (1984) "Calibration and Inherent Errors of a Two Hydrophone Sound Intensity Measurement System." Proc. Inst Acoustics Vol 6, Pt. 5.

Wendlan, W.L. (1983) "Boundary Element Methods and their Asymptotic Convergence", publ. for the Internbational Centre for Mechanical Science by Springer Venlag Wien, New York.

Whittome, T.R. and Dodds, C.J. (1983) "Monitoring of Offshore Structures by Vibration Techniques", Design in Offshore Structures, Thomas Telford Ltd., LONDON pp 93-100.

APPENDIX A

CALIBRATION TABLES FOR BRÜEL & KJÆR TYPE 3360 INTENSITY ANALYZERS

All calibrations were carried out using the B & K Type 3541 Sound Intensity Calibrator. However, the Pistonphone sound source used with the system was not the original supplied with the system, and the calibration values for Intensity and Particle Velocity levels measured are slightly different from the values given for the calibration system.

Calibration Values for Sound Intensity Calibrator Type 3541, Serial Number 1449489.

Sound Pressure Level

117.9 dB re 20 μPa $\pm$ 0.2 dB

Particle Velocity Level

117.6 dB re 50 nm/s $\pm$ 0.3 dB (nominal microphone spacing 50 mm)

130.0 dB re 50 nm/s $\pm$ 0.3 dB (nominal microphone spacing 12 mm)

136.0 dB re 50 nm/s $\pm$ 0.3 dB (nominal microphone spacing 6 mm)

Sound Intensity Level

117.7 dB re 1 pW/m^2 $\pm$ 0.25 dB (nominal microphone spacing 50 mm)

123.9 dB re 1 pW/m^2 $\pm$ 0.25 dB (nominal microphone spacing 12 mm)

126.9 dB re 1 pW/m^2 $\pm$ 0.25 dB (nominal microphone spacing 6 mm)

The calibration and instrument error measurements were carried out using the software routine 'INTENS_CAL'.

Unit 1. Serial Number 1336918.

Calibrations using 1/2" microphone pair Type 4181 serial number 1335832.

Nominal spacing of 12 mm:

Pressure Calibration, Channel A : 117.9 dB

Pressure Calibration, Channel B : 117.9 dB

Intensity Calibration : 124.4 dB

Residual Intensity Index and Phase Error Measurements

Freq. (Hz.)	L_{PR} (dB)	L_{IR} (dB)	L_{KO} (dB)	Phase Error
100	67.6	59.1(+)	-8.5	0.19°
125	71.7	65.9(+)	-5.8	0.43°
160	71.2	60.3(-)	-10.9	0.17°
200	71.5	58.6(+)	-12.9	0.13°
250	71.4	55.5(+)	-15.9	0.08°
315	71.2	56.0(+)	-15.2	0.12°
400	69.9	40.0(+)	-29.9	0.01°
500	67.5	53.9(+)	-13.6	0.29°
630	65.3	51.0(+)	-14.3	0.32°
800	63.8	50.4(+)	-13.4	0.48°
1000	64.1	46.0(+)	-18.1	0.20°
1250	65.6	49.0(+)	-16.6	0.36°
1600	67.4	50.5(+)	-16.9	0.43°
2000	62.7	46.5(+)	-16.2	0.64°
2500	61.9	45.3(+)	-16.6	0.72°
3150	55.6	40.0(+)	-15.6	1.14°
4000	62.9	44.9(+)	-18.0	0.83°
5000	62.4	43.6(+)	-18.8	0.86°

Nominal spacing of 50 mm

Pressure Calibration, Channel A : 117.9 dB

Pressure Calibration, Channel B : 117.9 dB

Intensity Calibration : 118.4 dB

Residual Intensity Index and Phase Error Measurements

Freq. (Hz)	L_{PR} (dB)	L_{IR} (dB)	L_{KO} (dB)	Phase Error ϕ_{err}
31.5	66.0	52.5(+)	-13.5	0.08°
40	60.2	49.0(+)	-11.2	0.17°
50	60.5	40.0(+)	-20.5	0.02°
63	63.9	52.9(-)	-11.0	0.28°
80	64.5	54.3(-)	-10.2	0.42°
100	68.2	40.0(+)	-28.8	0.01°
125	72.4	50.6(+)	-21.8	0.05°
160	72.6	52.7(+)	-19.9	0.09°
200	72.0	51.8(-)	-20.2	0.10°
250	71.6	52.3(+)	-19.3	0.16°
315	70.9	48.7(+)	-22.4	0.10°
400	70.3	46.6(+)	-23.7	0.09°
500	67.9	48.9(+)	-19.0	0.34°
630	65.8	45.6(+)	-20.2	0.34°
800	64.5	40.0(+)	-24.5	0.15°
1000	64.6	43.0(+)	-21.6	0.38°
1250	65.9	43.9(+)	-22.0	0.43°

Unit 2. Serial Number 1336920.

Calibrations using 1/2" microphone pair Type 4181 serial number 1335821.

Nominal Spacing 12 mm

Pressure Calibration, Channel A : 117.9 dB

Pressure Calibration, Channel B : 117.9 dB

Intensity Calibration : 124.6 dB

Particle Velocity Calibration : 131.2 dB

Residual Intensity Index and Phase Error Measurements

Freq. (Hz)	L_{PR} (dB)	L_{IR} (dB)	L_{KO} (dB)	Phase Error ϕ_{err}
100	69.4	65.5(+)	-3.9	0.53°
125	69.4	66.7(+)	-2.7	0.88°
160	70.4	66.4(+)	-4.0	0.83°
200	70.9	65.9(+)	-5.0	0.83°
250	71.1	62.3(+)	-8.8	0.43°
315	71.1	56.5(+)	-14.6	0.14°
400	69.4	48.8(+)	-20.6	0.05°
500	67.5	48.9(-)	-18.6	0.09°
630	66.0	51.3(-)	-14.7	0.29°
800	64.3	50.3(-)	-14.0	0.42°
1000	63.7	51.4(-)	-12.3	0.77°
1250	66.0	52.1(-)	-13.9	0.67°
1600	67.3	53.7(-)	-13.6	0.91°
2000	62.7	48.5(-)	-14.2	1.00°
2500	62.5	48.7(-)	-13.8	1.37°
3150	57.4	44.4(-)	-13.0	2.07°
4000	57.5	43.4(-)	-14.1	2.04°
5000	59.0	44.1(-)	-14.9	2.12°

Nominal spacing of 50 mm:

Pressure Calibration, Channel A : 117.9 dB

Pressure Calibration, Channel B : 117.9 dB

Intensity Calibration : 118.5 dB

Particle Velocity Calibration : 118.5 dB

Residual Intensity Index and Phase Error Measurements

Freq. (Hz)	L_{PR} (dB)	L_{IR} (dB)	L_{KO} (dB)	Phase Error ϕ_{err}
31.5	61.9	66.7(+)	4.8	5.19°
40	57.3	61.0(+)	3.7	5.12°
50	57.7	60.1(+)	2.4	4.74°
63	59.2	57.9(+)	-1.3	2.63°
80	61.7	40.0(+)	-21.7	0.03°
100	63.7	59.0(+)	-4.7	1.85°
125	68.2	58.1(+)	-10.1	0.67°
160	68.1	60.7(+)	-7.4	1.59°
200	68.0	57.9(+)	-10.1	1.07°
250	67.7	55.5(+)	-12.2	0.82°
315	67.3	54.0(+)	-13.3	0.80°
400	66.0	47.0(-)	-19.0	0.27°
500	63.9	45.6(+)	-18.3	0.40°
630	61.6	40.0(+)	-21.6	0.25°
800	60.5	41.4(-)	-19.1	0.54°
1000	60.6	42.9(-)	-17.7	0.93°
1250	61.9	44.6(-)	-17.3	1.27°

Unit 3. Serial Number 1375391.

Calibrations using 1/2" microphone pair Type 4181 serial number 1425303

Nominal Spacing 12 mm

Pressure Calibration, Channel A : 117.9 dB

Pressure Calibration, Channel B : 117.9 dB

Intensity Calibration : 124.3 dB

Residual Intensity Index and Phase Error Measurements

Freq. (Hz)	L_{PR} (dB)	L_{IR} (dB)	L_{KO} (dB)	Phase Error ϕ_{err}
100	68.9	60.9(-)	-8.0	0.21°
125	70.6	62.8(+)	-7.8	0.27°
160	71.9	58.1(-)	-13.8	0.09°
200	71.0	57.7(+)	-13.3	0.12°
250	72.1	57.9(+)	-14.2	0.12°
315	71.7	55.6(+)	-16.1	0.10°
400	69.7	55.5(+)	-14.2	0.20°
500	67.7	53.0(+)	-14.7	0.22°
630	65.8	51.3(+)	-14.5	0.30°
800	64.1	48.2(+)	-15.9	0.27°
1000	64.4	46.0(+)	-18.4	0.19°
1250	66.0	46.4(+)	-19.6	0.18°
1600	67.4	49.2(+)	-18.2	0.32°
2000	62.6	42.1(+)	-20.5	0.23°
2500	61.9	40.0(+)	-21.9	0.21°
3150	56.1	40.0(+)	-16.1	1.01°
4000	61.6	40.3(+)	-21.3	0.39°
5000	61.4	40.0(+)	-21.4	0.47°

Nominal spacing of 50 mm:

Pressure Calibration, Channel A : 117.9 dB

Pressure Calibration, Channel B : 117.9 dB

Intensity Calibration : 118.3 dB

Residual Intensity Index and Phase Error Measurements

Freq. (Hz.)	L_{PR} (dB)	L_{IR} (dB)	L_{KO} (dB)	Phase Error ϕ_{err}
31.5	65.2	61.6(-)	-3.6	0.75°
40	61.6	51.5(+)	-10.1	0.21°
50	62.4	48.0(+)	-14.4	0.10°
63	64.1	59.0(+)	-5.1	1.10°
80	66.3	53.3(+)	-13.0	0.22°
100	67.4	54.0(-)	-13.4	0.25°
125	71.9	50.1(-)	-21.8	0.05°
160	71.2	54.7(+)	-16.5	0.20°
200	71.7	52.0(-)	-19.7	0.12°
250	71.9	46.7(+)	-25.2	0.04°
315	71.4	49.4(+)	-22.0	0.11°
400	70.1	42.4(+)	-27.7	0.04°
500	67.5	44.7(-)	-22.8	0.14°
630	65.7	44.8(-)	-20.9	0.29°
800	64.4	40.7(-)	-23.7	0.19°
1000	64.1	41.3(-)	-22.8	0.29°
1250	65.8	40.0(-)	-25.8	0.18°

APPENDIX B

CONTOUR MAP

AND

VECTOR MAP

INTERPRETATION

CONTOUR MAP

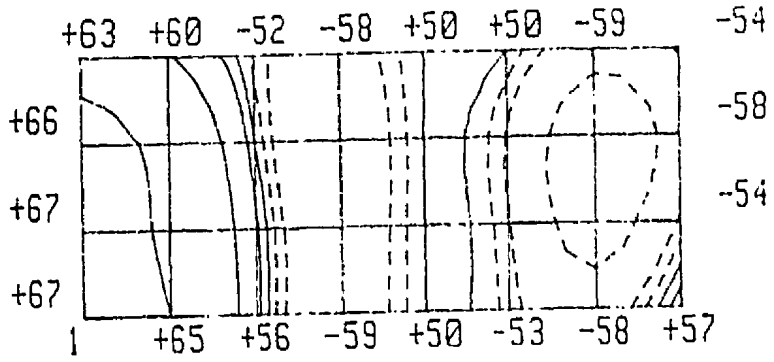

i) Except where noted, the contour map is always used to show energy flowing in the Z-direction i.e normal to the plate. Positive intensity is taken as being away from the plate; negative intensity is towards the plate.

ii) The lower left hand corner, numbered 1, is the start point for the measurement grid. This is at the pont 0,0 (see Figures 4.13 and 4.14).

iii) The grid cell width is 50 mm; the grid cell height is 20 mm (Beam I) or 25 mm (Beam II).

iv) The numerical values around the grid give the intensity level in dB measured at the edge grid locations.

v) The contour lines are interpolated mathematically from the intensity levels at each grid point. Solid lines are positive intensity i.e. radiating away from the plate; negative intensity (toward the plate) is shown by dashed lines.

VECTOR MAP

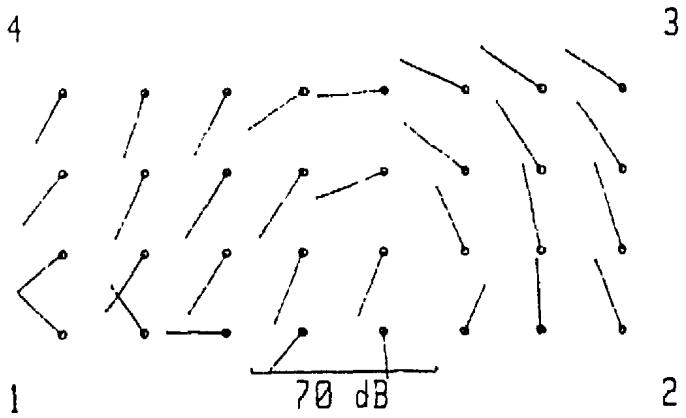

i) The vector map is used to show energy flowing in the X-Y plane of the plate.

ii) The lower left hand corner, numbered 1, is the start point for the measurement grid. This is at the pont 0,0 (see Figures 4.13 and 4.14).

iii) The grid cell width is 50 mm; the grid cell height is 20 mm (Beam I) or 25 mm (Beam II).